THE UNIVERSITY OF OKLAHOMA

GRADUATE COLLEGE

A STUDY OF THE DEPYRIDINATION OF DICHLOROHEXAKIS(PYRIDINE)COBALT(II)

A DISSERTATION

SUBMITTED TO THE GRADUATE FACULTY

in partial fulfillment of the requirements for the

degree of

DOCTOR OF PHILOSOPHY

BY

LYMAN CLIFFTON LEWIS II

Norman, Oklahoma

1967

A STUDY OF THE DEPYRIDINATION OF

DICHLOROHEXAKIS(PYRIDINE)COBALT(II)

APPROVED BY

Norman Fogel

J. J. Colbert

Bernard O. Halpern

Edwin H. Klehr

Stanley C. Nealy

ACKNOWLEDGEMENT

The author wishes to express his appreciation to Dr. Norman Fogel for the suggestion of this research topic and for his patient direction throughout the course of the investigation.

The author also gratefully acknowledges the aid of Dr. S. D. Christian of this department who provided helpful suggestions and discussions.

TABLE OF CONTENTS

LIST OF TABLES

LIST OF FIGURES

A STUDY OF THE DEPYRIDINATION OF DICHLOROHEXAKIS(PYRIDINE)COBALT(II)

CHAPTER I

INTRODUCTION

Pyridine Complexes of Cobalt(II) Chloride

Pyridine (C_5H_5N) is well known as one of the common ligands in transition metal coordination compounds (1). Judging from the number and variety of compounds formed, pyridine is apparently comparable to ammonia or water in its complexing ability. This behavior is satisfactorily explained by considering the formation of a coordinate covalent bond between the nitrogen atom of the pyridine molecule and the transition metal cation. Considering an sp^2 hybridized nitrogen, the five valence electrons (i.e. those in the second main energy level) will be distributed as follows: two are involved in the formation of covalent sigma bonds with adjacent carbon atoms, one is contained within a p type orbital perpendicular to the plane of the ring (which along with one electron from each of the carbons comprises the aromatic system), while the other two

remain as a lone pair in a nonbonded state. (This is analogous to the availability of nonbonding electrons in the ammonia molecule.) Thus a bond could be formed by overlapping of the nitrogen sp^2 hybrid orbital containing the lone pair with orbitals of appropriate symmetry on a transition metal cation such as Co(II).

Cobalt(II) chloride does, indeed, form a series of pyridine adducts with the general formula $Co(py)_nCl_2$.

Dichlorohexakis(pyridine)cobalt(II), the compound formed in the presence of excess pyridine, undergoes a stepwise, thermal decomposition with the evolution of pyridine vapor. Accompanying this reaction is a progressive color change from the deep, red-violet $Co(py)_6Cl_2$, through what is apparently a series of intermediate compounds of varying violet and blue coloration, to the pale blue of the ultimate product of this decomposition, $CoCl_2$. The compounds of general formula $Co(py)_nCl_2$ observed in this sequence are those with n = 6, 4, 2, 1, 2/3.

Survey of Previous Study

The preparation of $Co(py)_6Cl_2$ is reported (2), but this compound remains essentially uncharacterized. The visible reflection spectrum of $Co(py)_6(NO_3)_2$ (3), the solution spectrum of $CoCl_2$ dissolved in pyridine (4), and the spectra of $Co(NO_3)_2$ in pyridine solutions with other solvents (5) are reported. However, the solid structure or even the constitution of the inner coordination sphere (other than the probability

of octahedral geometry) in $Co(py)_6Cl_2$ remains undetermined.

In addition to a general preparation of $Co(py)_4Cl_2$ (2)(6), an x-ray structure analysis has been completed (7). Magnetic susceptibility measurements at room temperature (8)(6) as well as the reflection spectrum in the visible region (3) are reported.

$Co(py)_2Cl_2$ has produced the most intensive study since it exists in two temperature dependent, isomeric forms (9). $\alpha Co(py)_2Cl_2$ was first prepared in 1894 (10) and is stable at room temperature. A high temperature form, $\beta Co(py)_2Cl_2$, was initially prepared in 1927 (11). The α form is a pale violet color which changes upon heating above 100°C in a sealed tube to a deep blue color which is characteristic of the β modification. It was initially proposed that the α and β forms represented cis and trans isomers (8); however, on the basis of spectral (3)(13), x-ray (14)(15), and magnetic susceptibility (1)(16) data, the conclusion was drawn that the α and β forms represent respectively octahedral and tetrahedral coordination isomers. (The tetrahedral species is not, as might be expected, $CoCl_4^=$ (12)(17), but on the basis of further x-ray and spectral analysis, $Co(py)_2Cl_2$.) This constituted the first definite case of a bivalent metal possessing simple coordination derivatives with different configurations (12).

The infrared spectra of $Co(py)_4Cl_2$ (18) and $Co(py)_2Cl_2$ (18)(19) shows each band of the pyridine spectrum

reproduced with only minor shifts or splitting. The conclusion must be, therefore, that the electron density over the ring system remains relatively unchanged in the complexes since it is well known that for other aromatic systems, such as benzene, changes in the electron density produce wide differences in the observed spectrum (20). Such a constant electron level can result from either backbonding by the cobalt or external donation from some electron rich source in the system.

Some recent work (21), however, has shown that pyridine ring vibrations at 640 and 420 cm^{-1} are sensitive to the complex symmetry or crystal structure and some preliminary correlations have been made with known structures.

The complex $Co(py)Cl_2$ was initially thought to be an equimolar mixture of $Co(py)_2Cl_2$ and $CoCl_2$ (22). Later, however, this was found to be a definite compound (23)(24). No x-ray, magnetic, or spectral data is reported.

$Co(py)_{2/3}Cl_2$, which may be better represented empirically as $Co_3(py)_2Cl_6$, is mentioned once in the literature as one of the products of a thermogravimetric analysis of α $Co(py)_2Cl_2$ (23). It is reported that a plateau corresponding to this composition exists around 280°C. In this analysis only alkaline vapors (uncharacterized) were evolved and the final residue obtained was determined to be $CoCl_2$.

A summary of information pertaining to the pyridinates is shown in table 1 and figure 1.

TABLE 1

PYRIDINATE DATA

n (moles py) / (Mole $CoCl_2$)	Color	Site Symmetry	Magnetic Moment (B.M.)
6	Dark Red-Violet (2)	- - -	- - -
4	Red-Violet (2)	D_{4h} (7)	4.87 (13) 4.85 (20^{o}) (8,6)
α2	Violet (2,25)	D_{2h} (15)	5.34 (20^{o}) (16,26)
β2	Deep Blue (12)	C_{2v} (14)	4.60 (20^{o}) (16)
1	Pale Blue Violet	- - -	- - -
2/3	Pale Blue Violet	- - -	- - -
0	Pale Blue	O_h (27)	5.29 (8) 5.38 (28)

Fig. 1 -- Depyridination Sequence (including temperature at which reaction occurs in vacuuo)

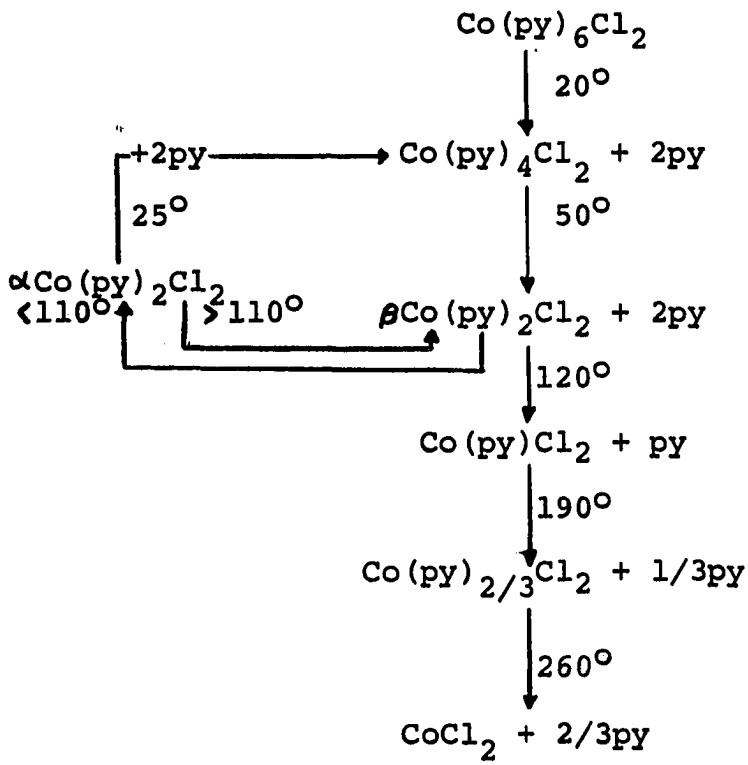

The Complexes in Solution

The pyridinates are all appreciably soluble in water giving a pink solution in which the predominate species present is probably $Co(H_2O)_6^{+2}$. The compounds also dissolve in pyridine and methyl alcohol to give similarly colored solutions. The predominant cobalt species present in these "red" solutions is octahedrally coordinated (although perhaps distorted and, therefore, actually possessing lower symmetry than O_h). Solutions containing the octahedral species can be generally characterized by an adsorption band centered at about 500 mμ (3).

$Co(py)_6Cl_2$, $Co(py)_4Cl_2$, α and β $Co(py)_2Cl_2$ and to a much lesser extent $Co(py)Cl_2$ and $Co(py)_{2/3}Cl_2$ are soluble in chloroform yielding a deep blue solution. It is known that if either α or β $Co(py)_2Cl_2$ is dissolved in chloroform, the predominant species is of tetrahedral configuration characterized by an absorption band at 600 mμ (4).

It was initially proposed (17) that the species present was tetrahedral $CoCl_4^=$ since the spectrum resembles that of $CoCl_2$ in concentrated hydrochloric acid and since the spectrum was virtually identical with that obtained with chloroform solutions of a compound where quinoline (C_9H_7N) replaces pyridine. It was argued that if pyridine were directly coordinated with the Co(II) ion, then replacement with the higher molecular weight quinoline would cause a spectral shift due to a mass effect as seen, for instance, in the series $CoCl_4^=$, $CoBr_4^=$, and $CoI_4^=$. This argument is faulty since quinoline and pyridine nitrogens have almost identical ring environments and electron donor ability. In both compounds, coordination would be through the nitrogen. Since the constitution of the inner coordination sphere would be almost the same with either ligand, similar spectra would be expected. (The effect of the coordination sphere on spectra will be discussed in some detail later in Chapter IV.) Some spectral deviation (which may or may not be significant) would, however, be expected to occur as the result of slightly different coordination sphere geometries

due to steric effects arising from the larger quinoline ring structure. It has been shown that the species present is definitely tetrahedral $Co(py)_2Cl_2$. (4)

Apparent molar absorbtivities at 600 mμ (Table 2) as well as the identical appearance of the spectra indicates that the same species is predominately present in chlorofrom solutions of $Co(py)_6Cl_2$ and $Co(py)_4Cl_2$. In chloroform solutions of $Co(py)_4Cl_2$ (and analogously $Co(py)_6Cl_2$) the situation is best represented by the equilibrium, $Co(py)_4Cl_2 = Co(py)_2Cl_2 + 2py$ for which $K = 8 \times 10^{-2}$ (4) (determined spectrophotometrically (29)). This indicates that if, for instance, the formal concentration of $Co(py)_4Cl_2$ were 10^{-4}M then the equilibrium concentration of $Co(py)_2Cl_2$ would be nearly 10^{-4}M.

Similar blue solutions are obtained with acetone, benzene and ethyl alcohol. The solubility decreases with decreasing pyridine content in all solvents and the lower pyridinates $Co(py)Cl_2$ and $Co(py)_{2/3}Cl_2$ are insoluble in nonpolar solvents such as benzene (30). Molar absorbtivity studies and general spectral appearance indicate that the same tetrahedral species is present (as by far the predominant species) in all of these solvents.

The molar absorbtivities were obtained from Beer's Law plots in the concentration range from 1×10^{-4} to 16×10^{-4} M. One centimeter quartz cells and the Beckman DK - 1 spectrophotometer were employed. The results are

summarized in Table 2 and typical experimental data is shown in Table 3 and Figure 2.

TABLE 2

APPARENT MOLAR ABSORBTIVITIES OF SOME "TETRAHEDRAL" SPECIES

Compound	Solvent	Absorbtivity (M^{-1}), 600 mμ
$Co(py)_6Cl_2$	Chloroform	7.1×10^4
$Co(py)_4Cl_2$	Chloroform	6.5×10^4
$\alpha,\beta\ Co(py)_2Cl_2$	Chloroform	6.2×10^4
$\alpha\ Co(py)_2Cl_2$	Acetone	5.8×10^4
$\alpha Co(py)_2Cl_2$	Benzene	6.0×10^4
$Co(py)_4Cl_2$	Benzene	5.8×10^4

TABLE 3

BEER'S LAW PLOT DATA

Compound	Solvent	Average Absorbance	Concentration x 10^4 (m)
$\alpha Co(py)_2Cl_2$	Chloroform	29.0	5.38
		44.5	7.99
		60.5	10.76
		78.5	13.45
		97.0	16.14
$Co(py)_4Cl_2$	Chloroform	23.0	3.38
		42.0	6.76
		59.5	9.46
		85.5	13.52
$Co(py)_6Cl_2$	Chloroform	26.5	3.63
		52.0	7.26
		63.0	8.70
		73.0	10.10
$\alpha Co(py)_2Cl_2$	Acetone	17.0	3.95
		27.5	5.95
		37.5	7.90
		49.5	9.90
		60.5	11.85

Fig. 2 -- Beer's Law Plots for Pyridinates in Solution

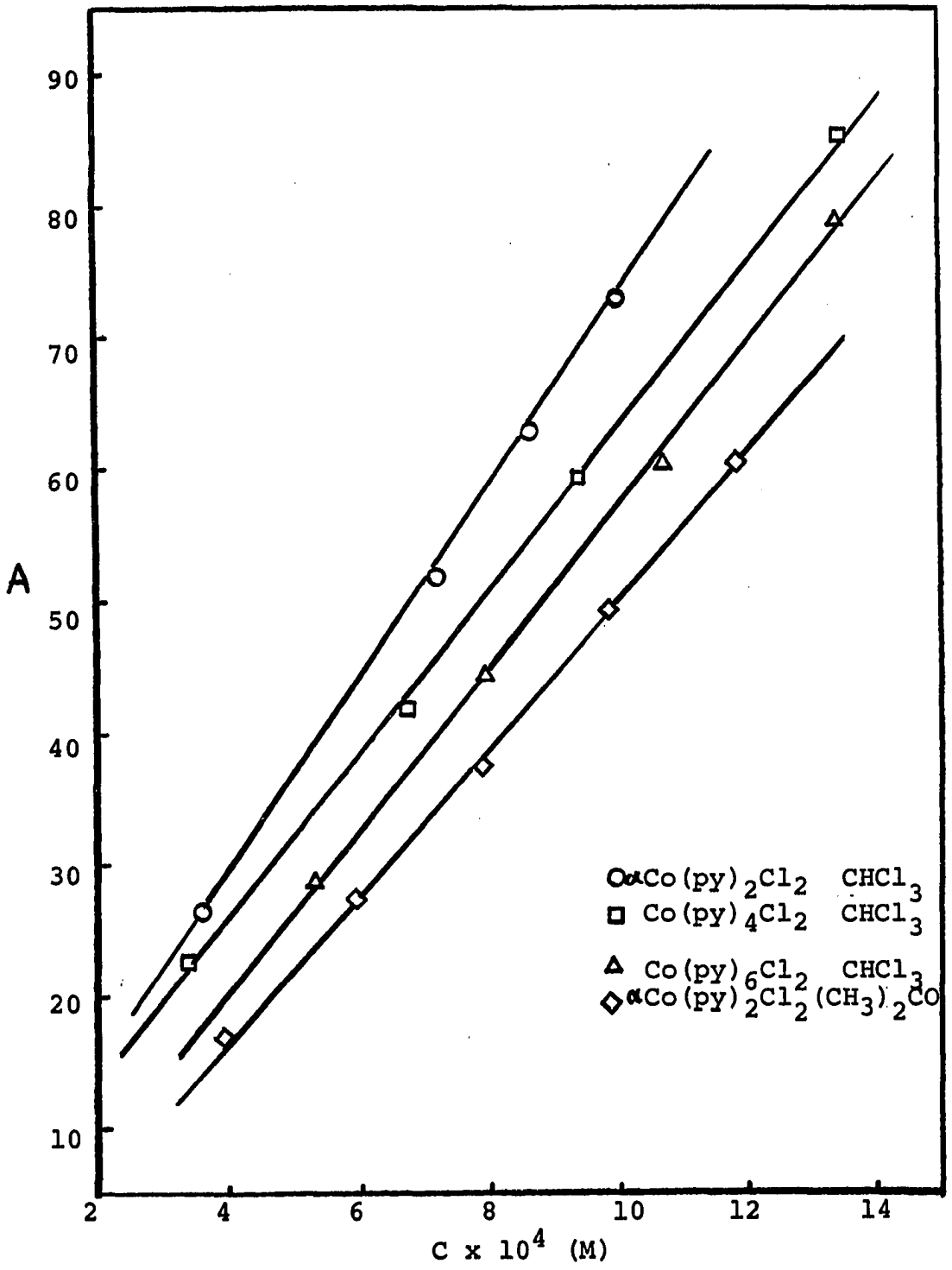

Complex Structures

It is not at all surprising to find tetrahedral and octahedral modifications present in both solution and solid phases within the series of pyridinates. Tetrahedral $CoCl_4^=$ is known to exist in solid Cs_3CoCl_5 (31) and K_2CoCl_4 (32) as well as in concentrated hydrochloric acid solutions of $CoCl_2$ (33). Equally well documented is the presence of octahedrally coordinated Co(II) such as in $CoCl_2$ itself (27) and in numerous complexes.

The most general argument for the stability of both tetrahedral and octahedral forms is based upon the relatively small differences between their respective crystal field stabalization energies (CFSE) as shown below in Table 4. Assuming that Dq (tetrahedral) is approximately 0.5 Dq (octahedral), the difference in CFSE is only 2Dq (octahedral) which is only about 5 kcal/mole for divalent ion Dq values of approximately 1000 cm^{-1}. Such a difference in stability energy may be easily overcome by particular solution or formation conditions; hence it is difficult to predict structures or site symmetries for those pyridinates which are presently uncharacterized.

TABLE 4

CFSE FOR Co(II), $3d^7$ GROUND STATE

	Octahedral	Tetrahedral
Ground State Electronic Configuration	$t_{2g}^5 e_g^2$	$e^4 t_2^3$
CFSE	-8Dq(oct.)	-12Dq(tet.) (-6Dq(oct.))

The Pyridinates in Practical Usage

In general, the pyridinates of cobalt(II) chloride have very limited practical significance. $Co(py)_4Cl_2$ and $Co(py)_2Cl_2$ are employed industrially as catalysts (34) (i.e. the Co(II) ion) in the polymerization of butadiene. These compounds are readily soluble in the reaction mixture and introduce a relatively insignificant contamination.

Objectives

The purpose of this work is, in general, to further elucidate the possible structural rearrangements occurring in connection with the depyridination. To this end, three separate studies have been completed which are, however, all related to either molecular or crystal structure and which may be correlated to yield the desired information:

(1) Reaction and formation thermodynamic functions have been calculated and related to structural changes.

This information was obtained by measuring the dissociation vapor pressure of the stepwise depyridinations at a constant temperature and also as a function of temperature.

(2) Magnetic susceptibilities were determined which are clearly indicative of the cobalt ion environment.

(3) The reflection spectra have been interpreted, in terms of the effect of perturbing ligand field potentials imposed upon the 3d orbitals of the cobalt ion and definitive structural data obtained.

When taken together and interrelated the results of the three studies yield sufficient evidence for an adequate interpretation and explanation of the structural rearrangements.

Incidentally, but not unimportantly, this study has hopefully further contributed to the development of methods of more general application, especially in the treatment of spectral and thermodynamic data.

CHAPTER II

COMPOUND PREPARATION AND ANALYSIS

Preparation

Dichlorohexakis(pyridine)cobalt(II) was prepared by the method of Katzin (2). One part by weight of reagent grade (Fisher's Certified) $Co(H_2O)_6Cl_2$ was stirred with 1.1 parts pyridine (Merck) dissolved in an equal volume of chloroform. The chloroform layer was separated and the solid residue extracted with ice cold chloroform two or three times. $Co(py)_6Cl_2$ was crystallized from the total extract in a desiccator under a dry air draft. The crystals formed were separated from the mother liquor and dried for a short time on a sintered glass disc under dry air. The apparent purity was unaffected by recrystallization.

Dichlorotetrakis(pyridine)cobalt(II) was also prepared by the method of Katzin with the exception that benzene was used as the solvent. The first three benzene extracts were discarded prior to the final extraction of the residual solid with ice cold chloroform. The red-violet crystals of $Co(py)_4Cl_2$ were recovered by evaporation in a draft and drying on a sintered glass disc. $Co(py)_4Cl_2$ may also be conveniently prepared from $Co(py)_6Cl_2$ under vacuum at a

temperature below 20°C by pumping to constant weight. It was found that, contrary to the observations of Katzin (2), $Co(py)_4Cl_2$ does indeed have an appreciable vapor pressure at room temperature. Preparation of $Co(py)_4Cl_2$ from $Co(py)_6Cl_2$ at a temperature much above 20°C resulted in the appearance of a blue compound, the composition of which was found to be $Co(py)_2Cl_2$ and which from the color must be the β modification. This is probably the same phenomenon observed by Friend and Mellor (6) who prepared $Co(py)_4Cl_2$ from trans $(Co(py)_4Cl_2)Cl$ and noted that the red-violet crystals kept indefinitely in a stoppered tube but turned blue in air.

α-Dichlorobis(pyridine)cobalt(II) was prepared (Ocone, (25)) by slowly adding 45 grams of pyridine to 35 grams of anhydrous $CoCl_2$ dissolved in 250 ml of absolute ethanol. The violet precipitate was recovered by filtration and dried on a disc. Final drying was completed over P_2O_5 or concentrated H_2SO_4 at room temperature. Pure $\alpha Co(py)_2Cl_2$ may also be prepared from either $Co(py)_4Cl_2$ or $Co(py)_6Cl_2$ by simply allowing either of those two compounds to stand over concentrated H_2SO_4 in a desiccator at room temperature. The samples reach constant weight after several months. $\alpha Co(py)_2Cl_2$ may, furthermore, be obtained as well formed needles by the slow evaporation of chloroform or acetone solutions in a desiccator at room temperature. The needles are apparently stable indefinitely in a stoppered tube, but break down within a few hours upon exposure to the atmosphere.

$\alpha Co(py)_2Cl_2$ has no appreciable vapor pressure at room temperature and no pyridine will be evolved. Compounds having simultaneous pyridine and water coordination are characterized (2) and, therefore, might well be expected to form as a result of a reaction of $\alpha Co(py)_2Cl_2$ with atmospheric water vapor. This would cause the α crystals to break down or become opaque.

β-Dichlorobis(pyridine)cobalt(II) is conveniently prepared by several methods from $\alpha Co(py)_2Cl_2$ (12). Simply heating in a sealed tube at 110°C produces the deep blue β isomer. The latter is apparently stable for long periods at room temperature in the absence of atmospheric water vapor or pyridine vapor. In the presence of trace amounts of water or pyridine vapor, the β to α transition is rapid. At relatively low temperatures (e.g. around dry ice temperature, -78°C) the transition to the stable α form occurs rapidly. $\beta Co(py)_2Cl_2$ may be obtained as well developed, six-sided, deep blue, columnar crystals by evaporation from a chloroform solution of $\alpha Co(py)_2Cl_2$ under partial reflux at a temperature just below the boiling point. The crystals break down to a blue powder which changes to violet very rapidly upon exposure to air. $\beta Co(py)_2Cl_2$ may also be obtained directly from $Co(py)_4Cl_2$ under vacuum at 60°C. It is the case that even though the α to β transition is above 100°C (110-135° (35)), the β isomer is preferentially formed from the higher pyridinates at temperatures between

room temperature and 110°C. This is a fact which will later complicate the vapor pressure study of this dissociation reaction.

$Co(py)Cl_2$ and $Co(py)_{2/3}Cl_2$ were obtained only as products of the depyridination reactions. $Co(py)Cl_2$ is obtained from $\beta Co(py)_2Cl_2$ at 120° - 130°C and $Co(py)_{2/3}Cl_2$ at 210° - 220°C. Both are definite compounds as indicated by plateaus in the vapor pressure-composition curves and breaks in the curves at the proper compositions.

Finally, $CoCl_2$ was obtained under vacuum at 260° - 280°C.

Analysis

Compound analysis was accomplished by standard methods. Chloride was determined gravimetrically by the precipitation of silver chloride with silver nitrate from dilute nitric acid solutions (36). The precipitate was dried to constant weight at 110°C. Duplicate samples were analyzed. No further determinations on a particular compound were made if reasonable agreement with the theoretical percentages was obtained.

Cobalt was determined by electrodeposition from ammoniacal solution on a Sargent-Stomin Electrolytic Analyzer equipped with rotating platinum gauze anode and platinum gauze cathode (37). No attempt was made to control the cathode potential since there were no other metallic cations present. The potential was adjusted to slightly

greater than four volts so that a moderate current of approximately two amps would flow. The electrolysis was allowed to continue (usually approximately one hour) with only occasional adjustments of the current until electrodeposition was complete as indicated by the failure of the blue $Co(SCN)_4^{=}$ to form in acidified, alcoholic NH_4SCN solution. Duplicate depositions were made.

Pyridine was determined in the case of $Co(py)_6Cl_2$, $Co(py)_4Cl_2$, and $Co(py)_2Cl_2$ by complete thermal depyridination and analysis of the condensed vapors. The pyridine vapors were trapped in a tube at -78°C (dry ice-acetone), taken up quantitatively in glacial acetic acid. The perchloric acid was prepared by mixing 72% perchloric acid with glacial acetic acid and dehydration with a slight excess of acetic anhydride according to standard procedures (38). The perchloric acid was standaridzed against reagent grade (Merck) pyridine. The titrations were quite satisfactorily followed potentiometrically using a Beckman Model 62 pH meter with glass electrode and calomel reference electrode (39).

The pyridine content of $Co(py)Cl_2$ and $Co(py)_{2/3}Cl_2$ was not directly determined since the weight of either of these two compounds required to produce a reasonable weight of pyridine for titration is relatively large and the compounds are not readily available in large amounts. Furthermore, the chloride and cobalt analyses agreed closely

with the theoretical percentages; therefore, a direct pyridine analysis was not considered of vital importance.

$Co(py)_6Cl_2$, $Co(py)_4Cl_2$, and $Co(py)_2Cl_2$ when prepared by the method of Katzin show no detectable water content with Karl Fischer titration (2). However, the pyridinates in general show a tendency to react with water vapor such as atmospheric moisture. Only if a water impurity is present is there any possibility of hydrolysis accompanying depyridination. At higher temperatures a probable hydrolysis reaction would be, for example,

$$Co(C_5H_5N)_2Cl_2 + H_2O \longrightarrow CoO + 2C_5H_5NH^+Cl^-.$$

The pyridinium chloride formed has similar physical properties to ammonium chloride such as extensive sublimation above 200°C (40). Therefore, if water is present, a white salt should be sublimed off the sample and collect in the upper part of the sample chamber; furthermore the sample would contain cobalt oxides, the presence of which would be reflected in the percentages of cobalt and chloride.

The analysis is summarized in Table 5. It is noted that the analyses agree closely with the theoretical calculations. The only significant deviation is in the case of the pyridine analysis for $Co(py)_6Cl_2$ which is rather low. This is explained by the fact that the dissociation vapor pressure is high and pyridine is evolved rapidly when the compound is exposed to air; therefore, it is very difficult to transfer or work with and maintain the exact $Co(py)_6Cl_2$ composition.

TABLE 5

COMPOUND ANALYSIS

Compound	Percentages					
	Co		Cl		C_5H_5N	
	Theo.	Exper.	Theo.	Exper.	Theo.	Exper.
$CoCl_2$	45.39	45.6±.2	54.61	54.0±.1		
$Co(py)_{2/3}Cl_2$	32.28	32.5	38.84	38.2		
$Co(py)Cl_2$	28.20	28.0	33.94	33.9		
$Co(py)_2Cl_2$	20.64	20.8	24.62	24.3	54.91	55.0±.5
$Co(py)_4Cl_2$	13.20	13.3	15.89	16.0	70.91	70.0
$Co(py)_6Cl_2$	9.75	10.1	11.73	11.9	78.51	77.2

CHAPTER III

DISSOCIATION PRESSURE STUDY

Preliminary Discussion

The depyridination reaction studied is generalized,

$$Co(py)_nCl_2(s) = Co(py)_{n-m}Cl_2(s) + mpy(v)$$

n:	6	4	$\alpha 2$	$\beta 2$	1	2/3
m:	2	2	0	1	1/3	2/3

The equilibrium may be shifted to the right by the removal of pyridine vapor. If pyridine is continually removed, cobalt(II)chloride is eventually obtained as the final product.

The equilibrium constants are given by,

$$K = \frac{P_{py}^m \left[Co(py)_{n-m}Cl_2(s) \right]}{\left[Co(py)_nCl_2(s) \right]}$$

and since the solid compounds are present in their standard state, $K = P_{py}^m$ (atmospheres).

The vapor pressure data, therefore, will yield two different types of information: (1) thermodynamic constants may be calculated from the temperature dependence of the equilibrium constants and, (2) following the vapor pressure as a function of weight will show, as breaks in the curve, the exact composition of the intermediate pyridinates.

Apparatus and Technique

The apparatus used to obtain the vapor pressures is similar to those previously described (41)(32). The apparatus is most simply described as a sealed sample chamber with a closed end manometer attached. Provision is made for evacuation of the system through a stopcock and for the determination of sample composition at any point in a particular depyridination step.

Specifically two methods were employed to follow the changing sample composition: (1) a weighed amount (several grams) of a known compound was introduced into the sample chamber. Pyridine was removed by vacuum pumping and collected in a cold trap at dry ice temperature; the amount of pyridine removed was then determined by titration or weight difference of the trap. (2) A weighed amount of sample (on the order of 0.5 grams) contained within a small (0.2 grams), plastic lined, aluminum foil bucket was suspended inside of the sample chamber by a quartz fibre spring (Worden Labs). The quartz springs which were employed have a total weight capacity of one gram and are seven to eight centimeters long when fully extended with this weight. The extension of a particular spring is, of course, a function of the spring constant and suspended weight. The movement of an individual spring (as observed with a cathetometer) may, however, be easily calibrated with known weights in terms of millimeters extension per milligram weight. In this manner, the change in sample weight with

vacuum pumping was followed. The particular spring used had a force constant of 11.45 gmf/cm or the reciprocal in more useful units, 0.0873 mm/mg. Although both methods were employed satisfacotrily, it was found that the first method was the more convenient.

The apparatus when thermostated in either water or oil baths could be used to obtain vapor pressure-composition or pressure-temperature curves (at constant sample composition).

The lower temperature work was done in a constant temperature water bath into which the entire vapor pressure apparatus could be submerged. The temperature regulation system consisted of a mercury capillary temperature sensor and electric resistance heater working through an electronic relay (Precision Scientific 62690). Provision was made for water circulation by means of stirring motors. At higher water temperatures fine control was adequately obtained working against external room temperature; around room temperature and below room temperature, cold water was circulated through a copper tubing coil submerged in the bath. Maximum temperature deviation was $\pm 0.05^{\circ}C$.

The pressures at higher temperatures were obtained with only the sample chamber submerged in a silicone oil bath. This constant temperature apparatus consisted of a solid aluminum cylinder (approximately eight inch base diameter and six inch height) into which holes were drilled to

accommodate the sample tube, a thermometer, and a temperature sensing switch (all of which were immersed in silicon oil). The block was wrapped with heating tapes and insulated on all sides with rock wool. Silicon oil was used since it may be heated to 350°C without appreciable decomposition. Temperative control was maintained (depending on the temperature region) at ±1 - 2°C. The magnitude of the dissociation pressure at the higher temperatures is, therefore, limited to the vapor pressure of pyridine at room temperature for a maximum.

If the basic vapor pressure system is modified to include a sintered glass disc with mercury seal above the sample chamber, a known weight of pyridine can be introduced into the evacuated system through the mercury by pipette and the system equilibrated. In this manner, the sample composition could be varied. This method proved to be very useful in studying the $Co(py)_4Cl_2 = \alpha Co(py)_2Cl_2$ equilibrium, as will be discussed. However, this method was not employed for other reactions since the time required for absorption and equilibration was generally prohibitive. The equilibration time could be markedly reduced by freezing the pyridine directly onto the solid sample as it is introduced through the mercury seal into the sample chamber. Furthermore, by holding the sample at 0°C, liquid pyridine could be kept in contact with the solid and the reaction was facilitated.

Another modification which was found to be useful is shown in Figure 3.

Figure 3: Constant Composition Vapor Pressure Apparatus

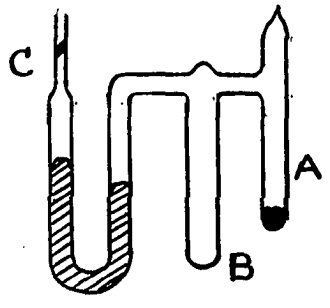

This apparatus can be made very compact and is easily immersed in the constant temperature bath. In addition it may be used with greater facility at higher temperatures and is completely leak free, having no standard taper joints, stopcocks, or mercury seals. It is, however, as shown in the Figure, useful only for obtaining pressure-temperature curves at one composition. That is, a sample of known composition is introduced into tube A and the top sealed. The system is evacuated through tube C while the mercury is in tube B. The sample may be cooled if necessary to prevent decomposition. While still evacuating, the mercury is poured into the manometer and the apparatus sealed at tube C.

Experimental Results

Figure 4 shows a thermogravimetric analysis curve which was constructed from experimental data compiled. (Tables 6-10) The plot is of temperature versus composition expressed in terms of the weight fraction $f = \frac{\text{weight compound}}{\text{weight } CoCl_2}$.

Each plateau corresponds to an equilibrium between two definite compounds. At a given temperature (at which one compound has a significant vapor pressure), pyridine will be evolved under vacuum until the weight fraction corresponding to the composition of the lower pyridinate is reached. The temperature must then be increased until the newly formed compound begins to evolve pyridine at a measurable vapor pressure in order to continue the decomposition. The curve (page 28) demonstrates that each of the pyridinates previously discussed does, indeed, occur under the depyridination conditions employed.

The pressure versus f curves which were obtained for the individual reactions are given in Figures 5-7. This type of curve is explained by application of the phase rule, F = C-P+2. Assuming that the components are pyridine and cobalt(II)chloride (C=2), the phases present are $Co(py)_nCl_2(s)$, $Co(py)_{n-m}Cl_2(s)$ and pyridine vapor (P=3), and the temperature of the system is held constant, then F = 2-3+1=0. Thus, a plateau in the P versus f curve should result (i.e. the pressure will be constant so long as two different pyridinates are present representing two solid phases).

In the case of the $Co(py)_6Cl_2 = Co(py)_4Cl_2$ reaction, a flat plateau is not obtained. This may be explained by assuming that $Co(py)_6Cl_2$ and $Co(py)_4Cl_2$ (perhaps having

Fig. 4 -- Thermogravimetric Analysis of $Co(py)_6Cl_2$

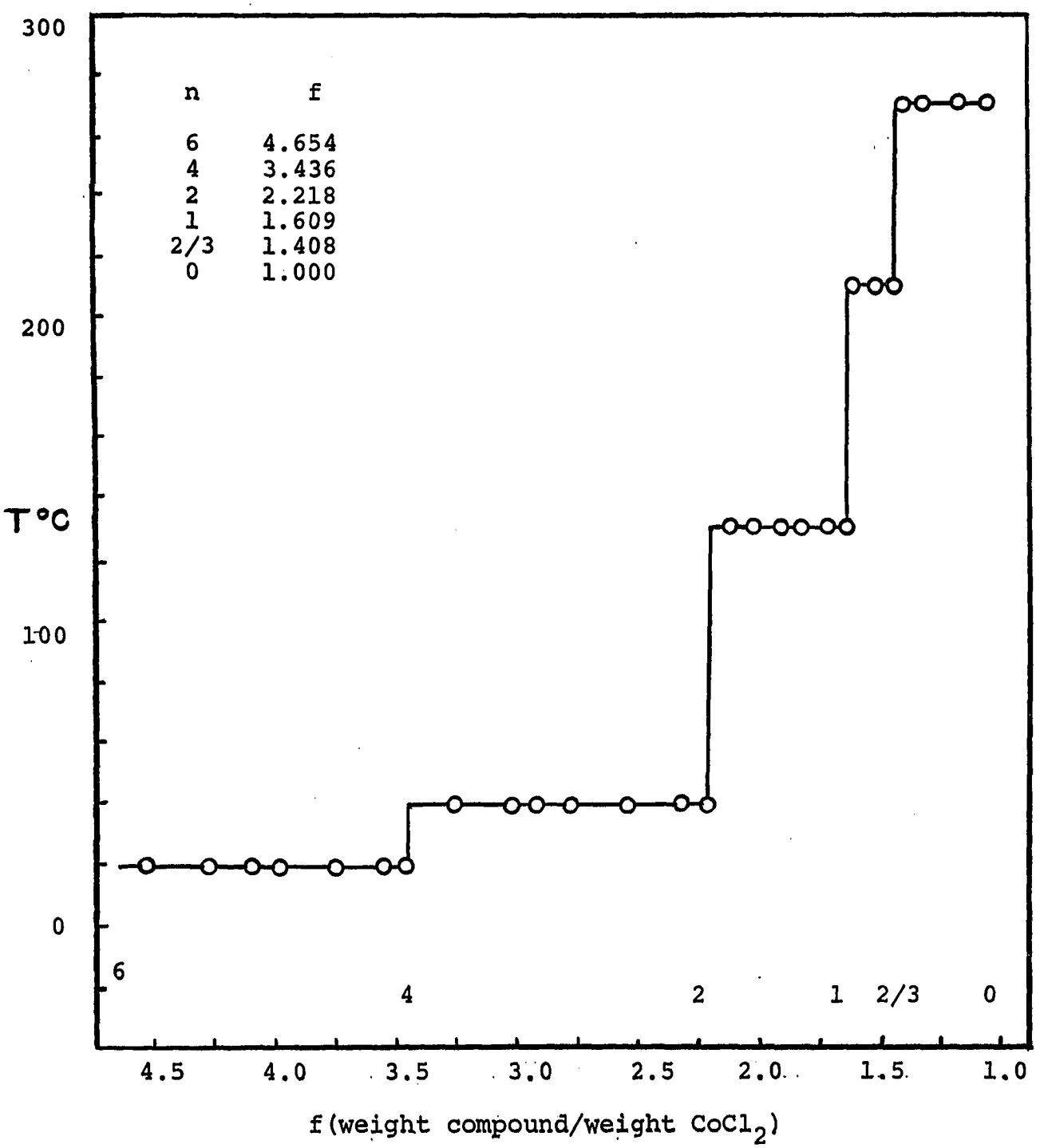

similar structures) form a solid solution (one solid phase) instead of two separate and distinct solid phases. From the phase rule, if P=2 then F=1 and the pressure would not be constant.

A similar situation may well exist for the other equilibria. In general, a weak interaction between the solid phases would not be unexpected thereby causing a slight plateau slope. Nevertheless, reasonably flat plateaus are obtained in all cases.

The equilibrium constants were, however, evaluated by taking the pressure-temperature data at a composition such that

$$\frac{[Co(py)_{n-m}Cl_2(s)]}{[Co(py)_nCl_2(s)]} = 1.$$

A difficulty is encountered in the depyridination of $Co(py)_4Cl_2$ in that, as mentioned previously, it is the $\beta Co(py)_2Cl_2$ rather than $\alpha Co(py)_2Cl_2$ which is formed by the removal of pyridine. Furthermore, the β to α transition is catalyzed by the presence of pyridine vapor (i.e. at temperatures below the transition temperature, the compound formed by reaction of the stoichiometric amount of pyridine with any lower pyridinate should be the α form). Therefore, the reaction occuring with the depyridination of $Co(py)_4Cl_2$ is as follows,

$$Co(py)_4Cl_2(s) = \begin{bmatrix} \alpha Co(py)_2Cl_2(s) \\ \| \\ \beta Co(py)_2Cl_2(s) \end{bmatrix} + 2py(v).$$

Fig. 5 -- Vapor Pressure vs. f
$Co(py)_6Cl_2(s) = Co(py)_4Cl_2(s) + 2py(v)$

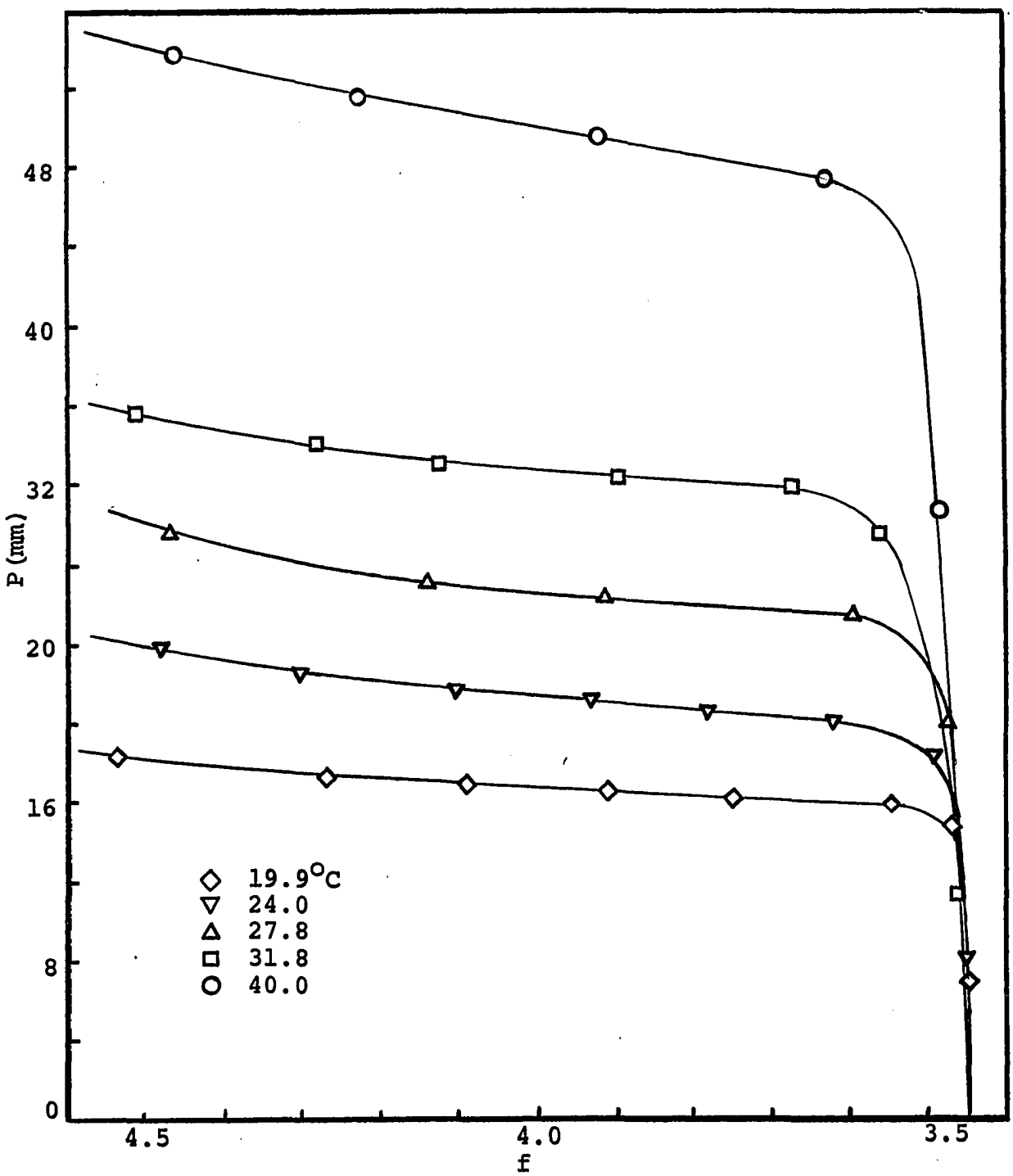

Fig. 6 -- Vapor P vs. f

$Co(py)_4Cl_2(s) = \alpha Co(py)_2Cl_2(s) + 2py(v)$

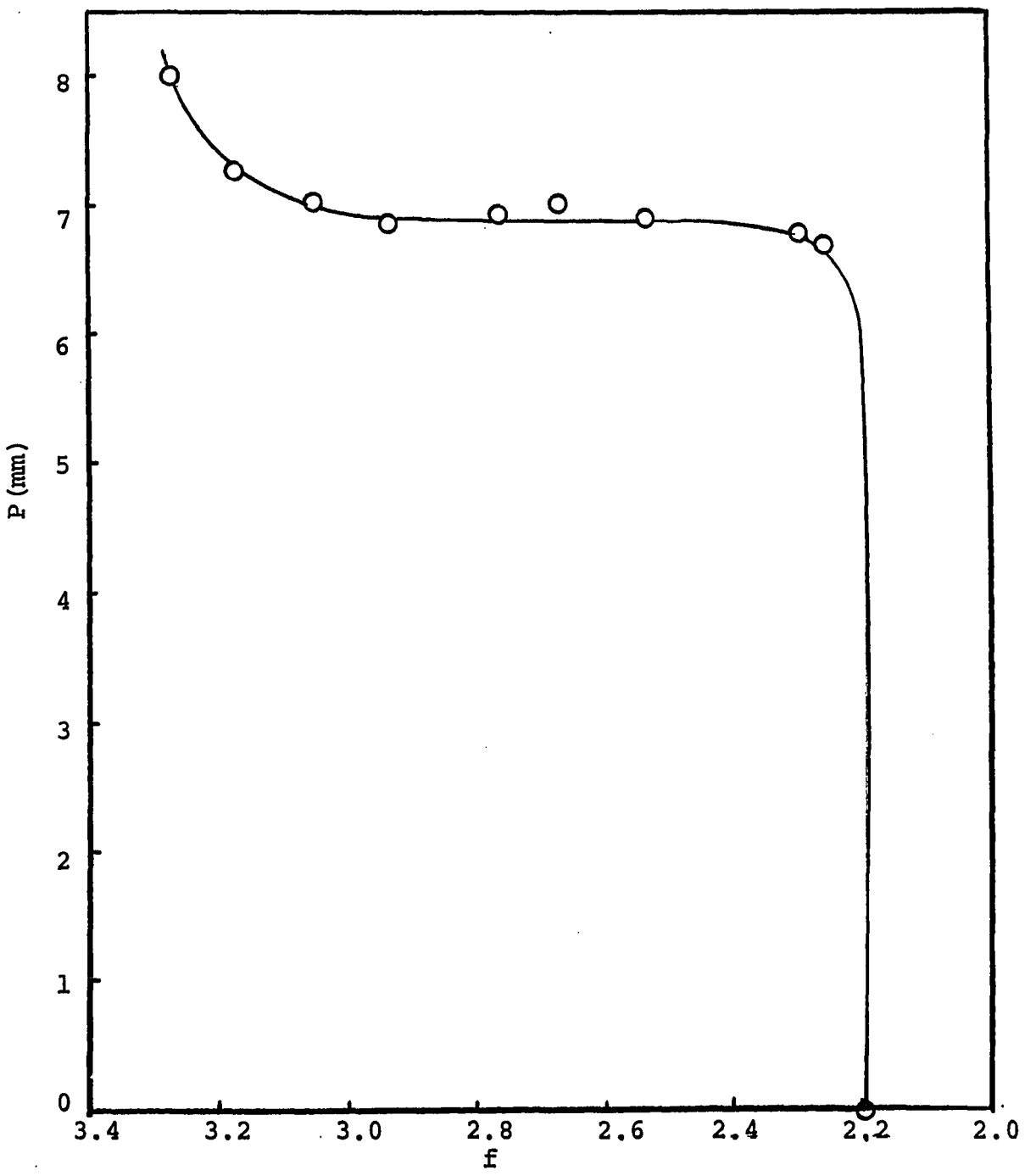

Fig. 7 -- Vapor Pressure vs. f
$\beta Co(py)_2Cl_2 = Co(py)Cl_2 + py$
$Co(py)Cl_2 = Co(py)_{2/3}Cl_2 + 1/3\ py$
$Co(py)_{2/3}Cl_2 = CoCl_2 + 2/3\ py$

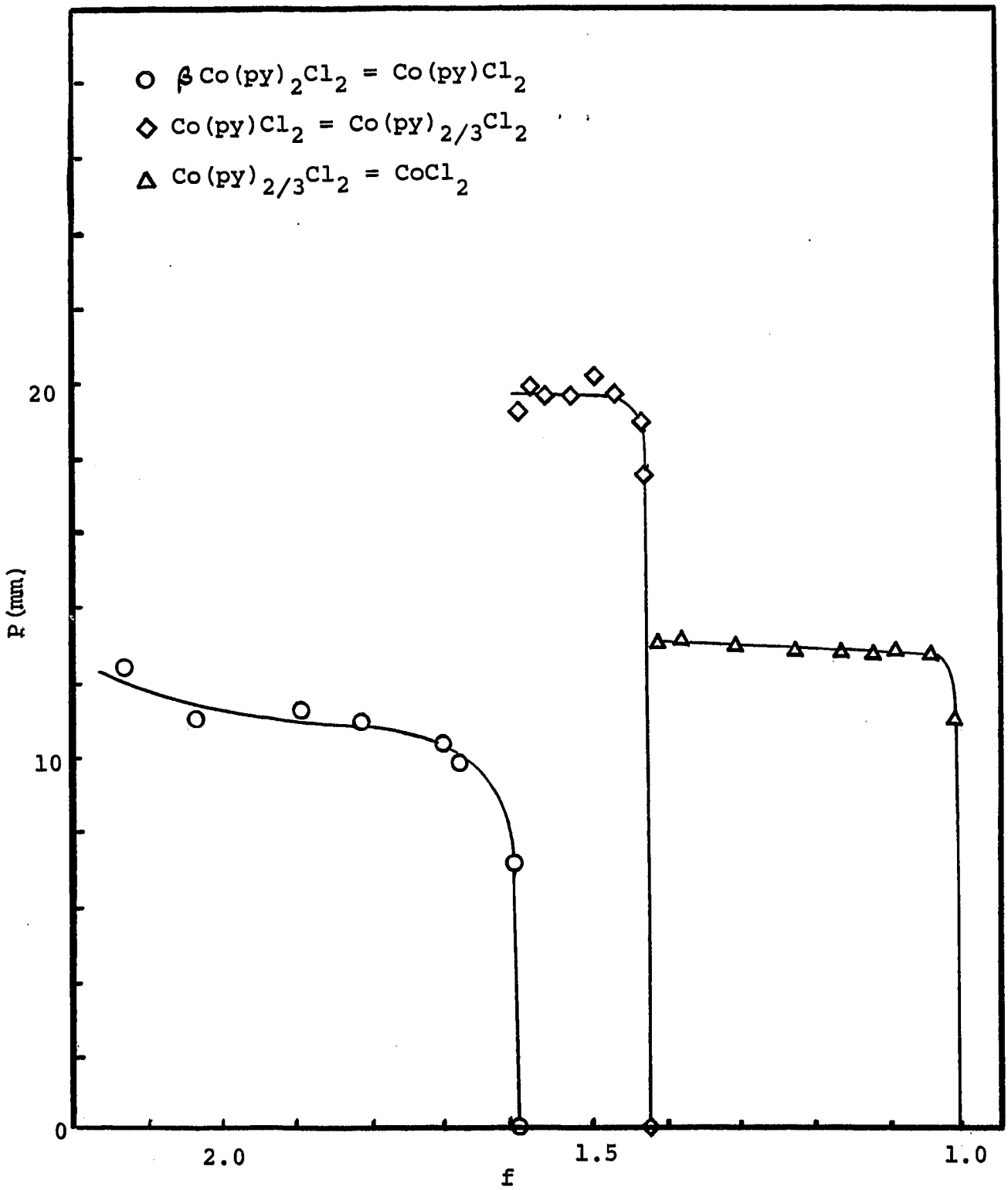

TABLE 6

VAPOR PRESSURE DATA $Co(py)_6Cl_2(s) = Co(py)_4Cl_2(s) + 2py(v)$

T^oC	f	$\bar{P}$ (mm)	T^oC	f	$\bar{P}$ (mm)	T^oC	f	$\bar{P}$ (mm)
19.9	4.542	18.60	27.8	4.463	29.95	40.0	4.455	53.90
	4.271	17.41		4.209	28.19		4.232	51.70
	4.092	17.20		4.125	27.45		3.917	49.80
	3.908	16.80		3.903	26.58		3.630	47.78
	3.752	16.50		3.743	26.10		3.483	31.27
	3.549	16.07		3.594	25.75		3.483	31.27
	3.476	14.73		3.475	20.23		3.433	10.64
	3.452	6.91		3.451	6.97			
24.0	4.486	23.98	31.8	4.514	36.12			
	4.305	22.90		4.274	34.40			
	4.105	22.01		4.118	33.45			
	3.929	21.42		3.887	32.79			
	3.780	20.77		3.670	32.25			
	3.622	20.25		3.540	29.74			
	3.488	18.64		3.474	11.63			
	3.455	8.15						

TABLE 7

VAPOR PRESSURE DATA
$Co(py)_4Cl_2(s) = \alpha Co(py)_2Cl_2(s) + 2py(v)$

T°C	f	P (mm)
41.3	3.271	8.04
	3.171	7.30
	3.054	7.07
	2.936	6.91
	2.768	6.99
	2.673	7.08
	2.535	6.95
	2.298	6.83
	2.261	6.73
	2.192	0.0

TABLE 8

VAPOR PRESSURE DATA
$\beta Co(py)_2Cl_2(s) = Co(py)Cl_2(s) + py(v)$

T°C	f	P (mm)
129	2.126	12.3
	2.035	11.0
	1.895	11.2
	1.810	10.9
	1.702	10.3
	1.677	9.8
	1.603	7.1
	1.595	0

TABLE 9

VAPOR PRESSURE DATA
$Co(py)Cl_2(s) = Co(py)_{2/3}Cl_2(s) + 1/3py(v)$

T^oC	f	P(mm)
209	1.595	19.3
	1.582	19.9
	1.562	19.6
	1.545	19.8
	1.524	19.7
	1.499	20.2
	1.466	19.7
	1.436	19.0
	1.432	17.5
	1.422	0

TABLE 10

VAPOR PRESSURE DATA
$Co(py)_{2/3}Cl_2(s) = CoCl_2(s) + 2/3py(v)$

T^oC	f	P(mm)
269	1.406	13.0
	1.382	13.1
	1.306	12.9
	1.225	12.8
	1.159	12.8
	1.120	12.7
	1.091	12.8
	1.043	12.7
	1.081	11.0

If the solid phases present are $Co(py)_4Cl_2$, $\alpha Co(py)_2Cl_2$ and $\beta Co(py)_2Cl_2$ then P = 4 and F = -1. This indicates that the pressure would be undefined at an arbitrary temperature. This system was observed to approach what was an apparent equilibrium (as indicated by constant pressure) after a period of several weeks. However, it is strongly suspected that this represented a pseudo-equilibrium and not a true equilibrium for either $Co(py)_4Cl_2 = \alpha Co(py)_2Cl_2$ or $Co(py)_4Cl_2 = \beta Co(py)_2Cl_2$ since by visual examination of the sample α and β forms were obviously present.

The pressure-composition curve obtained by adding pyridine to a sample of $\alpha Co(py)_2Cl_2$ (Figure 6) shows a flat plateau. Pressure-temperature data for $Co(py)_4Cl_2 = \alpha Co(py)_2Cl_2$ was obtained from this sample.

Calculations and Data Treatment

From the thermodynamic relationship,

$$\Delta F^o = -RT \ln K = \Delta H^o - T\Delta S^o \text{ (at constant T)}$$

the following expression is obtained by substitution for the equilibrium constant ($K = P_{py}^m$),

$$\log P_{py} = \frac{-\Delta H^o}{2.303mRT} + \frac{\Delta S^o}{2.303Rm}$$

which is of the form y = mx + b. A plot of log P(atm) versus $1/T^oA$ should yield a straight line with slope $-\Delta H^o/2.303mR$ and intercept on the log P axis of

$\Delta S^{o}/2.303mR$. (This is assuming that the heat capacity is constant over the temperature range employed.)

The pressure-temperature data (Table 11) was subjected to a least squares analysis with,

$$m = \frac{N\sum(1/T \log K_p) - \sum \log K_p \sum(1/T)}{N\sum(1/T)^2 - (\sum(1/T))^2} = \frac{-\Delta H^{o}}{2.303mR}$$

and,

$$b = \frac{\sum \log K_p \sum(1/T)^2 - \sum(1/T)\sum(1/T)\log K_p}{N\sum(1/T)^2 - (\sum(1/T))^2} = \frac{\Delta S^{o}}{2.303mR}$$

The values of the thermodynamic constants for the individual reactions obtained in this manner are shown in Table 12 and the log K_p versus 1/T curves are given in Figures 8 and 9.

Having once obtained the thermodynamic constants for each depyridination step, and using the values for the standard enthalpies of formation for cobalt chloride (solid) and pyridine (vapor) at 25°C (298°A), respectively -77.8 kcal/mole (42) and 33.5 kcal/mole*, the standard enthalpies of formation of each of the pyridinates may be calculated.

$$\Delta H^{o}_{f}\ Co(py)_nCl_2(s) = \Delta H^{o}_{f}\ Co(py)_{n-m}Cl_2(s) + m\ \Delta H^{o}_{f}\ py(v) - \Delta H^{o}_{R}$$

---

* $\Delta H^{o}_{f}\ py(l) = 23.9$ kcal/mole (43)

$\Delta H_{vap} = 9.6$ kcal/mole (44)

$\Delta H^{o}_{f}\ py(v) = 33.5$ kcal/mole

TABLE 11

PRESSURE-TEMPERATURE AND LEAST SQUARED DATA FOR LOG P vs 1/T

n	m	f	P(mm)	P x 10^3 (atm)	-Log P (atm)	T^oA	$1/T^oA \times 10^3$	-slope x 10^3	b
6	2	4.05	17.10	22.50	1.6478	292.1	3.423	2.05	5.37
			21.82	28.68	1.5424	297.0	3.367		
			27.01	35.53	1.4494	300.8	3.324		
			33.20	43.68	1.3597	304.8	3.281		
			50.33	66.18	1.1793	313.0	3.194		
4	2	2.83	2.97	3.91	2.4080	299.0	3.344	2.88	5.83
			4.10	5.40	2.2680	306.5	3.263		
			6.00	7.90	2.1026	311.9	3.206		
			7.90	10.40	1.9820	316.0	3.165		
			9.80	12.90	1.8894	319.3	3.132		
			12.27	16.15	1.7917	323.0	3.096		
			14.79	19.46	1.7111	325.7	3.070		
			19.53	25.70	1.5901	330.4	3.027		
2	1	1.91	5.24	6.89	2.1552	383.5	2.608	3.34	6.56
			7.30	9.61	2.0173	389.5	2.567		
			9.44	12.42	1.9038	394.5	2.534		
			11.92	15.69	1.8044	400.5	2.496		
			14.81	19.48	1.7104	405.5	2.466		
			18.59	24.46	1.6118	410.5	2.436		
1	$\frac{1}{3}$	1.51	5.21	6.85	2.1644	455.8	2.194	4.82	8.42
			6.46	8.50	2.0706	460.5	2.172		
			9.14	12.02	1.9200	466.5	2.144		
			12.19	16.04	1.7945	472.3	2.117		
			16.49	21.70	1.6635	478.0	2.092		
			19.57	25.75	1.5893	483.5	2.068		
$\frac{2}{3}$	$\frac{2}{3}$	1.20	5.97	7.86	2.1048	524.5	1.907	5.52	8.55
			6.46	8.50	2.0706	527.5	1.896		
			8.37	11.01	1.9575	534.0	1.873		
			11.00	14.47	1.8393	539.0	1.855		
			12.81	16.86	1.7734	542.0	1.845		
			14.80	19.47	1.7106	545.0	1.835		
			16.91	22.25	1.6526	548.0	1.825		
			19.20	25.26	1.5976	550.5	1.817		
			20.70	27.24	1.5664	552.5	1.810		

TABLE 12

THERMODYNAMIC CONSTANTS FOR THE REACTION,
$Co(py)_nCl_2(s) = Co(py)_{n-m}Cl_2(s) + mpy(v)$ at 25°C

n	6	4	α2	β2	1	2/3	
m	2	2	0	1	1/3	2/3	
ΔH°	18.9	26.5	3.4	15.4	7.4	16.9	kcal/mole
ΔS°	49.4	53.5	-11.4	30.2	12.9	26.2	eu/mole
ΔF°	4.0	10.5	0.0	6.4	3.4	9.1	kcal/mole

TABLE 13

ENTHALPIES AND ENTROPIES OF FORMATION AT 25°C

Compound	ΔH_f°(kcal/mole)	S_f°(eu/mole)	$S^\circ_{f(n-m)} - S^\circ_{f(n)}$
$CoCl_2$	-77.8	25.4	
			-23.9
$Co(py)_{2/3}Cl_2$	-72.4	49.3	
			-12.2
$Co(py)Cl_2$	-68.5	61.5	
			-45.0
$\beta Co(py)_2Cl_2$	-50.5	106.5	
			11.4
$\alpha Co(py)_2Cl_2$	-53.9	95.1	
			-96.9
$Co(py)_4Cl_2$	-13.4	192.0	
			-101.1
$Co(py)_6Cl_2$	34.7	293.0	

Fig. 9 -- Log P(atm) vs. 1/T; $Co(py)_6Cl_2$ = $Co(py)_4Cl_2$

$Co(py)_4Cl_2$ =α$Co(py)_2Cl_2$;β$Co(py)_2Cl_2$ = $Co(py)Cl_2$

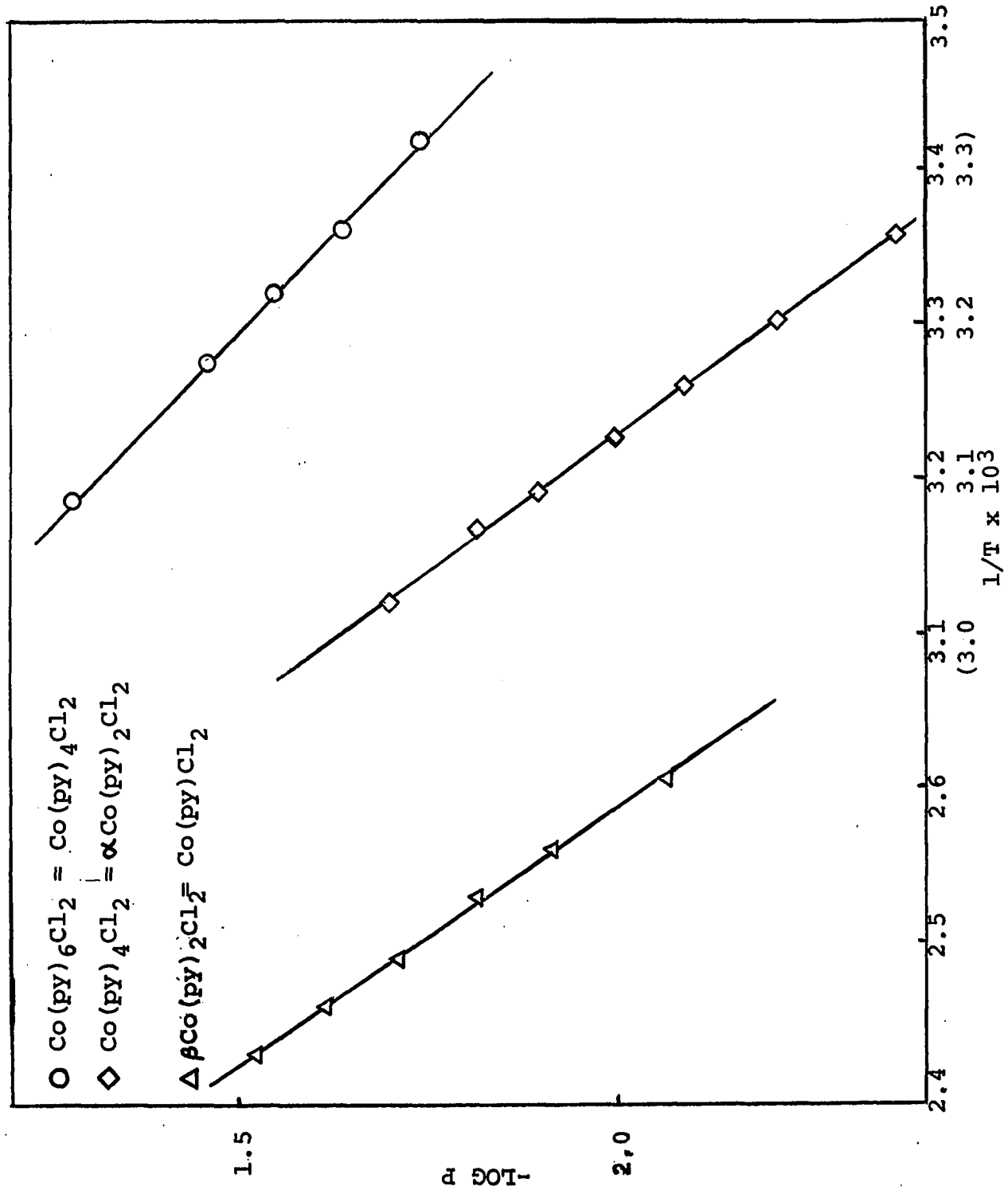

Fig. 8 -- Log P(atm) vs. 1/T
$Co(py)_{2/3}Cl_2 = CoCl_2$; $Co(py)Cl_2 = Co(py)_{2/3}Cl_2$

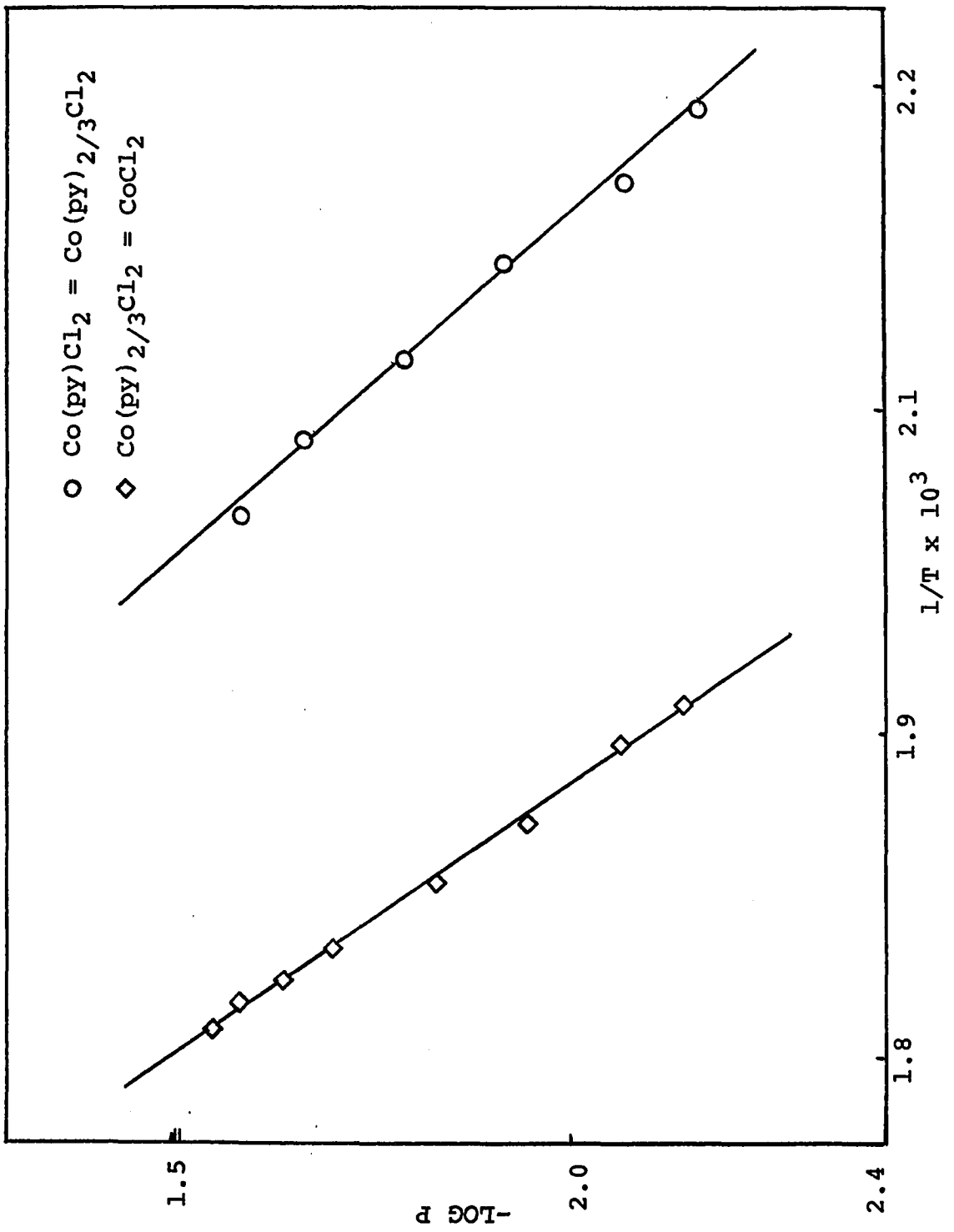

Similarly, entropies of formation may be calculated from the reaction entropies and the entropy of formation of cobalt(II)chloride and pyridine vapor at 25°C, respectively 25.4 eu/mole (42) and 75.2 eu/mole* (Table 13).

The enthalpy of the $\alpha \rightarrow \beta$ transition was obtained calorimetrically from heat of solution data. Since the α and β isomers form the same species in chloroform solution as shown previously, it is possible to make use of the following cycle which includes the heats of solution of $\alpha Co(py)_2Cl_2$ and $\beta Co(py)_2Cl_2$ ($\Delta H_{s\alpha}$, $\Delta H_{s\beta}$) to calculate the transition enthalpy (ΔH_T),

$$\alpha Co(py)_2Cl_2(s) \xrightarrow{\Delta H_T} \beta Co(py)_2Cl_2(s) \xrightarrow{\Delta H_{s\beta}} Co(py)_2Cl_2(soln.)$$

$$\alpha Co(py)_2Cl_2(s) \xrightarrow{\Delta H_{s\alpha}} Co(py)_2Cl_2(soln.)$$

The heats of solution were determined in a simple calorimeter which consisted of a 500 ml. vacuum flask fitted with a motor driven, glass stirrer and Beckman thermometer. The samples were added through a glass funnel. The top of the flask was fitted with a cork to prevent evaporation and further insulate the system. Chloroform (initially at 25°C) was used as solvent.

The general procedure was that a sample was added (by weight difference from a weighing bottle) and the

---

*$S^o_f py(l)$ = 42.8 eu/mole (45)

ΔS_{vap} = 32.4 eu/mole (44)

$\therefore S^o_f py(v)$ = 75.2 eu/mole

temperature lowering was noted (as shown in Figure 10). Then to the same chloroform solution, another sample was added, etc. The ratio of moles $CHCl_3$/mole complex was purposely kept large so that ΔH_S would approach the total enthalpy of solution and, therefore, the difference in heats of solution would yield the enthalpy of transition. Table 14 shows the results of three sample additions to a known weight of chloroform.

From the data, the heat of solution was calculated,

$$\Delta H_S = \frac{-(C_c + C_p m)\ \Delta T}{n}$$

where C_c is the heat capacity of the calorimeter (determined to be 30.1 cal/^oC with KCl), C_p is the heat capacity of chloroform (0.24 cal/gram ^oC(40)), m is the solution weight, and n is the number of moles of solute.

The heat of transition was determined therefore,

$$\Delta H_T = \Delta H_{S\alpha} - \Delta H_{S\beta}$$

$$\Delta H_T = 3.4 \text{kcal/mole}$$

TABLE 14

HEAT OF SOLUTION DATA

Compound	$\frac{(\text{Moles } CHCl_3)}{(\text{Moles complex})_{ave.}}$	$\Delta T_{ave.}$	ΔH_S (kcal/mole)
$\alpha Co(py)_2Cl_2$	438.0	-0.33	7.1
$\beta Co(py)_2Cl_2$	353.9	-0.21	3.7

Fig. 10 -- TEMPERATURE DEPRESSION FOR α $Co(py)_2Cl_2$ in CHLOROFORM

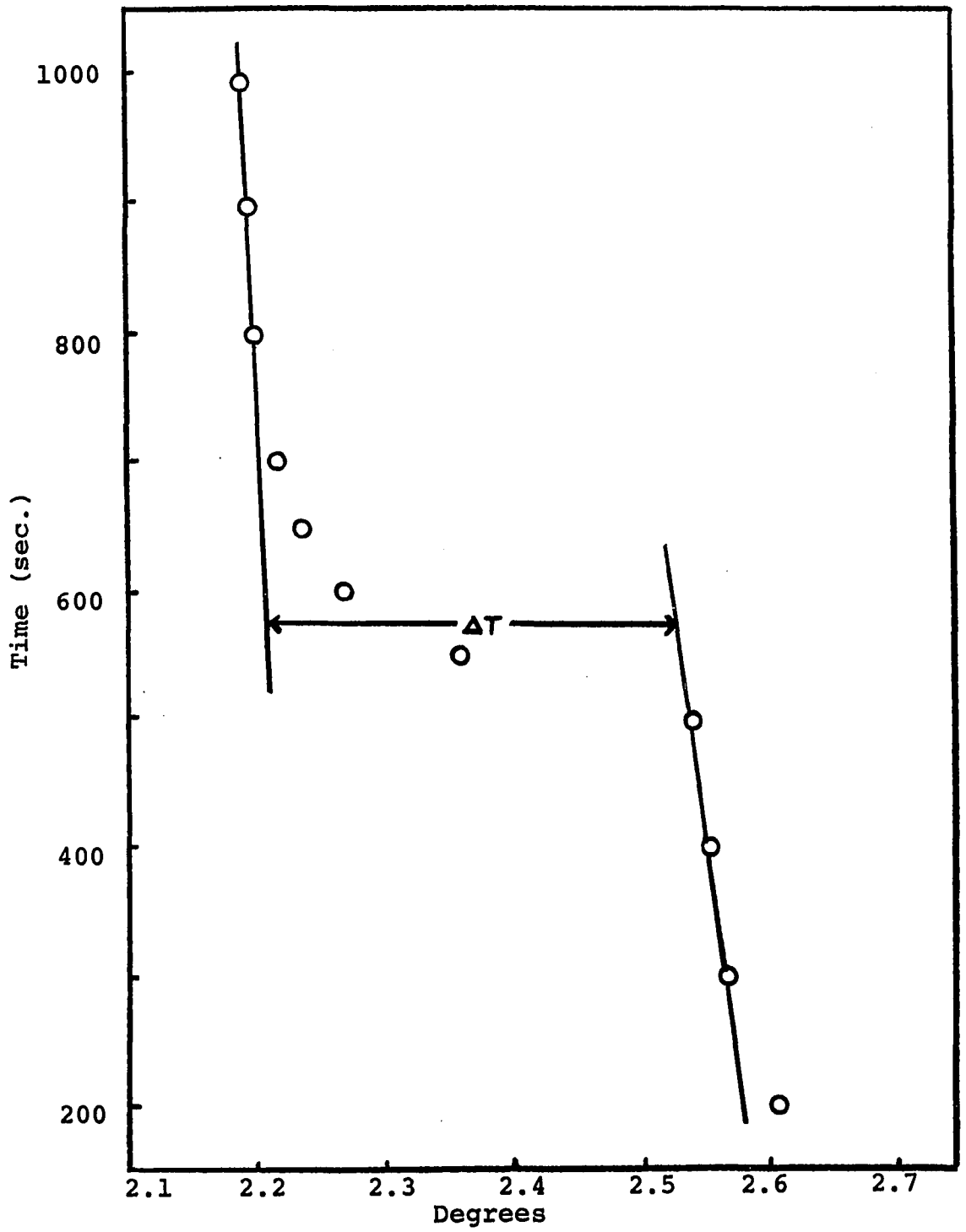

Complete enthalpies and entropies of formation are presented in Table 13.

The formation constants compare favorably with enthalpies which may be calculated from heat of reaction data for compound formation from solid cobalt(II) chloride and liquid pyridine by the reaction,

$$CoCl_2(s) + npy(l) \xrightarrow{\Delta H_R} Co(py)_nCl_2(s)$$

$$\Delta H_f^\circ\ Co(py)_nCl_2 = \Delta H_f^\circ\ CoCl_2(s) + n\,\Delta H_f^\circ py(l) + \Delta H_R$$

TABLE 15

ENTHALPIES OF FORMATION FROM LITERATURE DATA (46)

n	ΔH_R (kcal/mole)	$\Delta H_f^\circ\ Co(py)_nCl_2$ (kcal/mole)	T°C
1	-15.4	-69.3	20
α2	-25.5	-55.5	
4	-35.3	-17.5	

The heats of formation for $Co(py)Cl_2$ and $\alpha Co(py)_2Cl_2$ agree reasonably well (in the case of $Co(py)Cl_2$ within 0.8 kcal/mole and for $\alpha Co(py)_2Cl_2$ within 1.6 kcal/mole). The values for $Co(py)_4Cl_2$ are similar but do differ to the extent of 4.1 kcal/mole. The logical explanation is that the heats of formation obtained in this study are subject to cumulative errors which would not occur in a direct calorimetric determination. In further explanation, the ΔH_f° values here determined are calculated

from experimental heats of reaction which are, of course, subject to error. Each successive calculation, therefore, contains the total of the previous error to the extent that a total error on the order of 4 kcal/mole has accumulated in the calculated value of the fourth enthalpy of formation. This indicates an average error of 1 kcal/mole in the heats of reaction which corresponds to a change in slope of approximately 0.3×10^3 or about 5% in the case of the $Co(py)_{2/3}Cl_2 = CoCl_2$ reaction.

CHAPTER IV

SPECTRA

Preliminary Discussion

The absorption spectra of the cobalt(II) chloride pyridinates are characterized by a series of bands appearing in the visible and near IR regions. These absorptions are attributed to electronic transitions within the 3d level as a result of a nonsymmetric perturbation produced by a particular ligand electric field, the exact nature of which is determined by the geometry of ligand arrangement. In this respect, a correct analysis of the nature of the perturbation leads to an effective elucidation of the spectrum and, hence, the environment of the cobalt ion (i.e. the site symmetry of the complex).

The crystal structure of cobalt(II) chloride (27), as well as the spectra in the visible and near IR regions (47) is well characterized (assuming that the major perturbation is due to an interaction of electron spin and orbital angular momentum moments). Transitions to excited states of maximum multiplicity as well as to low spin states are

defined. However, considering as an approximation that the site symmetry is exactly O_h, the spectrum can also be fit reasonable well using elementary crystal field approximations.

Assuming a ground state configuration (d^7), $t_{2g}^5 e_g^2$ ($^4T_{1g}$), with excited states, $t_{2g}^4 e_g^3$ ($^4T_{2g}$, $^4T_{1g}$) and $t_{2g}^3 e_g^4$ ($^4A_{2g}$), then the transition energies in terms of the octahedral splitting parameter Dq, calculated on the energy basis t_{2g}(-4Dq) and e_g(+6Dq), are given:

1. $^4T_{1g}(F) \longrightarrow {}^4T_{2g}$: 8Dq
2. $\longrightarrow {}^4A_{2g}$: 18Dq
3. $\longrightarrow {}^4T_{1g}(P)$: 6Dq + ΔE

$$\Delta E = E(^4P) - E(^4F)$$

Using Dq as a parameter, the cobalt chloride spectrum (Figure 14) was fit, and the results are shown in Table 27 (Part III (47) and Part V using Dq and ΔE as parameters).

In regard to the pyridinates, either a direct comparison with the cobalt(II) chloride spectrum or to energy calculations made on the basis of the known structures of $Co(py)_4Cl_2$, $\alpha Co(py)_2Cl_2$ and $\beta Co(py)_2Cl_2$ (as discussed in the following) provides the foundation for spectral analysis.

Theory

The energy of a given electronic state may be

calculated in theory by the evaluation of an integral of the type,

$$E_n = \int_{\text{ALL SPACE}} \psi_n^* H \psi_n \, d\tau$$

ψ_n is the normalized wave function of the state and H is the energy operator, the form of which is given,

$$H = H_F = V_{r_i} + V$$

where H_F = the free ion Hamiltonian(48)

$V_{r_i} = \sum \frac{1}{\sqrt{4\pi}} R_o(r_i)$ (A spherically symmetrical ($\ell = 0$) perturbation potential, the effect of which is to uniformly increase all energy levels).

$V = \frac{f(1)}{(r_j)}$ (A perturbation potential whose form is dependent on the geometrical arrangement of ligands about the central metal ion).

The ligand symmetries presently of interest are O_h (octahedral) and D_{4h} (tetragonally distorted octahedral). It may be shown (49a) that the octahedral ligand potential (V_o) has the form,

$$V_o = Y_{4,0} + \sqrt{\frac{15}{4}} (Y_{4,4} + Y_{4,-4})$$

since any potential may be expanded in terms of the spherical harmonics ($Y_{l,m}$) centered at the origin (50). In general, the ligand field will not be of true O_h symmetry but rather the actual potential may be assumed to arise from the superposition of a tetragonal perturbation potential (V_T) component upon the purely octahedral potential. Under D_{4h},

the spherical harmonics of order less than five which are invariant with respect to the symmetry (i.e. those which transform as a_{1g}) are $Y_{2,0}$, $Y_{4,0}$, and $Y_{4,\pm4}$. Therefore, the total ligand field potential is given by,

$$V = V_o + V_T = aY_{2,0} + bY_{4,0} + c(Y_{4,4} + Y_{4,-4}).$$

Substituting for V_o,

$$V_T = aY_{2,0} + bY_{4,0} + c(Y_{4,4} + Y_{4,-4}) - Y_{4,0} - \sqrt{\frac{15}{4}}(Y_{4,4}+Y_{4,-4}).$$

The spherical harmonics with $m = \pm4$ may be eliminated from the potential (49b) if it is assumed that the tetragonal potential results from ligand substitution along the + and -z axis in which case, as a first approximation, the form of the potential in the xy plane would be essentially identical under both O_h and D_{4h}, the only difference being the actual magnitude of the perturbation (i.e. the orbitals in the xy plane are only changed in energy, not distorted). One may also consider on this basis that the $Y_{4,\pm4}$ harmonics do not contain z vector components; therefore,

$$V_T = AY_{2,0} + BY_{4,0}$$

where,

$$Y_{2,0} = \sqrt{\frac{5}{4\pi}}\sqrt{\frac{1}{4}}\quad\frac{3z^2 - r^2}{r^2}$$

$$Y_{4,0} = \sqrt{\frac{9}{4\pi}}\sqrt{\frac{1}{64}}\quad\frac{3z^4 - 30z^2r^2 + 3r^4}{r^4}$$

with $r^2 = x^2 + y^2 + z^2$. Now since $\hat{\ell}_z\,[-i\hbar(x\,\partial/\partial y - y\,\partial/\partial x)]$ transforms exactly as z under D_{4h}, z may be replaced with $\hat{\ell}_z$ according to the operator equivalent method (51). Then,

also noting that $\hat{l}^2 = \hat{l}_x^2 + \hat{l}_y^2 + \hat{l}_z^2$ and that $\hat{l}^2(l,m_l) = l(l+1)\hbar(l,m_l)$,

$$V_T = A'\left[3\hat{l}_z^2 - l(l+1)\right] + B'\left[35\hat{l}_z^4 - 30(l)(l+1)\hat{l}_z^2 + 25\hat{l}_z^2 - 6l(l+1) + 3l^2(l+1)^2\right]$$

and since for d electrons, $l = 2$,

$$V_T = A''\left[(\hat{l}_z^2 - 2)\right] + B''\left[(35/12\,\hat{l}_z^4 - 155/12\,\hat{l}_z^2 + 6)\right]$$

The final form of the tetragonal potential may be obtained by replacing the constants A" and B" respectively with splitting parameters D_s and D_t.

Table 16 (49c) indicates the operation of the $\hat{l}_z^2$ and $\hat{l}_z^4$ terms on the 3d harmonics.

TABLE 16

ANGULAR MOMENTUM OPERATIONS
ON THE 3d WAVE FUNCTIONS (d±m)

Operator	Operation
$(\hat{l}_z^2 - 2)$	$d_o \longrightarrow -2d_o$
	$d_{\pm1} \longrightarrow -d_{\pm1}$
	$d_{\pm2} \longrightarrow 2d_{\pm2}$
$(\frac{35}{12}\hat{l}_z^4 - \frac{155}{12}\hat{l}_z^2 + 6)$	$d_o \longrightarrow 6d_o$
	$d_{\pm1} \longrightarrow -4d_{\pm1}$
	$d_{\pm2} \longrightarrow d_{\pm2}$

The d orbitals which correspond (either directly or in some linear combination) to the m values are as follows: m = 0, d_{z2}; m = ±1, d_{xz} and d_{yz}; m = ±2, d_{xy} and $d_{x2} - y^2$.

The signs chosen for the splitting parameters D_s and D_t determine which set of d orbitals will be stabalized. This is, of course, directly related to the geometry (particularly the respective ligand-central ion separations in the xy plane and along the z axis). The axial compression or elongation determines which orbital lies lowest and, hence, the symmetry of the ground electronic state. Table 17 shows the evaluation of the integrals (orbital energies) $(\psi_{3d} || \psi_{3d})$ in relation to the signs of D_s and D_t.

For example, examining the situation with D_s(+) and D_t(-), it is seen that the d_z^2 orbital lies lowest in energy since $(d_o || d_o)$ is $-(2D_s + 6D_t)$. This means

TABLE 17

INTEGRAL EVALUATION FOR 3d ORBITALS

D_s	D_t	z axis effect	$(d_{\pm2} \| d_{\pm2})$	$(d_{\pm1} \| d_{\pm1})$	$(d_o \| d_o)$
+	+	Elongation	$2D_s + D_t$	$-(D_s + 4D_t)$	$-(2D_s - 6D_t)$
-	+	Compression	$-(2D_s - D_t)$	$D_s - 4D_t$	$2D_s + 6D_t$
-	-	Compression	$-(2D_s + D_t)$	$D_s + 4D_t$	$2D_s - 6D_t$
+	-	Elongation	$2D_s - D_t$	$-(D_s - 4D_t)$	$-(2D_s + 6D_t)$

that relative to the other orbitals, electrons will preferentially fill the d_{z2}. In turn, this indicates that the ligand field potential along the z axis is reduced since approximately 70% of the probability space lies along the z axis. In respect to the present evaluation, therefore, an elongation of the z axis ligand-central ion distance with respect to the x and y axial distances is indicated.

There also exists a very useful energy correlation between the d^7 configuration of Co(II) and d^3 configuration energies. This relationship is shown in Table 18 for O_h (taking electrons in t_{2g} and e_g as having energies respectively, of $-4D_q$ and $+6D_q$),

TABLE 18

d^3 - d^7 ENERGY CORRELATION

Ionic State under O_h	Configuration d^3	Configuration d^7	Energy d^3	Energy d^7
$^4A_{2g}$	t_2^3g	$t_{2g}^3e_g^4$	-12Dq	+12Dq
$^4T_{2g}$; $^4T_{1g}$	$t_{2g}^2e_g$	$t_{2g}^4e_g^3$	-2Dq	+2Dq
$^4T_{1g}$	$t_{2g}e_g^2$	$t_{2g}^5e_g^2$	+6Dq	-6Dq

The relationship between state energies of d^3 and d^7 configurations is simply a sign change; thus the energies calculated in terms of D_s and D_t for d^3 may be directly related to d^7. Or more simply, the sign interconversion

may be accomplished by choice of sign for D_s and D_t.

The inverse sign relationship between d^n and d^{10-n} configurations (52) is frequently employed since the number of electrons involved in the d^n configuration is less than in the d^{10-n} case and as such wave functions are more easily handled. This correlation is qualitatively explained by assuming that the "absence of an electron" (i.e. a hole in the configuration) responds electrostatically as the opposite of an electron. Therefore, the energies of the d^n and d^{10-n} states are related by difference in sign. Energies calculated in terms of D_s and D_t for d^3 electronic states are directly related to d^7 energies by direct change in sign of D_s and D_t. Thus, for example, if energies are calculated with d^3 wave functions using $D_s(+)$ and $D_t(-)$, this is directly analogous to d^7 energies with $D_s(-)$ and $D_t(+)$.

Derivation of Wave Functions and Energy Calculations

The correlation between the electronic state symmetries under O_h and D_{4h} is given in Table 19.

TABLE 19

STATE CORRELATIONS, O_h - D_{4h}

O_h	D_{4h}
$^4A_{2g}$	$^4B_{1g}$
$^4T_{2g}$	$^4B_{2g} + {}^4E_g$
$^4T_{1g}$	$^4A_{2g} + {}^4E_g$

The wave functions which correspond to these ionic states under D_{4h} may now be determined. Specifically, wave functions will be derived for the d^3 configuration as discussed previously.

Since the $^4A_{2g}$ state arises from t_{2g}^3 (a half filled shell yields a_{2g} symmetry), only one wave function is possible (only one is implied by the A symmetry) according to the Pauli Exclusion Principle,

$$\chi = |(\overset{+}{x}z)(\overset{+}{y}z)(\overset{+}{x}y)| \quad *$$

This wave function transforms as b_{1g} ($a_{2g} \times b_{2g}$) under D_{4h} as would be expected since $^4A_{2g}(O_h)$ correlates with $^4B_{1g}(D_{4h})$. (Since d_{xz} and d_{yz} are degenerate under D_{4h}, this level is half filled and is of a_{2g} symmetry; d_{xy} under D_{4h} transforms as b_{2g}).

From the $t_{2g}^2 e_g$ configuration, $^4T_{2g}$ and $^4T_{1g}$ states arise. It is seen that since

$$\psi_1 = |(xz)(yz)(x^2 - y^2)|$$

transforms as $b_{2g}(a_{2g} \times b_{1g})$ under D_{4h}, ψ_1 must be a component of $^4T_{2g}(O_h)$ and likewise,

$$\psi_1 = |(xz)(yz)(z^2)|$$

transforms as $a_{2g}(a_{2g} \times a_{1g})$ and must, therefore, be a component of $^4T_{1g}(O_h)$. Four more configurations are required, two each for the ^4E_g states arising from $^4T_{1g}$ and $^4T_{2g}(O_h)$.

---

*Paraenthesis indicates the d orbital, sign indicates electron spin (+ for α spin, - for β spin). All spins in the following wave functions will be α.

These may be derived from ψ_1 and φ_1 by application of the C_3 operator and the orthogonality and normalization relations, $a^2 + b^2 = 1$ and $aa' + bb' = 0$. It is qualitatively quite easily seen that some linear combination of wave functions must result since there are several d orbital occupancies which fit the description $t_{2g}^2 e_g$ and are apparently equivalent. The functions derived are,

$$\psi_2 = -\sqrt{1/4}\ |(yz)(xy)(x^2-y^2)| + \sqrt{3/4}\ |(yz)(xy)(z^2)|$$
$$\psi_3 = -\sqrt{1/4}\ |(xy)(xz)(x^2-y^2)| - \sqrt{3/4}\ |(xy)(xz)(z^2)|$$
$$\varphi_2 = -\sqrt{1/4}\ |(yz)(xy)(z^2)| - \sqrt{3/4}\ |(yz)(xy)(x^2-y^2)|$$
$$\varphi_3 = -\sqrt{1/4}\ |(xy)(xz)(z^2)| + \sqrt{3/4}\ |(xy)(xz)(x^2-y^2)|$$

Finally for the states arising from $t_{2g} e_g^2$, the three wave functions are,

$$\Lambda_1 = |(xy)(z^2)(x^2 - y^2)|$$
$$\Lambda_2 = 1/\sqrt{2}\left[|(xz)(z^2)(x^2-y^2)| - |(yz)(z^2)(x^2-y^2)|\right]$$
$$\Lambda_3 = 1/\sqrt{2}\left[|(yz)(z^2)(x^2-y^2)| - |(xz)(z^2)(x^2-y^2)|\right]$$

Once having determined the wave functions of appropriate symmetry, the state energies under D_{4h} may be calculated in terms of D_s and D_t. The functions are summarized in Table 20.

The accompanying Table 21 shows the final energy calculation for situations of z axis compression and elongation. There are four sets of energies corresponding to the four possible orbital energy sets given in Table 17. The signs chosen for D_s and D_t are designated (top d_3, bottom d_7). In actually fitting the spectra (next section, Table 27) only two of these are used (i.e. one set for z axis elongation

and one for z axis compression chosen strictly for best fit with reasonable parameter size.

TABLE 20

STATE ENERGY INTEGRALS

State in D_{4h}	From	State in O_h	Energy $(\psi_n \lvert V_T \rvert \psi_n)$
$^4B_{1g}$		$^4A_{2g}$	$(\chi \lVert \chi)$
$^4B_{2g}$		$^4T_{2g}$	$(\psi_1 \lVert \psi_1)$
^4E_g		$^4T_{2g}$	$(\psi_2 \lVert \psi_2) = (\psi_3 \lVert \psi_3)$
$^4A_{2g}$		$^4T_{1g}$ (F)	$(\varphi_1 \lVert \varphi_1)$
^4E_g		$^4T_{1g}$ (F)	$(\varphi_2 \lVert \varphi_2) = (\varphi_3 \lVert \varphi_3)$
$^4A_{2g}$		$^4T_{1g}$ (P)	$(\Lambda_1 \lVert \Lambda_1)$
^4E_g		$^4T_{1g}$ (P)	$(\Lambda_2 \lVert \Lambda_2) = (\Lambda_3 \lVert \Lambda_3)$

In the case of axial elongation, the predicted ground state is $^4A_{2g}$ whereas under axial compression, ^4E_g is the ground state. That is, for d^7, since the ground state is $^4T_{1g}$ under O_h and this is split into $^4A_{2g}$ and ^4E_g states under D_{4h}, one of these two would be expected to be the D_{4h} ground state. For example, in the case of D_s, D_t sets I and II corresponding to z axis elongation, the $^4A_{2g}$ energies, $-(4D_s + 2D_t)$ and $(-4D_s + 2D_t)$

TABLE 21

STATE ENERGIES IN TERMS OF D_s and D_t

D_{4h}	O_h	Elongation I $\pm D_s$ $\pm D_t$	Elongation II $\pm D_s$ $\pm D_t$	Compression III $\mp D_s$ $\mp D_t$	Compression IV $\mp D_s$ $\pm D_t$
$^4A_{2g}$	$^4T_{1g}$ (F)	$-4D_s - 2D_t - 6D_q$	$-4D_s + 2D_t - 6D_q$	$4D_s + 2D_t - 6D_q$	$4D_s - 2D_t - 6D_q$
^4E_g	$^4T_{1g}$ (F)	$2D_s - 3/4D_t - 6D_q$	$2D_s + 3/4D_t - 6D_q$	$-2D_s + 3/4D_t - 6D_q$	$-2D_s - 3/4D_t - 6D_q$
$^4B_{2g}$	$^4T_{2g}$	$-7D_t + 2d_q$	$7D_t + 2D_q$	$7D_t + 2D_q$	$-7D_t + 2D_q$
^4E_g	$^4T_{2g}$	$7/4D_t + 2D_q$	$-7/4D_t + 2D_q$	$-7/4D_t + 2D_q$	$7/4D_t + 2D_q$
$^4B_{1g}$	$^4A_{2g}$	$-7D_t + 12D_q$	$7D_t + 12D_q$	$7D_t + 12D_q$	$-7D_t + 12D_q$
^4E_g	$^4T_{1g}$ (P)	$-D_s + 3D_t + \Delta E$	$-D_s - 3D_t + \Delta E$	$-2D_s - 8D_t + \Delta E$	$D_s + 3D_t + \Delta E$
$^4A_{2g}$	$^4T_{1g}$ (P)	$2D_s + 8D_t + \Delta E$	$2D_s - 80_t + \Delta E$	$D_s - 3D_t + \Delta E$	$-2D_s + 80_t + \Delta E$

when compared respectively with ^4E_g energies, $(2D_s-3/4D_t)$ and $(2D_s + 3/4D_t)$, are seen to be somewhat lower. Also, in Table 21, the octahedral d^7 state energies have been added to give the total energy. This must be done since, as discussed previously, the tetragonal potential was imposed as a perturbation upon the existing octahedral potential; therefore the energies derived in terms of D_s and D_t are only perturbation energies to be imposed over the octahedral energies in terms of D_q.

The ground state d orbital occupancy may be deduced on the basis of the ground state symmetries. The levels are listed in order of increasing energy.

z axis elongation ($^4A_{2g}$) : $e_g^4\ a_{1g}^1\ b_{2g}^1\ b_{1g}^1$

z axis compression (^4E_g) : $b_{2g}^2\ e_g^3\ b_{2g}^1\ a_{1g}^1$

Some of the states arising under O_h and D_{4h} are of the same symmetry and, as such, would be expected to interact. This may be considered as a second order perturbation and evaluated using a secular equation of the type (50),

$$\begin{vmatrix} H_{11} - E & H_{12} \\ H_{21} & H_{22} - E \end{vmatrix} = 0.$$

For example, considering the ^4E_g states from $^4T_{2g}$ and $^4T_{1g}$ in O_h, the interaction energies would be given as solutions of the equation,

$$\begin{vmatrix} (\psi_2 \| \psi_2) - E & (\psi_2 \| \varphi_2) \\ (\varphi_2 \| \psi_2) & (\varphi_2 \| \varphi_2) - E \end{vmatrix} = 0$$

in which $(\psi_2 \| \varphi_2) = (\varphi_2 \| \psi_2) = \sqrt{3/4}\ (x^2 - y^2 \| x^2 - y^2) - \sqrt{3/4}\ (z^2 \| z^2)$ and has the following values with $a = \sqrt{3}$ and $b = 5\sqrt{3/4}$:

D_s	D_t	$(\psi_2 \| \varphi_2)$
+	+	$aD_s - bD_t$
-	+	$-aD_s - bD_t$
-	-	$-aD_s + bD_t$
+	-	$aD_s + bD_t$

In general, the resulting quadratic equation cannot be solved exactly by the quadratic formula; however, it is usually possible to form a perfect square under the radical such that the remainder is close to unity with the numerical values of the parameters employed.

Considering as an approximation that the interaction between $^4E_g(T_{1g}F)$ and $^4E_g(T_{2g})$ is the most significant (i.e. that the effect of ^4E_g arising from the higher $^4T_{1g}(P)$ state may be neglected) then the perturbed energy levels may be calculated. The final state energies are given in Table 22.

The above analysis should apply directly to $Co(py)_4Cl_2$ since the site symmetry is exactly $D_{4h}(14)$. In the case

TABLE 22

FINAL ENERGIES

D_{4h}	O_h	Elongation I	Elongation II	Compression III	Compression IV
^4E_g	$T_{1g}(F)$	$D_s + 9/4D_t - 6D_q$	$D_s - 9/4D_t - 6D_q$	$-5D_s + 11/4D_t - 6D_q$	$-5D_s + 9/4D_t - 6D_q$
^4E_g	T_{2g}	$3D_s - 1/4D_t + 2D_q$	$3D_s + 1/4D_t + 2D_q$	$D_s - 19/4D_t + 2D_q$	$D_s + 19/4D_t + 2D_q$

of $\alpha Co(py)_2Cl_2$, there is a further lowering of symmetry to D_{2h} (15); however it has been demonstrated that such symmetries, in so far as spectral analysis is concerned, may be successfully apprxoimated as D_{4h} (53). Furthermore, it can be seen from the structures that $Co(py)_4Cl_2$ (with the chlorides along the z axis) represents a case of axial elongation (Co-Cl, 2.32Å Co-N, 1.99 Å) whereas in $\alpha Co(py)_2Cl_2$ (with the pyridines along the z axis) there is a compression (Co-Cl, 2.42 Å; Co - N, 2.14 Å).

Further Symmetry Consideration of α and β $Co(py)_2Cl_2$

Considering that $\alpha Co(py)_2Cl_2$ is subjected to a slight rhombic distortion, an analysis (52)(54) may be made which will further elucidate the spectrum under conditions of symmetry reduction to D_{2h} and which can be shown to correlate quite well with the previous derivation.

The essential development under D_{2h} is that the degeneracy of the d_{xz} and d_{yz} orbitals is removed. The complete correlation is given in Table 23. (55)

TABLE 23

D_{4h} - D_{2h} Correlation

D_{4h}	D_{2h}
$A_{2g} + E_g$	$B_{1g} + B_{2g} + B_{3g}$
B_{1g}	A_g
$B_{2g} + E_g$	$B_{1g} + B_{2g} + B_{3g}$

It is observed that crystals of α $Co(py)_2Cl_2$ when viewed through a microscope equipped with a light polarizer are strongly dichroic (i.e. absorptions are polarized with respect to certain crystal axes). Considering such transition moment integrals as, $\langle \psi_e^* \phi_v^* | \vec{r} | \psi_e \phi_v \rangle$ ψ_e^*, ψ_e and ϕ_v^*, ϕ_v represent respectively electronic and vibrational excited and ground state wave functions. Symmetries can be used to determine whether or not a given transition is vibronically allowed with respect to a particular polarization vector. In order for a transition to be allowed, the integrand must transform as a_{1g}. Since $\vec{r} = (i\vec{x} + j\vec{y} + k\vec{z})$ is an odd (u) function, the direct product of the symmetry of the wave functions $\psi_e^* \psi_e \phi_v^* \phi_v$ must be odd and, furthermore, contain at least one of the representations spanned by x, y, or z vectors under the particular point group in question. The d orbitals (Y_2m_1's) are all even (g) functions as is the vibrational ground state (a_{1g}). Therefore, the odd vibrational modes of D_{2h} must be determined. In other words, since $\psi_e^* \psi_e$ and ϕ_v are g functions, ϕ_v^* must be u so that the direct product will be u. Then the product of r(u) and this result (u) will be g. In order for the integrand to be a_{1g}, the two u symmetries must be identical.

Considering the internal coordinates (56) of the D_{2h} model in Figure 11, the reducible representations given

in Table 24 are derived.

Fig. 11 -- INTERNAL COORDINATES D_{2h}
ANGLES α_{nm}, VECTORS r_n

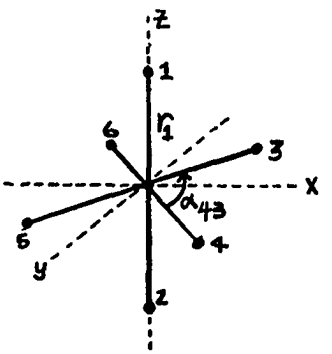

TABLE 24

REDUCIBLE REPRESENTATIONS FROM
INTERNAL COORDINATES UNDER D_{2h}

D_{2h}	E	$C_2(z)$	$C_2(y)$	$C_2(x)$	i	xy	xz	yz
Γ_α	12	0	2	2	0	4	2	2
Γ_r	6	2	0	0	0	4	2	2
$\Gamma_{vib.}$	18	2	2	2	0	8	4	4

The normal vibrational modes of D_{2h} may now be determined by decomposition of $\Gamma_{vib.}$ into its component irreducible representations using the equation,

$$a_i = 1/h \sum_i \chi \chi_i$$

where a_i is the coefficient of the ith irreducible representation of point group D_{2h}, h is the order of the group (=8), χ_i is the character of the ith irreducible representation, and χ the character of $\Gamma_{vib.}$ The vibrational modes are therefore,

$5A_g$, $2B_{1g}$, B_{2g}, B_{3g}, A_u, $2B_{1u}$, $3B_{2u}$, $3B_{3u}$.

Subtracting the modes which correspond to translation (B_{1u}, B_{2u}, B_{3u}) and to rotation (B_{1g}, B_{2g}, B_{3g}), the allowed, normal modes are,

$5A_g$, B_{1g}, A_u, B_{1u}, $2B_{2u}$, $2B_{3u}$ (3N - 6 = 12 modes).

Of this group only the odd modes need be considered as discussed previously.

Now since the physical explanation of vibronic absorption is that the vibrational modes must distort the complex in such a way that the center of symmetry is destroyed in which case a slight u character is imparted to the configurational electronic states and the transition becomes partially allowed, the A_{1u} mode (which is a symmetric vibration and as such will not destroy the center of symmetry of the complex) may be considered to be inactive.

Table 25 contains the symmetries of the elements $(\psi_e^* \vec{r} \psi_e)$ to be compared with the odd normal vibrational modes. From this table it can be seen that transitions 1, 2, and 3, for example would be vibronically forbidden for radiation vectors z, y, and x respectively.

TABLE 25

ELECTRONIC TRANSITION MOMENT SYMMETRIES

	Transition	x(b_{3u})	y(b_{2u})	z(b_{1u})
1.	$^4A_g \longleftrightarrow {}^4B_{1g}$	B_{2u}	B_{3u}	A_{1u}
2.	$\longleftrightarrow {}^4B_{2g}$	B_{1u}	A_{1u}	B_{3u}
3.	$\longleftrightarrow {}^4B_{3g}$	A_{1u}	B_{1u}	B_{2u}
4.	$^4B_{3g} \longleftrightarrow {}^4B_{1g}$	B_{1u}	A_{1u}	B_{3u}
5.	$\longleftrightarrow {}^4B_{2g}$	B_{2u}	B_{3u}	A_{1u}
6.	$\longleftrightarrow {}^4B_{3g}$	B_{3u}	B_{2u}	B_{1u}

In D_{2h}, choosing x as coincident with the needle axis (parallel to the polymer chain and crystal axis c) determines that it is the basis for the b_{3u} representation; z is similarly chosen perpendicular to the horizontal mirror plane.

In the case of "tetrahedral" $\beta Co(py)_2Cl_2$ (site symmetry C_{2v}) (14) some band splitting would be expected. A lowering of symmetry from T_d to C_{2v} might be considered as a modification of tetragonal distortion in that there is compression or elongation along the z axis (colinear with C_2). However, contrary to the tetragonal distortion of O_h, there is considerable d-orbital distortion (with respect to T_d

symmetry) in each of the coordinate planes under C_{2v}. This contributes to a rather complicated expression for the distortion potential. There is no apparent, reasonable simplification of the potential as employed under D_{4h}. It can be said, in general, that as the symmetry is decreased, the number of parameters required to express the perturbation potential increases. Specifically referring to $\beta Co(py)_2Cl_2$, it may be seen from the x-ray data that in the solid there is considerable deviation from regular T_d symmetry; therefore, the d orbitals would be considerably distorted which would produce extensive splitting. Quantitatively, however, the $\beta Co(py)_2Cl_2$ spectrum will be evaluated in terms of a single parameter system only; that is the simple, straight forward treatment as a T_d molecule.

Nevertheless, qualitatively, more can be said about the C_{2v} spectrum in terms of band splitting. Correlations between T_d states and those resulting under C_{2v} symmetry are shown in Table 26.

TABLE 26

T_d - C_{2v} CORRELATIONS

T_d	C_{2v}
A_2	A_2
T_1	$A_2 + B_1 + B_2$
T_2	$A_1 + B_1 + B_2$

Since the degeneracy of both the upper $^4T_1$ states in T_d is removed under C_{2v}, transitions from the $^4A_2$ ground state would be expected to consist of three distinct but overlapping bands in each of these cases. The lowest energy absorption (transition to the $^4T_2$ state) would also be expected to show splitting. This transition is, however, forbidden for electric dipole absorption under T_d but may have some intensity because of reduced site symmetry. The energy of this band is such that it would be overlapped by vibrational bands and, hence, very difficult to observe. As a matter of fact, it has never been definitely observed in the spectra of tetrahedral Co(II) complexes.

It may also be argued that spin-orbit coupling can produce a similar splitting. The structure of the bands in the spectrum of tetrahedral $CoCl_4^=$ (in Cs_3CoCl_5 and other compounds) is interpreted in terms of spin-orbit splitting (47). In this consideration there are two limitations: (1) the splitting due to a lowered symmetry is small compared to spin-orbit splitting, and, (2) vice versa. The spectrum of $\beta Co(py)_2Cl_2$ may well not be approximated successfully using either limiting case. In this complex, distortion is obviously large but since D_q for the tetrahedral case is small compared to octahedral D_q, the symmetry splitting may not be large compared to spin-orbit splitting but, rather, of the same magnitude.

The $\beta Co(py)_2Cl_2$ spectrum will, nevertheless, be discussed qualitatively within the limits of the second assumption.

Results and Applications

The spectra were obtained on powder samples of the pyridinates with the Beckman DK-1 recording spectrophotometer fitted with the Beckman model reflectance attachment. 15 mm. microscope well slides were used as sample containers. The samples were finely powdered, the slide well filled, and finally the sample was covered with a very thin glass cover slide held in place with cellophane tape. This effectively sealed the compounds from the atmosphere and prevented decomposition during the short time necessary for spectra recording (10-15 minutes). No measure of molar absorbtivity is possible and, therefore, spectra are simply plotted as wavelength (and frequency) versus approximate relative absorbance. The reflection spectra obtained are approximated in Figures 14-21 with descriptions in Table 28.

The shape and intensity of the reflection spectra absorbances are a function of particle size and packing, and, therefore, would be expected to vary to some extent even in different samples of the same compound. Even though the spectrum reflects primarily the site symmetry or ligand arrangement about the central metal ion, the spectra of two different compounds which have identical site symmetries but

different crystal symmetries must differ in details of peak position and intensity. This is simply explained by noting that the geometry of molecule arrangement within the unit cell imposes a certain particular potential upon the inner coordination sphere (the nearest neighbor perturbation) which influences to some extent the positioning of energy levels. Thus if the nearest neighbor perturbation is varied, the spectra would be expected to reflect this fact in terms of slightly different band positions and intensities.

The actual determination of peak position is, indeed, not always simple. All of the peaks seen in the spectra are composites of two or more separate absorptions which are so broadened that they are extensively overlapped. No cryostats were available for low temperature spectral work and all spectra were obtained at room temperature. The broadening will naturally occur as a result of lattice vibrational effects.

In some instances, especially in the case of a shoulder on the side of a large peak, the overlapping bands may be positioned by a second derivative plot of absorbance versus wavelength. Taking absorbances from the spectra at 5 or 10 mμ intervals and determining $\Delta^2 A / \Delta \lambda^2$ (i.e. the actual difference in the difference between adjacent absorbances) the shoulder absorbance is isolated. This procedure is limited, however, and gives less satisfactory results in those regions of the spectrum in which the absorbance is

relatively flat.

It is noted that the spectra of $Co(py)_4Cl_2$ and $Co(py)_6Cl_2$ are virtually identical. The spectra of $Co(py)Cl_2$, $Co(py)_{2/3}Cl_2$ and $CoCl_2$ are closely related. In this respect, the same parameters may be used to fit the $Co(py)_4Cl_2$ and $Co(py)_6Cl_2$ spectra assuming conditions of axial elongation. Analogously, the $Co(py)Cl_2$ and $Co(py)_{2/3}Cl_2$ spectra may be favorably compared with the known spectrum of $CoCl_2$.

In the $\beta Co(py)_2Cl_2$ spectrum, the two main band systems are each seen to be split into three discernible segments as was predicted for descent to C_{2v} symmetry.

The single crystal, polarized light spectrum of $\alpha Co(py)_2Cl_2$ shows by visual observation that the intensity of the absorption band at 610 mμ is greatly diminished with light polarized parallel to the needle axis. The spectrum fit using the axial compression, tetragonal distortion scheme indicates that this peak is the transition to the $^4B_{1g}$ state arising from $^4A_{2g}(O_h)$ (see Table 27). The ground state in $\alpha Co(py)_2Cl_2$ under D_{2h} must be $^4B_{3g}$ since as indicated in Table 25 this transition would have zero vibronic intensity with x polarized right. The ground state electronic configuration for $\alpha Co(py)_2Cl_2$ is, therefore,

z axis compression $(^4B_{3g})$: $b_{3g}^2\ a_g(x^2 - y^2)^2\ b_{2g}^1\ a_g(z^2)^1 b_{1g}^1$.

The energy level diagrams (as predicted by the results shown in Table 21 and verified by the results of

spectral fitting shown in Table 27 of the next section) are given in Figure 12 and Figure 13.

Fig. 12 -- ENERGY LEVEL ORDERING IN "OCTAHEDRAL" ENVIRONMENTS

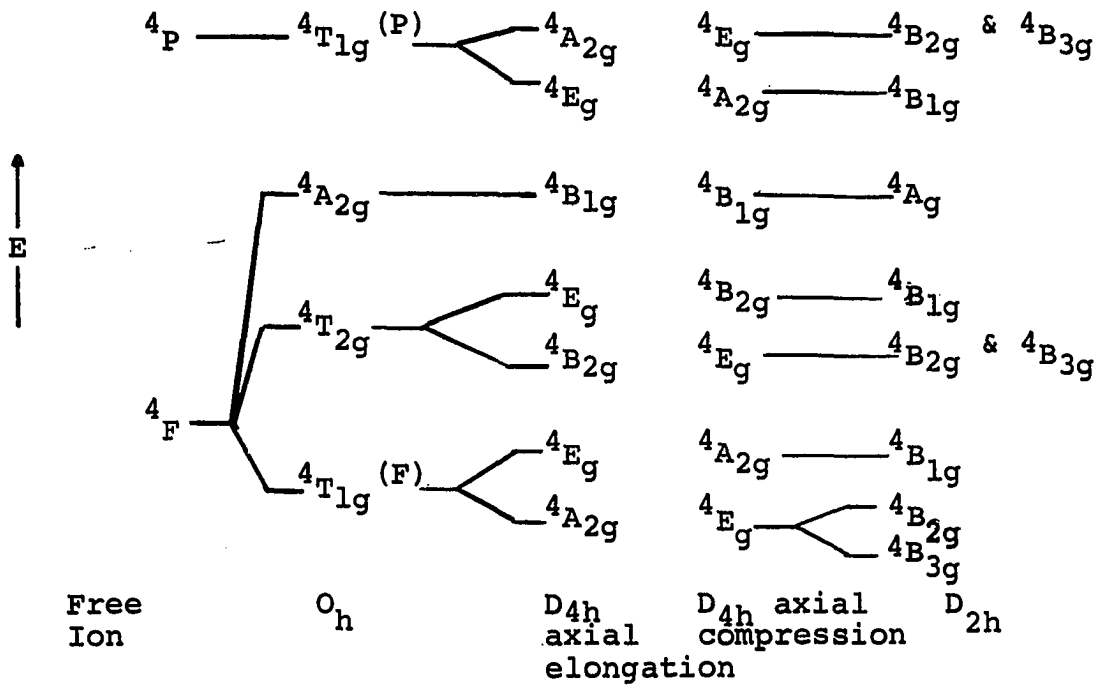

Fig. 13 -- ENERGY LEVEL ORDERING
IN "TETRAHEDRAL" ENVIRONMENTS

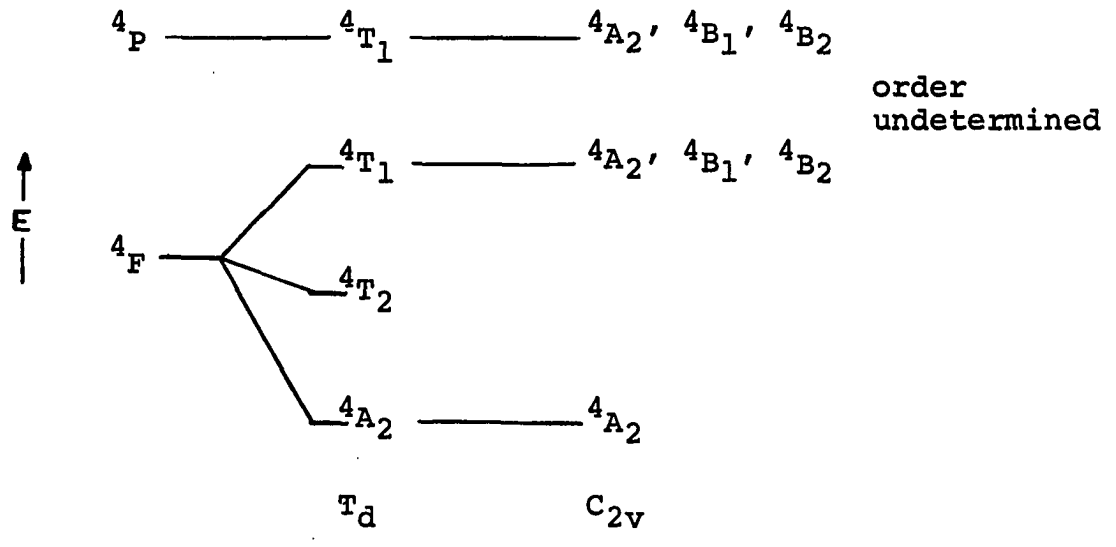

Spectral Fitting

One of the spectral parameters, $\Delta E(^4P - {}^4F)$, may be effectively estimated in the following manner.* In the spectrum of octahedrally coordinated $Co(py)_6^{+2}$ ion in solution (as present in pyridine solutions of $Co(ClO_4)_2$ or $Co(NO_3)_2$) the transitions ν_1: $^4T_{1g}(F) \longrightarrow {}^4T_{2g}$ and ν_3: $^4T_{1g}(F) \longrightarrow {}^4T_{1g}(P)$ can be identified at 20,400 cm^{-1} and 8500 cm^{-1} (Figure 21). Assuming that an interaction (repulsion) will occur between the two $^4T_{1g}$ states and that this will constitute the major perturbation within the configuration, the perturbation energy matrix (of usual form)

---

*The $^4P - {}^4F$ separation within the complex would be expected to differ appreciably from the spectroscopically determined value of 14,500 cm^{-1} in gaseous Co^{+2} (57).

is given,

$$\begin{vmatrix} \langle \psi(T_{1g}F) | V_o | \psi(T_{1g}F) \rangle - E & \langle \psi(T_{1g}F) || \psi(T_{1g}P) \rangle \\ \langle \psi(T_{1g}P) || \psi(T_{1g}F) \rangle & [E(^4P) - E(^4F)] - E \end{vmatrix} = 0$$

The matrix elements in question are best evaluated from wave functions derived by means of the application of the lowering operator upon an unambiguous electronic configurational state (49d). The matrix, upon evaluation of the elements in terms of the octahedral splitting parameter D_q, becomes,

$$\begin{vmatrix} -6D_q - E & 4D_q \\ 4D_q & \Delta E - E \end{vmatrix} = 0$$

The solutions to this equation (E_+ and E_-, the positive and negative root energies from the quadratic formula, correspond to energies relative to the ^4F as zero) must be such that, using ΔE and D_q as parameters,

$$\nu_1 = 2D_q + |E_-| = 8500 \text{ cm}^{-1}$$

$$\nu_3 = |E_-| + E_+ = 20{,}400 \text{ cm}^{-1}$$

In this manner a best fit value of ΔE may be obtained for this particular environment. In general, this separation may be considered to remain reasonably constant with minor complex environmental changes.

Using values of $\Delta E = 13{,}000 \text{ cm}^{-1}$ and $D_q = 925 \text{ cm}^{-1}$, ν_1 and ν_3 are calculated to be respectively 8,350 and 20,500 cm^{-1} which fits the spectrum reasonably well. This value of ΔE was used for the spectra fitting of the pyridinates.

The value of D_q for a complex in which the coordination sphere consists of more than one type of ligand may be estimated as the weighted average of D_q's for total coordination by each ligand separately. For example in the case of $Co(py)_4Cl_2$,

$$D_q = 4/6\ D_q\ [Co(py)_6^{+2}] + 2/6\ D_q\ [CoCl_2] \cong 850\ cm^{-1}.$$

This would not be the exact D_q value since $Co(py)_4Cl_2$ does not have O_h symmetry and D_q must be treated as a parameter within the D_{4h} potential; however, the value determined should be approximate.

Using the ΔE value obtained above and assumed values for D_q, D_s and D_t, the transition energies were calculated using the energy levels shown in Tables 21 and 22. Energy set I was found to give the best spectral fit in the case of $Co(py)_6Cl_2$ and $Co(py)_4Cl_2$ axial elongation situation while set IV was used for $\alpha\, Co(py)_2Cl_2$ axial compression. Simplified calculations with only the D_q parameter were made for $CoCl_2$ and $\beta\, Co(py)_2Cl_2$ as discussed previously and $Co(py)Cl_2$ and $Co(py)_{2/3}Cl_2$ spectra were fit in direct comparison with $CoCl_2$.

TABLE 27

COLLECTED SPECTRAL DATA

	Transition	Calculated (cm^{-1})	Calculated (mμ)	Observed (cm^{-1})
I.	$Co(py)_6Cl_2$ and $Co(py)_4Cl_2$			
	D_q = 875 cm^{-1}, D_s = 250 cm^{-1}, D_t = 125 cm^{-1}			
1.	$^4A_{2g} \longrightarrow {}^4B_{2g}(T_{2g})$	7,375	1,360	Overlapping Peaks 6700-10,000 cm^{-1}
2.	$\longrightarrow {}^4E_g(T_{2g})$	9,000	1,110	
3.	$\longrightarrow {}^4B_{1g}(A_{2g})$	16,125	630	16,400 (sh)
4.	$\longrightarrow {}^4E_g(T_{1g}P)$	19,625	510	19,600 (s)
5.	$\longrightarrow {}^4A_{2g}(T_{1g}P)$	21,000	480	20,400 (s)
6.	$\longrightarrow {}^4E_g(T_{1g}F)$	1,750	5,700	Not in region examined
7.	$^4E_g \longrightarrow {}^4B_{2g}(T_{2g})$	5,625	1,780	5150, 5260 cm^{-1}
8.	$\longrightarrow {}^4E_g(T_{2g})$	7,185	1,390	6900, 7090 cm^{-1}
9.	$\longrightarrow {}^4B_{1g}(A_{2g})$	14,375	695	
10.	$\longrightarrow {}^4E_g(T_{1g}P)$	17,875	560	
11.	$\longrightarrow {}^4A_{2g}(T_{1g}P)$	19,250	520	
II.	α $Co(py)_2Cl_2$: D_q = 825 cm^{-1}, D_s = 400 cm^{-1}, D_t = 100 cm^{-1}			
1.	$^4E_g \longrightarrow {}^4E_g(T_{2g})$	7,500	1,330	7,200 (m)
2.	$\longrightarrow {}^4B_{2g}(T_{2g})$	9,250	1,080	9,350 (m)
3.	$\longrightarrow {}^4B_{1g}(A_{2g})$	15,950	625	16,500 (m)
4.	$\longrightarrow {}^4A_{2g}(T_{1g}P)$	20,450	505	19,400 (s)
5.	$\longrightarrow {}^4E_g(T_{1g}P)$	19,750	490	18,500 (sh)
6.	$\longrightarrow {}^4A_{2g}(T_{1g}F)$	1,750	5,700	Not in region examined

TABLE 27 - Continued

Transition	Calculated (cm^{-1})	Calculated ($m\mu$)	Observed (cm^{-1})
II. $\alpha Co(py)_2Cl_2$			
7. $^4A_{2g} \longrightarrow {}^4E_g(T_{2g})$	4,500	2,220	
8. $\longrightarrow {}^4B_{2g}(T_{2g})$	6,100	1,640	6,200, 5,800 cm^{-1}
9. $\longrightarrow {}^4B_{1g}(A_{2g})$	12,750	785	14,300
10. $\longrightarrow {}^4A_{2g}(T_{1g}P)$	18,800	1,120	
11. $\longrightarrow {}^4E_g(T_{1g}P)$	16,600	600	
III. $CoCl_2$, $Co(py)_{2/3}Cl_2$, $Co(py)Cl_2$: D_q = 690 cm^{-1} ΔE = 13,000 cm^{-1} (47)			
1. $^4T_{1g}(F) \longrightarrow {}^4T_{2g}$	6,600	1,520	6,600 cm^{-1} (band center) (m)
2. $\longrightarrow {}^4A_{2g}$	13,300	750	13,000 (m)
3. $\longrightarrow {}^4T_{1g}(P)$	17,150	570	17,200 (s)
4. $\longrightarrow {}^2T_{2g}$	19,200	520	19,000 (sh)
5. $\longrightarrow {}^2A_g$	19,800	505	19,000 (sh)
IV. $\beta Co(py)_2Cl_2$: D_q = 400 cm^{-1}, ΔE = 13,000 cm^{-1}			
1. $^4A_2 \longrightarrow {}^4T_1(F)$	7,200	1,380	From 900 to 1600 $m\mu$
2. $\longrightarrow {}^4T_1(P)$	17,800	560	16,600 cm^{-1}, 600 $m\mu$
V. $CoCl_2$, $Co(py)_{2/3}Cl_2$, $Co(py)Cl_2$: D_q = 750 cm^{-1}, ΔE = 12,700 cm^{-1}			
1. $^4T_{1g}(F) \longrightarrow {}^4T_{2g}$	6,000	1,670	6,600
2. $\longrightarrow {}^4A_{2g}$	13,500	740	13,000
3. $\longrightarrow {}^4T_{1g}(P)$	17,200	580	17,200

TABLE 28

SPECTRAL DESCRIPTION (2000-400 m)

Compound	Peak Position (cm^{-1})	(mμ)	Description
$CoCl_2$	6,490	1,540	Center of Broad, moderate intensity band, (~1000mμ) ~ symmetrical
	8,000	1,250	Shoulder, weak
	13,000	770	Shoulder, moderate, flat and undefined
	17,540	570	Sharp (~100 mμ), intense strong band, apparently complex and unresolved
	19,050	525	Shoulder, moderate, on 570 mμ band system.
$Co(py)_{2/3}Cl_2$	6,450	1,550	Broad band, ill defined, moderate, ~ symmetrical
	7,500	1,330	Shoulder, moderate
	12,820	780	Clearly defined shoulder on 580 mμ peak, moderate
	17,240	580	Strong peak, sharp (~50 mμ) unresolved
	18,350	545	Shoulder on 580 mμ system
$Co(py)Cl_2$	6,670	1,500	Broad band (~1000mμ), moderate, ~symmetrical
	7,940	1,260	Weak shoulder
	13,500	740	Shoulder on 560 mμ band moderate
	17,860	560	Strong band, (~100 mμ), unresolved

TABLE 28 - Continued

Compound	Peak Position (cm^{-1})	($m\mu$)	Description
$Co(py)Cl_2$	18,900	530	Shoulder on 560 mμ band, moderate
$\beta Co(py)_2Cl_2$	6,900	1,450 (center)	Broad band (800 mμ). At least two peaks centered at 1,370 mμ(7,300 cm^{-1}), and 1,530 mμ(6,540 cm^{-1}), moderate
	10,200	980	Round band definitely separated from 1,450 mμ system, broad (~300 mμ), moderate
	14,710	680	Shoulder on 600 mμ system strong
	16,670	600	Sharp, very strong, perhaps complex
	17,700	565	Shoulder, strong
$\alpha Co(py)_2Cl_2$	5,800 6,200 7,200	1,730 1,610 1,390	Band system extending from 5,400 cm^{-1} to 7,500 cm^{-1}, moderate, peak at 1,610 mμ is pyridine.
	9,350	1,070	Broad band (300 mμ), moderate
	14,300	700	Shoulder on 605 mμ, moderate
	16,550	605	Sharp peak, strong
	18,560 19,420 20,000	540 515 500	Strong band system, shoulders on center peak at 515, fairly symmetrical

TABLE 28 - Continued

Compound	Peak Position (cm^{-1})	($m\mu$)	Description
$Co(py)_4Cl_2$	5,260	1,900	Weak band, sharp
	6,210	1,610	Moderate, sharp, attributed to pyridine
	6,900 7,410 9,100	1,450 1,300 1,100	Broad, complex band, from 1,500 mμ to 800 mμ , moderate intensity
	16,260	610	Shoulder on 500 mμ peak, moderate
	18,500	540	Shoulder, more intense
	19,200	525	Strong band, sharp
	20,000	500	Strong band, sharp
$Co(py)_6Cl_2$	5,150	1,940	Small, weak, fairly sharp peak
	6,010	1,665	Sharp, moderate, pyridine
	7,090 7,580 8,930	1,410 1,320 1,120	Broad, complex band, from 1,550 mμ to 850 mμ , and unresolved, moderate
	16,100	620	Shoulder on 500 mμ
	18,200 19,230 20,800	550 520 480	Complex band, strong, definite shoulders, unresolved, but sharp.

Fig. 14 -- $CoCl_2$ Spectrum

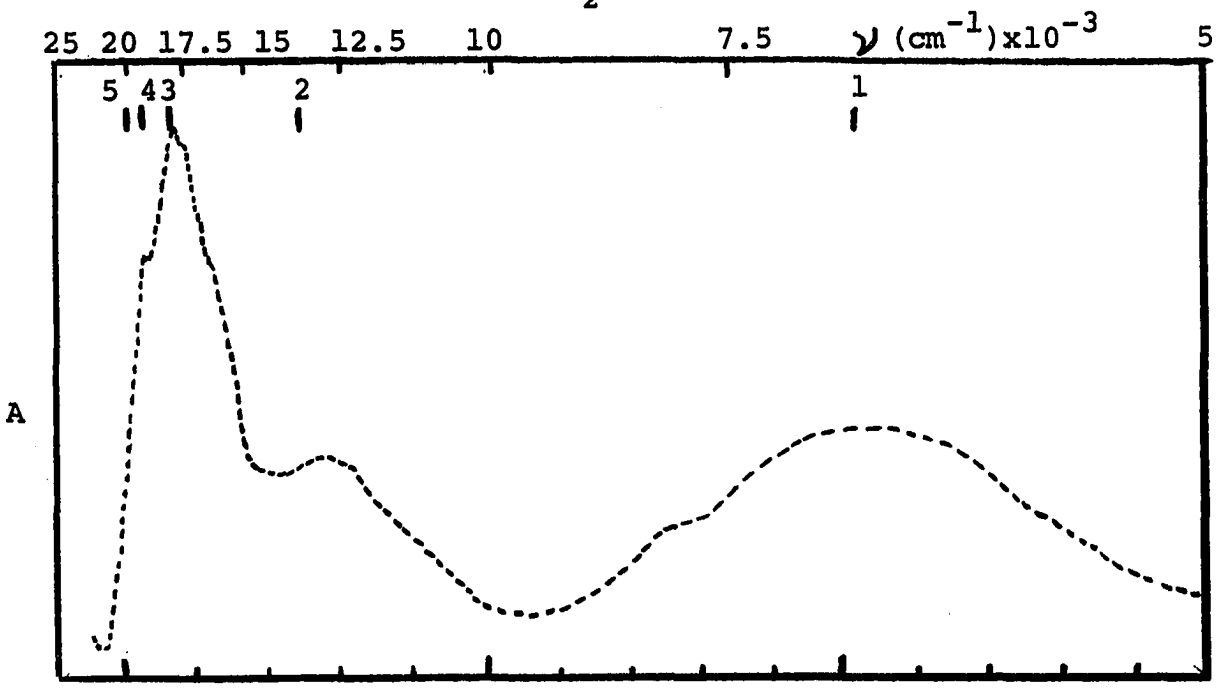

Fig. 15 -- $Co(py)_{2/3}Cl_2$ Spectrum

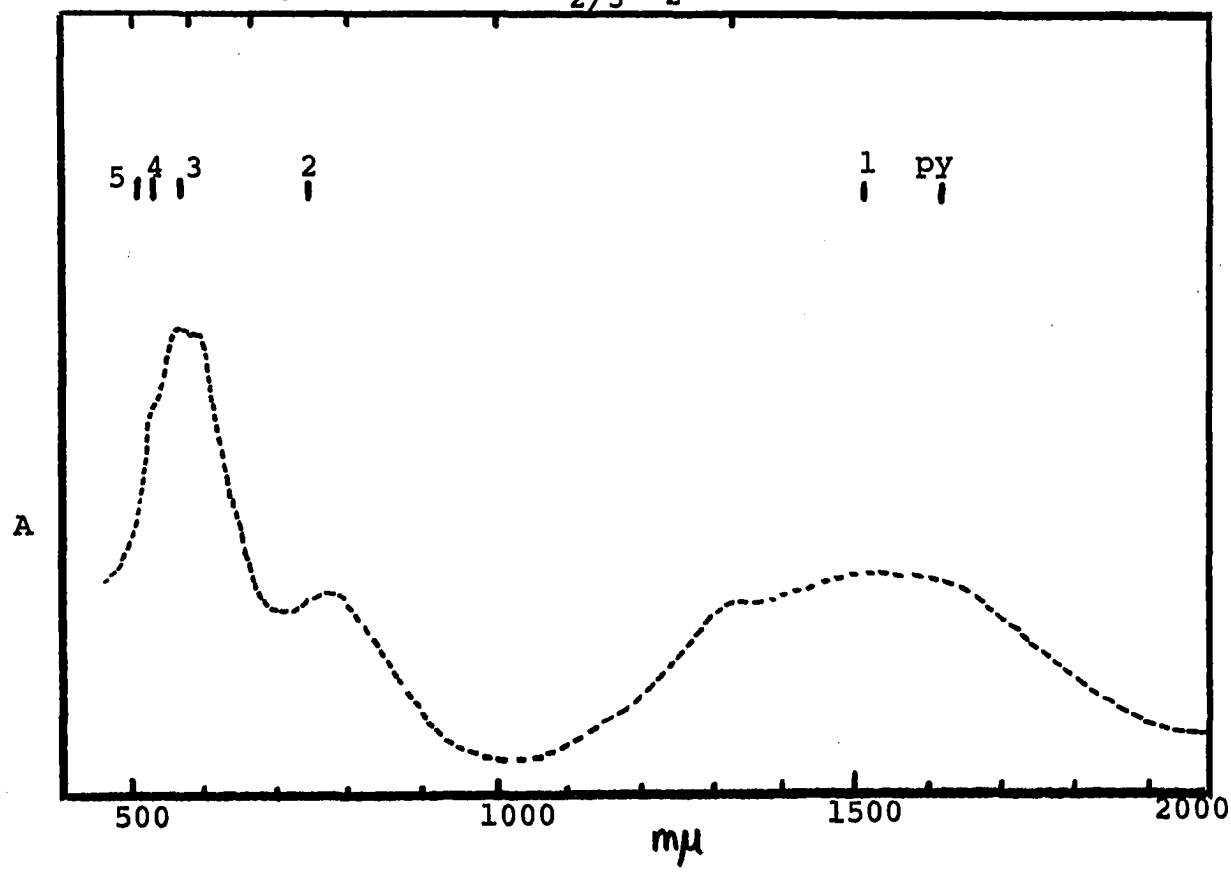

Fig. 16 -- $Co(py)Cl_2$ Spectrum

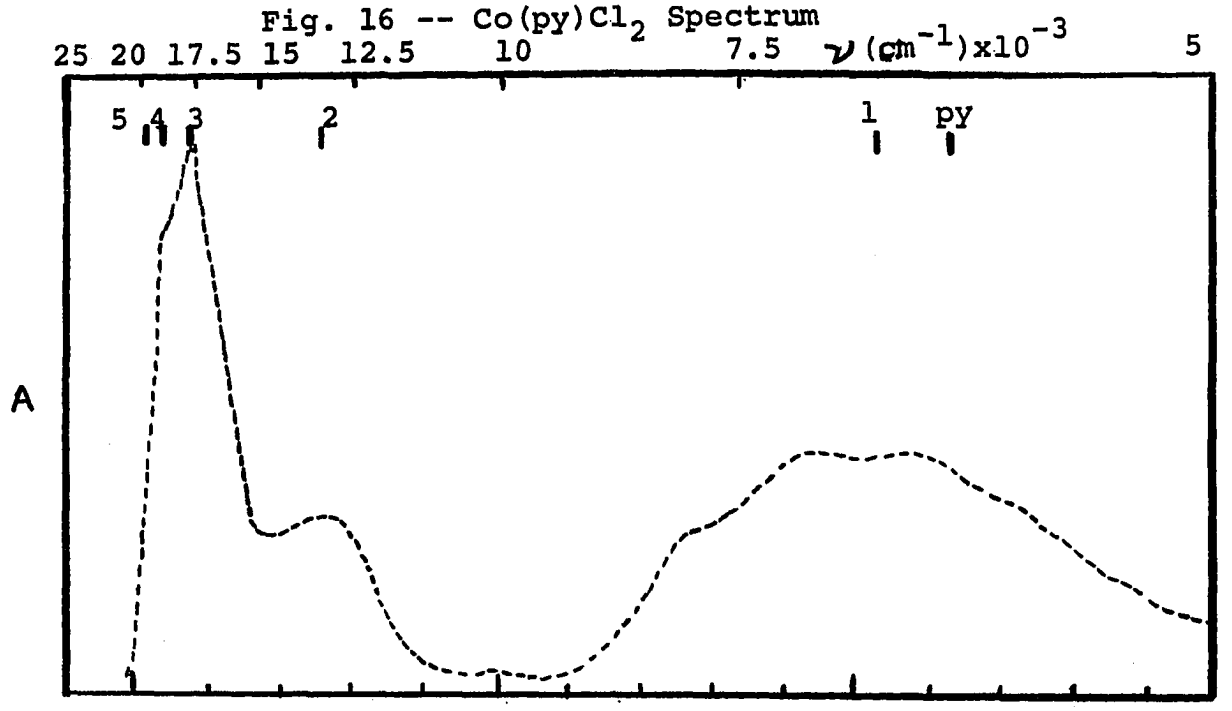

Fig. 17 -- $\beta Co(py)_2Cl_2$ Spectrum

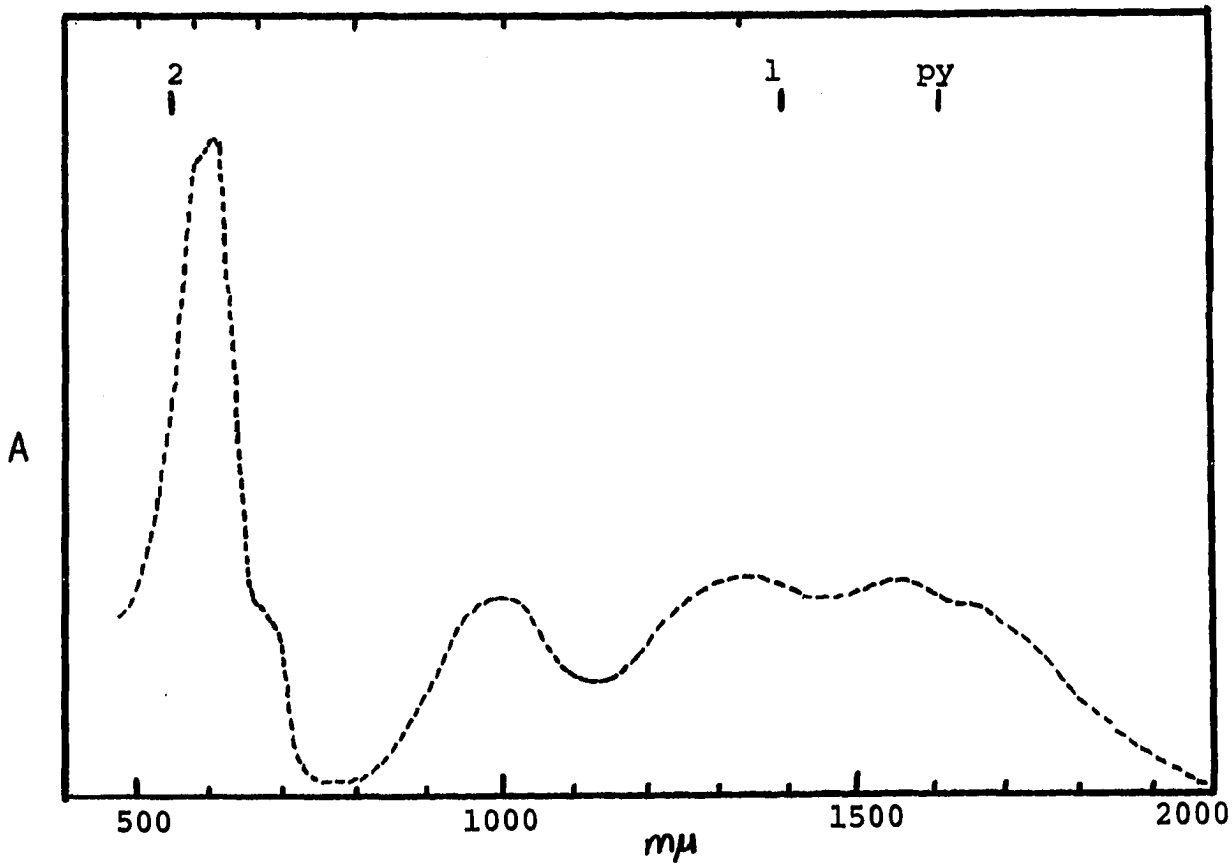

Fig. 18 -- $Co(py)_2Cl_2$ Spectrum

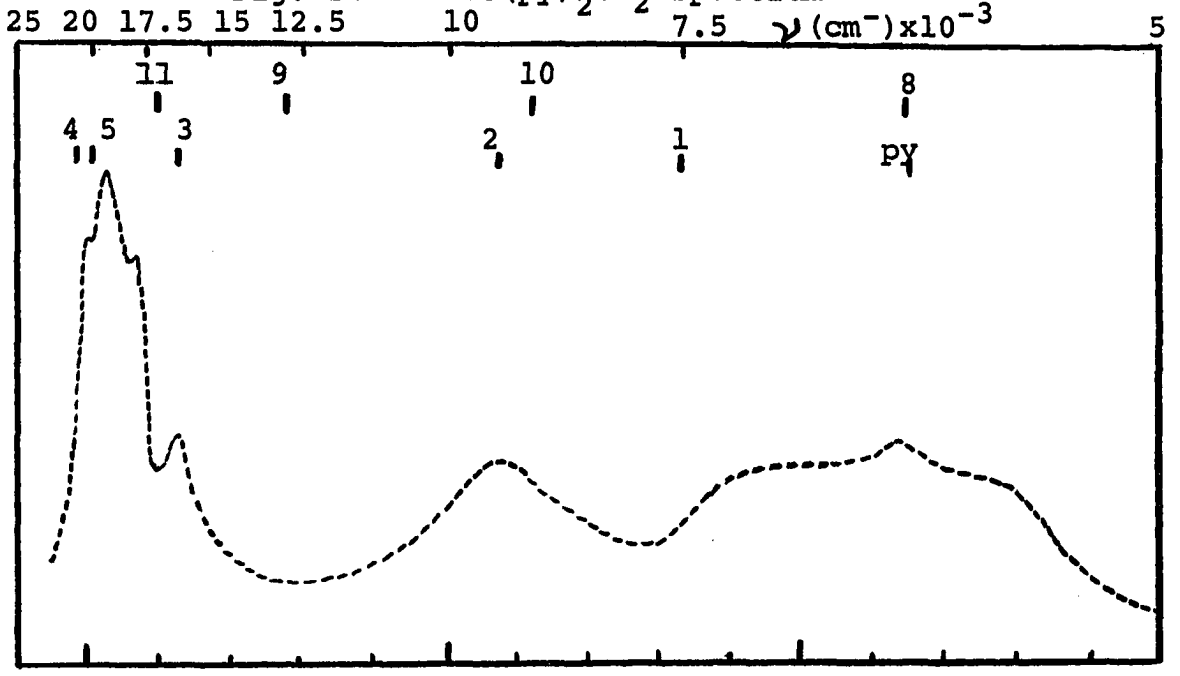

Fig. 19 -- $Co(py)_4Cl_2$ Spectrum

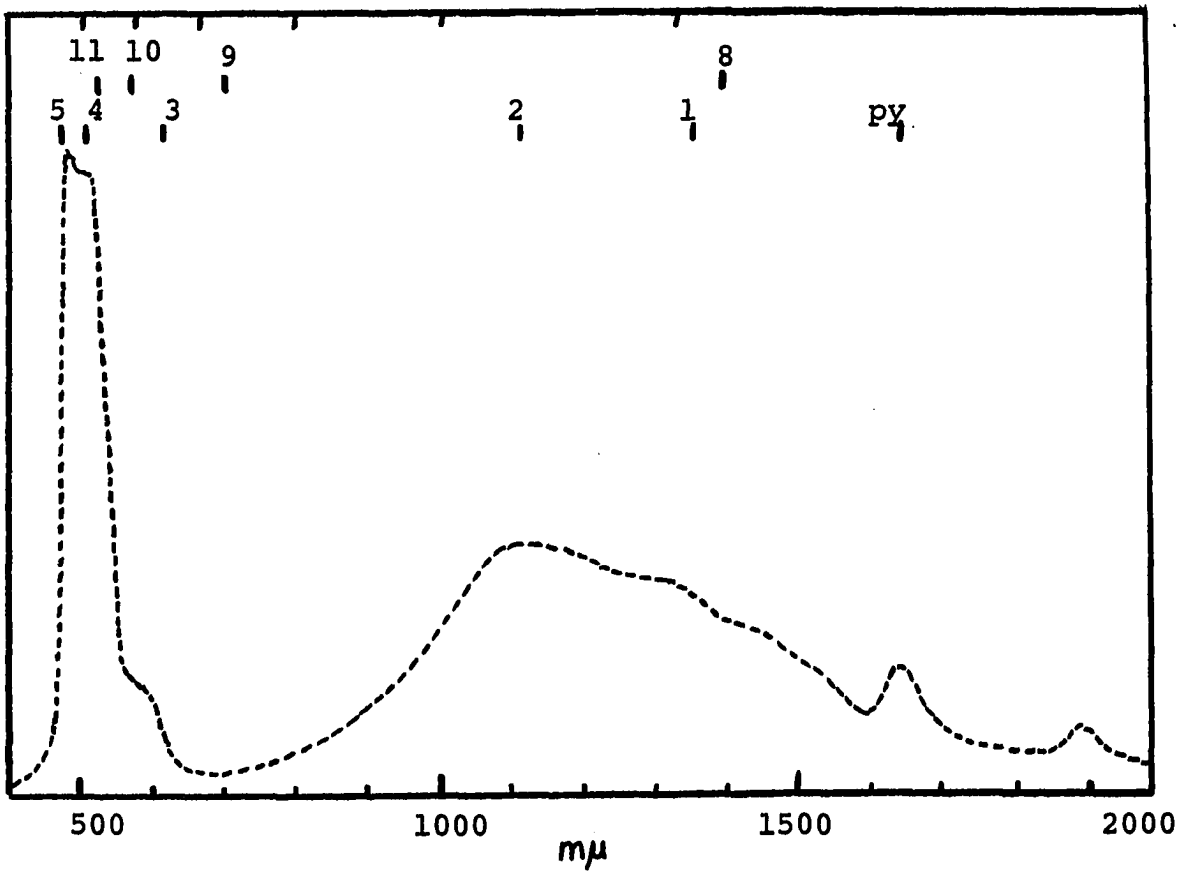

Fig. 20 -- $Co(py)_6Cl_2$ Spectrum

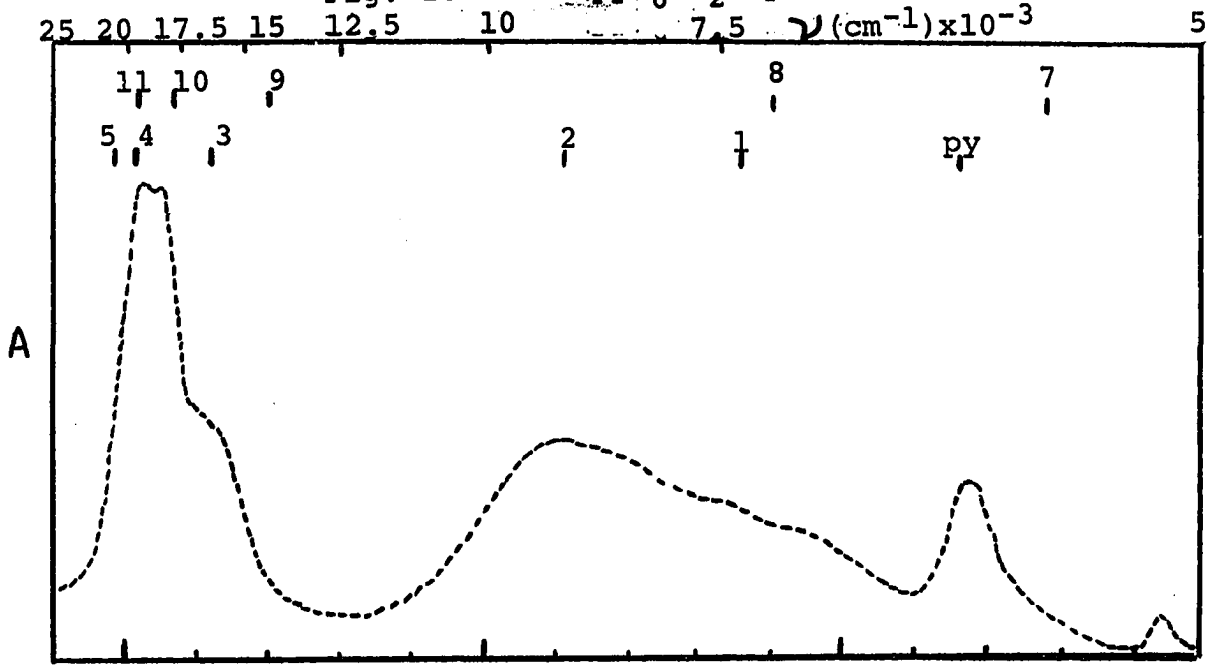

Fig. 21 -- $Co(py)_6(NO_3)_2$ in py vs. py Reference

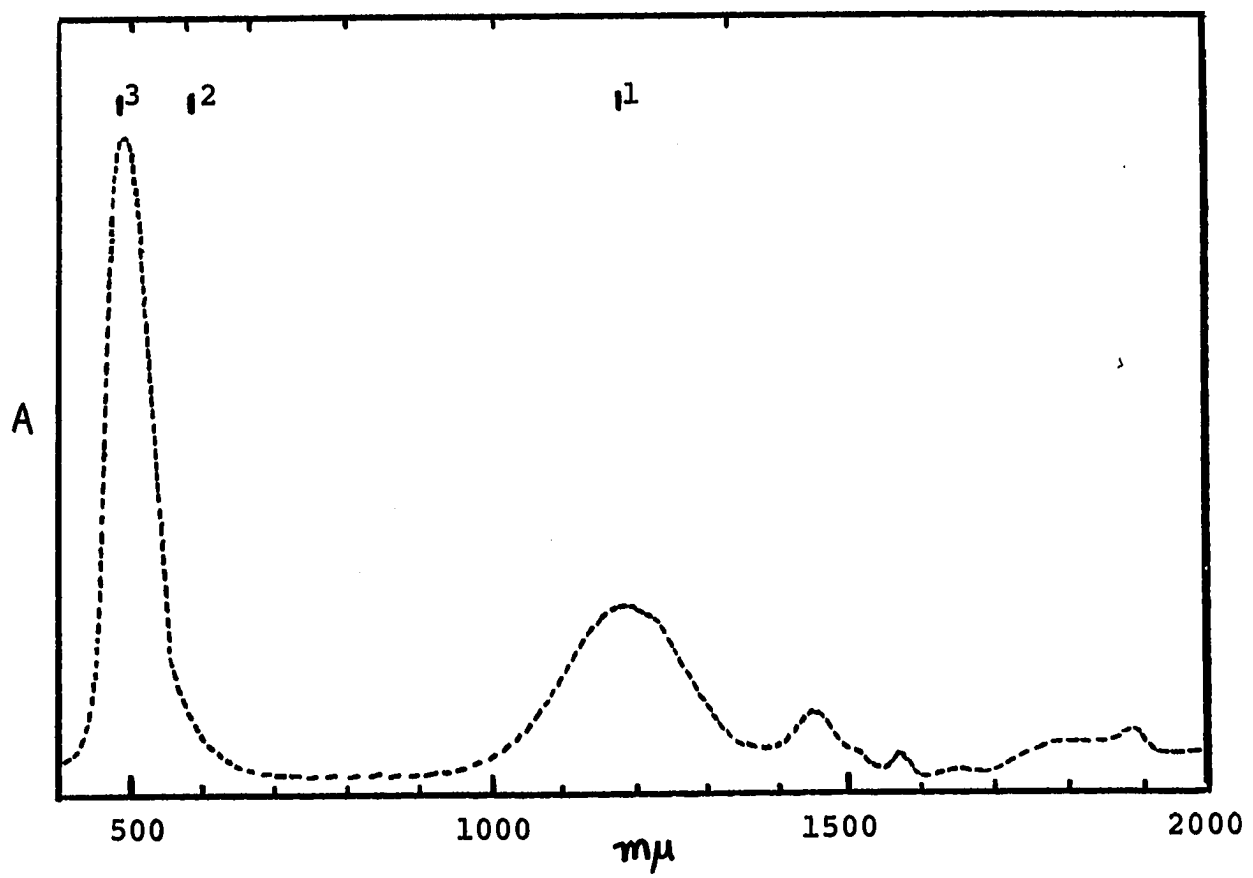

CHAPTER V

MAGNETIC SUSCEPTIBILITY

Preliminary Discussion

Measurement of magnetic susceptibility can aid in a structure determination since the number of unpaired electrons is dependent on the 3d orbital splitting or the magnitude of the splitting. The strength of the ligand field or the extent of the interaction between ligand and central ion determines the magnitude of the d orbital splitting. In cases where the energy separation between adjacent d levels in the complex is greater than the electron pairing energy (the strong field case), electrons will preferentially pair in the lower orbitals rather than occupy the higher energy orbitals. In the weak field situation, the opposite effect will be noted. Thus, on the basis of the number of unpaired electrons, the site symmetry and ligand field strength may frequently be determined.

In Co(II)(d^7), the number of unpaired electrons is the same in either octahedral or tetrahedral environments (weak field).

Tetrahedral: $e^4 t_2^3$ (3 unpaired)

Octahedral: $t_{2g}^5 e_g^2$ (3 unpaired)

Other configurations of Co(II) are very rare and the ligands chloride and pyridine are definitely weak field; therefore, no other situations are considered.

The total susceptibility is, however, influenced by factors other than the number of unpaired electrons. The major component is, of course, due to the interaction of the electron spin moment of the unpaired electron with a magnetic field. Secondarily, there may be a contribution from excited states (which have the same multiplicity as the ground state and significant population at the temperature of measurement) mixed in by spin-orbit coupling. Furthermore, the octahedral susceptibility would have an additional contribution from the electron orbital angular momentum adding to the total which does not occur in the tetrahedral case, (i.e. the tetrahedral ground state consists of a completely filled e level and a half filled t_2 level which represents a completely symmetrical electron arrangement and as such would possess no net moment about a given axis; whereas in the ground state octahedral, the t_{2g} level contains five electrons and as a consequence of the lack of symmetry has a net moment which can constitute an orbital angular momentum contribution.)

Experimental

The magnetic susceptibilities were measured on a Curie-Chevenaux type balance which has been previously described (58)(32). This type of apparatus consists of a quartz fibre torsion balance from one arm of which the sample, contained in a glass bucket, was suspended by a long, rigid glass fibre into the sample chamber. The sample and balance chambers are interconnected so that the entire apparatus can be evacuated and a nitrogen atmosphere (at reduced pressure) may be substituted. Furthermore, the sample chamber is enclosed with a specially made, high vacuum flask which allows the sample to be thermostated by placing constant temperature liquids or mixtures (such as ice-water, dry ice-acetone, liquid nitrogen, etc.) in contact with the sample chamber and maintaining the particular temperature for some time during which measurements could be completed. Provision is made for the slow passage of a double pole permanent magnet by the sample chamber and the movement (deflection) of the sample in the magnetic field is determined by following the movement of a point on the glass fibre with a cathetometer.

A unique balance constant was determined from measurements of a compound of known susceptibility and application of the equations,

$$\chi_g = kd/m \quad \text{and} \quad \chi_m = \chi_g \bar{M}$$

where χ_g is the gram susceptibility of a compound of mass m grams, χ_m is the molar susceptibility, d is the total up and down deflection of the sample in the magnetic field (the sum of the deflection due to the paramagnetic sample (d_p) and the lesser deflection due to the diamagnetism of the glass bucket (d_d). A plot of m versus d should give a straight line with slope k/χ_g and intercept d_d on the d axis. This plot also determines whether or not the quartz balance is deflecting linearly. The constant was determined to be 1.026×10^{-6} (Figure 22)* using as a standard $H_gCo(SCN)_4$ which may be made in high purity and has a molar susceptibility of 16.44×10^{-6} c.g.s. units at 20°C with a temperature dependence of -0.05 c.g.s. per degree (59).

Furthermore, the susceptibilities of the pyridinates were determined as a function of temperature. The chosen temperatures were: liquid nitrogen (78°A), dry ice-acetone (195°A), ice-water (273°A), room temperature (300°A), and steam-water (373°A). Temperatures at the wall of the sample chamber were measured using a double copper-constantan thermocouple (against an ice-water (0°C) junction) and galvanometer for measuring the current.

---

*These values were obtained in conjunction with Arthur M. Stevens.

Fig. 22 -- d vs. m for $Hg Co(SCN)_4$

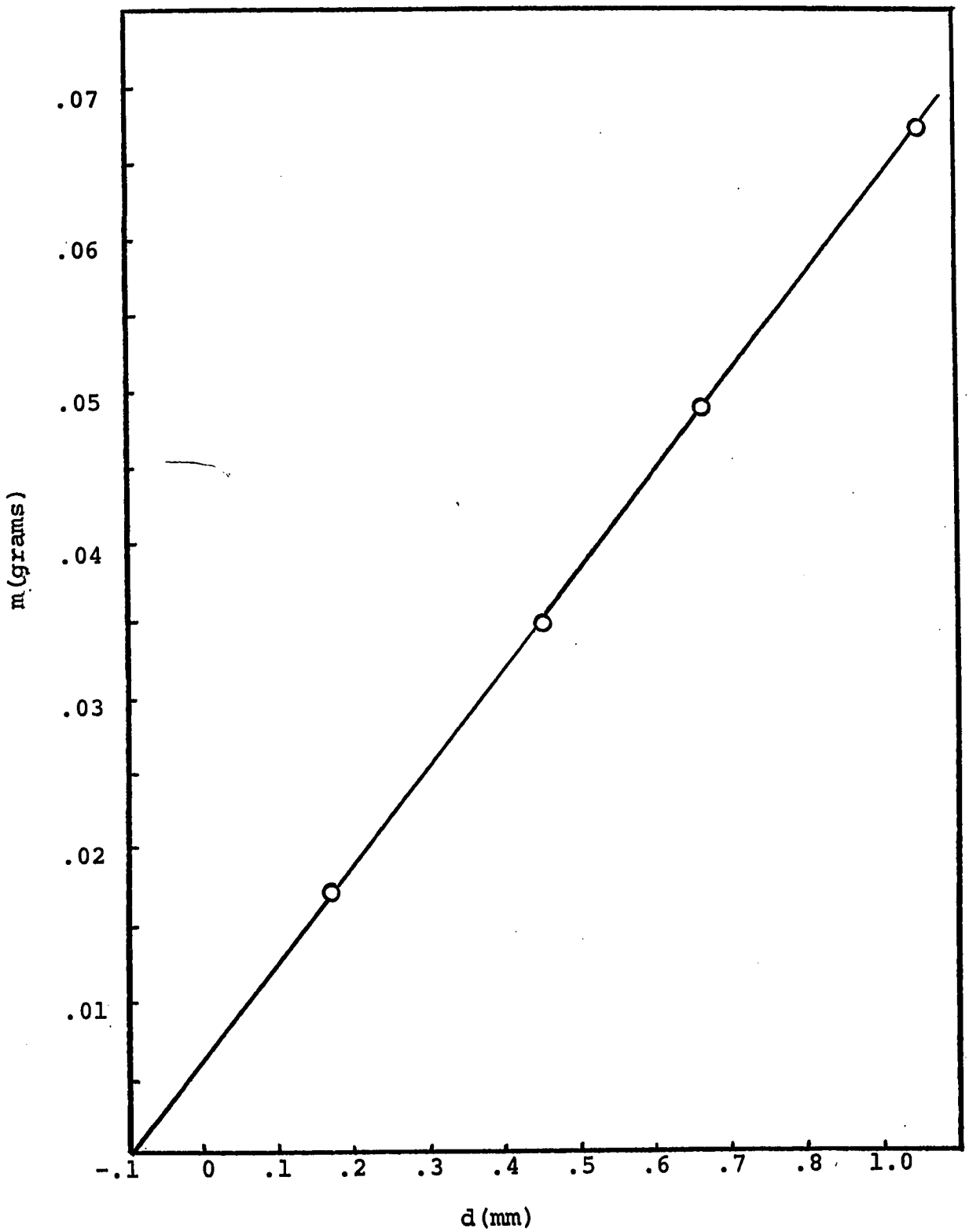

Measurements on the $Co(py)_6Cl_2$ and $Co(py)_4Cl_2$ were not made at steam temperature due to rapid decomposition. The low temperature measurements of $\beta Co(py)_2Cl_2$ were considered to be in error since they showed considerable deviation from the extrapolated line of the higher temperature points. It was observed that during the period of several hours allowed for temperature equilibration at the lower temperatures, the transition to the α form occurred to an appreciable extent. The observed susceptibility corresponds to what would be expected of a mixture of α and β $Co(py)_2Cl_2$.

The magnetic susceptibility data obtained is shown in Table 28. The corrected molar susceptibility ($\chi_m^{corr.}$) shown considers the molar diamagnetism of the compound constituents: pyridine, 50 x 10^{-6}c.g.s. (40); cobalt(II), 13 x 10^{-6}c.g.s.; chloride, 23 x 10^{-6}c.g.s. (60).

Calculations and Data Evaluation

Following non-rigorously, Van Vleck's deriviation for molar paramagnetic susceptibility (60) of a particular configuration with the simplification that the separation between ground state and excited state energy levels is large compared to kT and that $\beta_g H \ll kT$ (i.e. the separation of the energy levels within the ground state is small compared to kT), it can be shown that,

$$\chi_m = (N\beta^2/3kT)\, g^2 S(S+1),$$

TABLE 29

MAGNETIC SUSCEPTIBILITY DATA

Compound	T°A	$\chi_g \times 10^6$ (c.g.s.)	$\chi_m^{corr} \times 10^6$ (c.g.s.)	$1/\chi_m^{corr.}$	$1/T-\theta \times 10^3$
$CoCl_2$	373	76.82	9,910	101.0	2.87
	300	97.21	12,540	79.7	3.64
	273	107.83	13,910	71.8	4.03
	195	157.28	20,290	49.2	5.88
	78	504.57	65,090	15.3	18.90
$Co(py)_{2/3}Cl_2$	373	50.00	9,220	109.5	2.79
	300	69.55	12,790	78.7	3.51
	273	62.92	11,580	87.0	3.88
	195	99.89	18,330	54.8	5.55
	78	286.36	52,380	19.1	15.90
$Co(py)Cl_2$	373	32.78	9,550	105.9	2.85
	300	57.08	12,040	83.8	3.60
	273	66.49	13,320	75.7	3.98
	195	45.87	19,260	51.3	5.78
	78	201.35	58,100	17.2	17.85

TABLE 29 - Continued

Compound	T°A	χ_g x 10^6 (c.g.s.)	χ_m^{corr} 10^6 (c.g.s.)	$1/\chi_m^{corr.}$	$1/T-\theta$ x 10^3
$\beta Co(py)_2Cl_2$	373	22.64	6,780	153.4	2.79
	300	28.37	8,430	122.3	3.51
	273	31.35	9,260	111.1	3.88
	195	54.56	15,960	63.6	5.55
	78	150.49	43,600	23.1	15.90
$\alpha Co(py)_2Cl_2$	373	30.17	8,950	115.1	2.77
	300	38.68	11,200	89.8	3.47
	273	42.01	12,360	82.6	3.83
	195	60.28	17,560	51.6	5.46
	78	165.03	47,790	21.0	15.15
$Co(py)_4Cl_2$	300	22.92	10,490	97.8	3.51
	273	25.36	11,580	88.3	3.88
	195	36.54	16,570	61.3	5.55
	78	104.45	46,880	21.5	15.90
$Co(py)_6Cl_2$	300	15.83	9.930	104.5	3.42
	273	17.48	10,930	94.6	3.77
	195	24.91	15,420	66.4	5.35
	78	65.80	40,140	25.1	14.30

where β is the Bohr magneton, g is the Lande' factor which holds within the Russell-Saunders coupling scheme, and S is the spin quantum number ($\sum s_i$). N, k, and T have their usual meanings. This is compared to the empirical Curie-Weiss formula (where Θ is the Weiss constant and C_m the Curie constant),

$$\chi_m = C_m/(T-\Theta) = N\beta^2 \mu^2_{eff.}/3k(T-\Theta)$$

and a new term, μ_{eff}, the experimentally measured, "effective magnetic moment" is defined,

$$\mu_{eff} = \beta g \sqrt{S(S+1)}.$$

Substituting g = 2 (61) and S = n/2 where n is the number of unpaired electrons,

$$\mu_{eff} = \beta\sqrt{n(n+2)} = \sqrt{n(n+2)} \text{ Bohr Magneton (B.M.) units}$$

Therefore, for d^7 octahedral and tetrahedral weak field situations, n = 3 and μ_{eff} = 3.88 B.M. This is usually referred to as the spin only moment ($\mu_{s.o.}$).

Rearranging the above equation for χ_m and evaluating the constants,

$$\mu_{eff} = 2.84\sqrt{\chi_m(T-\Theta)} \text{ B.M.}$$

Furthermore,

$$C_m = \chi_m(T-\Theta) = \mu^2/(2.84)^2 = \mu^2/8$$

therefore,

$$\chi_m = \frac{\mu^2/8}{T-\Theta}$$

and,

$$T = \mu^2/8\,\chi_m + \theta$$

From this last equation, it can be seen that a plot of T versus $1/\chi_m$ will yield a straight line with a slope of $\mu^2/8$ and an intercept on the T axis of θ.

In addition, there will exist a small temperature independent susceptibility (T.I.P.) arising from excited state contribution such that,

$$\chi_m = C_m/(T - \theta) + \text{T.I.P.}$$

The T.I.P. may be evaluated as the χ_m intercept of a plot of χ_m vs. $1/(T - \theta)$ or θ and T.I.P. may be taken as parameters and the last equation fit to a best straight line (62). The best straight line was taken to be that line on which the points did not deviate from the least squares line by more than the maximum error in χ_m and $1/(T - \theta)$.

The data analyzed in the above manner gave values for μ, θ, and T.I.P. shown in Table 29. Plots are shown in Figures 23-30. On Figure 27, the least squares points are obtained from the equation

$$\chi_m = 3.450/(T-\theta) - 3 \times 10^{-4}.$$

The magnetic moments agree reasonably well with literature values. Most of the other moments were calculated from susceptibility measurements taken at one temperature and as such should not be expected to represent the most accurate results.

TABLE 30

MAGNETIC DATA SUMMARY*

Compound	μ (B.M.)	θ (^{o}A)	T.I.P. (cgs x 10^{6})
$CoCl_2$	5.25, 5.29 (8) 5.38 (28)	25, 38 (8)	300
$Co(py)_{2/3}Cl_2$	5.10	19	50
$Co(py)Cl_2$	5.14	22	250
β $Co(py)_2Cl_2$	4.35, 4.60(16) 4.42 (1)	11, -4.8 (19)	0
α $Co(py)_2Cl_2$	5.05, 5.34(16) 5.15 (1) 5.10(13)	13, 8.3 (43)	100
$Co(py)_4Cl_2$	4.87, 4.85 (8)	16	300
$Co(py)_6Cl_2$	4.80	8	400

*(The second figure(s) is (are) from the literature)

There is no particular theoretical significance attached to θ other than that it is simply an empirical quantity which measures how far the origin of paramagnetism departs from the ideal basis upon which the Curie Law is derived. Deviations from a strict temperature dependence can be caused by T.I.P. or the thermal occupation of levels above the ground state level.

T.I.P. arises since the ground state is mixed to some extent with higher states which lie more than kT above the ground level such that thermal distribution between the levels does not occur and hence a contribution occurs which is independent of temperature. The main significance of the experimental T.I.P. is that they are small and therefore, the above description of the situation is satisfactory.

Fig. 23 -- $T^{o}A$ vs. $1/\chi_m^c$ for $CoCl_2$, $Co(py)Cl_2$ and $Co(py)_{2/3}Cl_2$

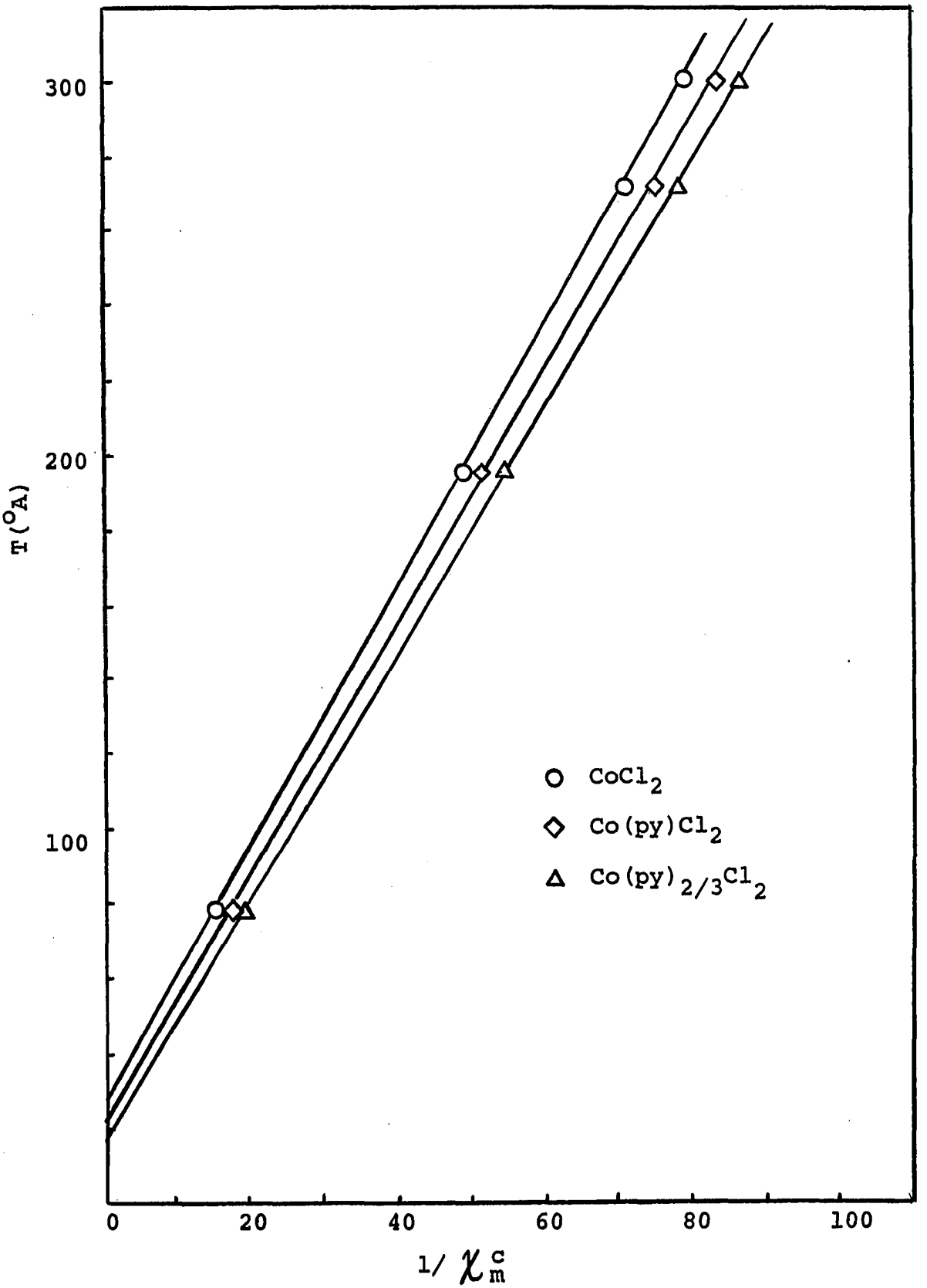

Fig. 24 -- $T^{o}A$ vs. $1/\chi_m^c$ for $\beta Co(py)_2Cl_2$

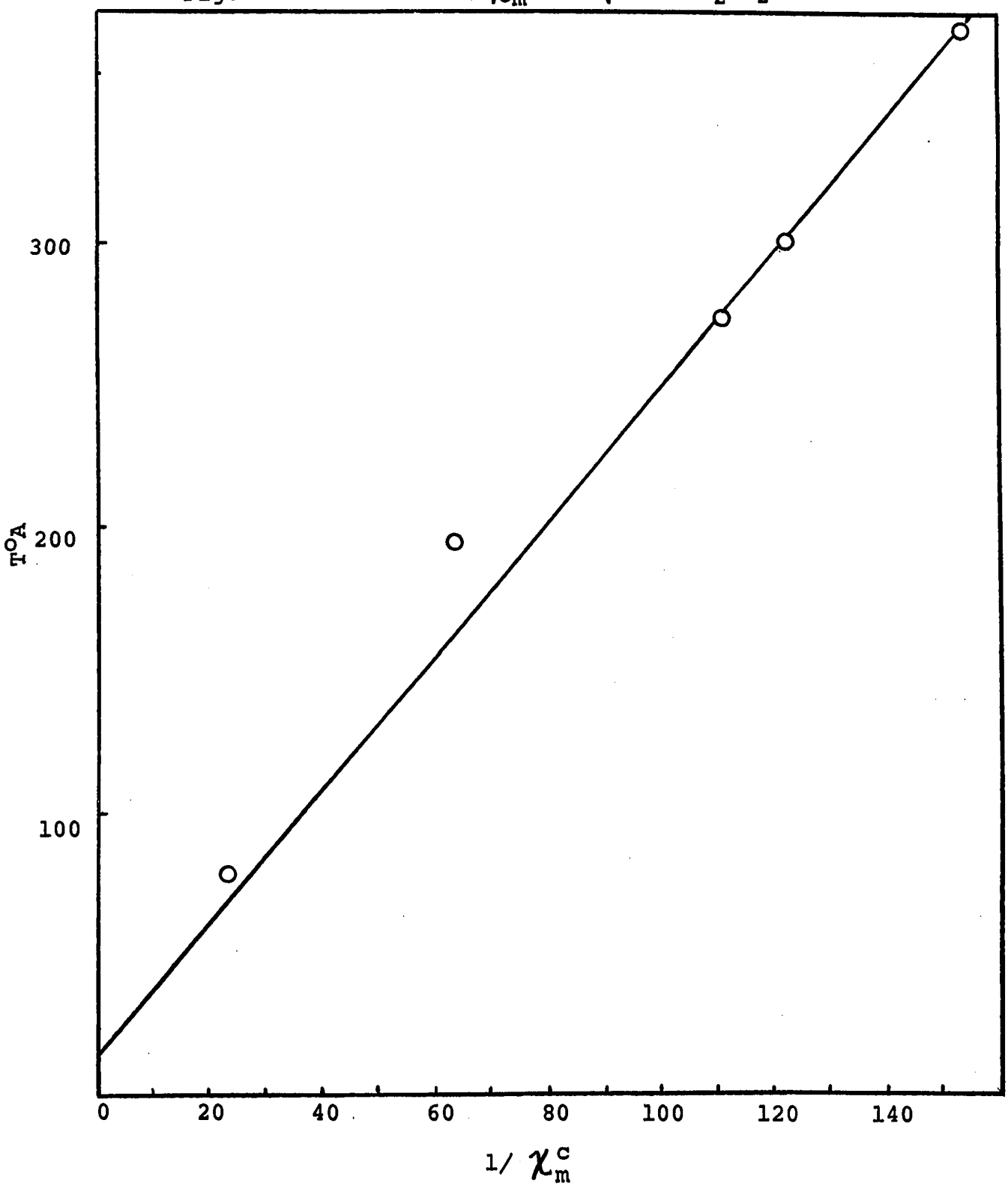

Fig. 25 -- $T^{o}A$ vs. $1/\chi_m^c$ for $\alpha Co(py)_2Cl_2$

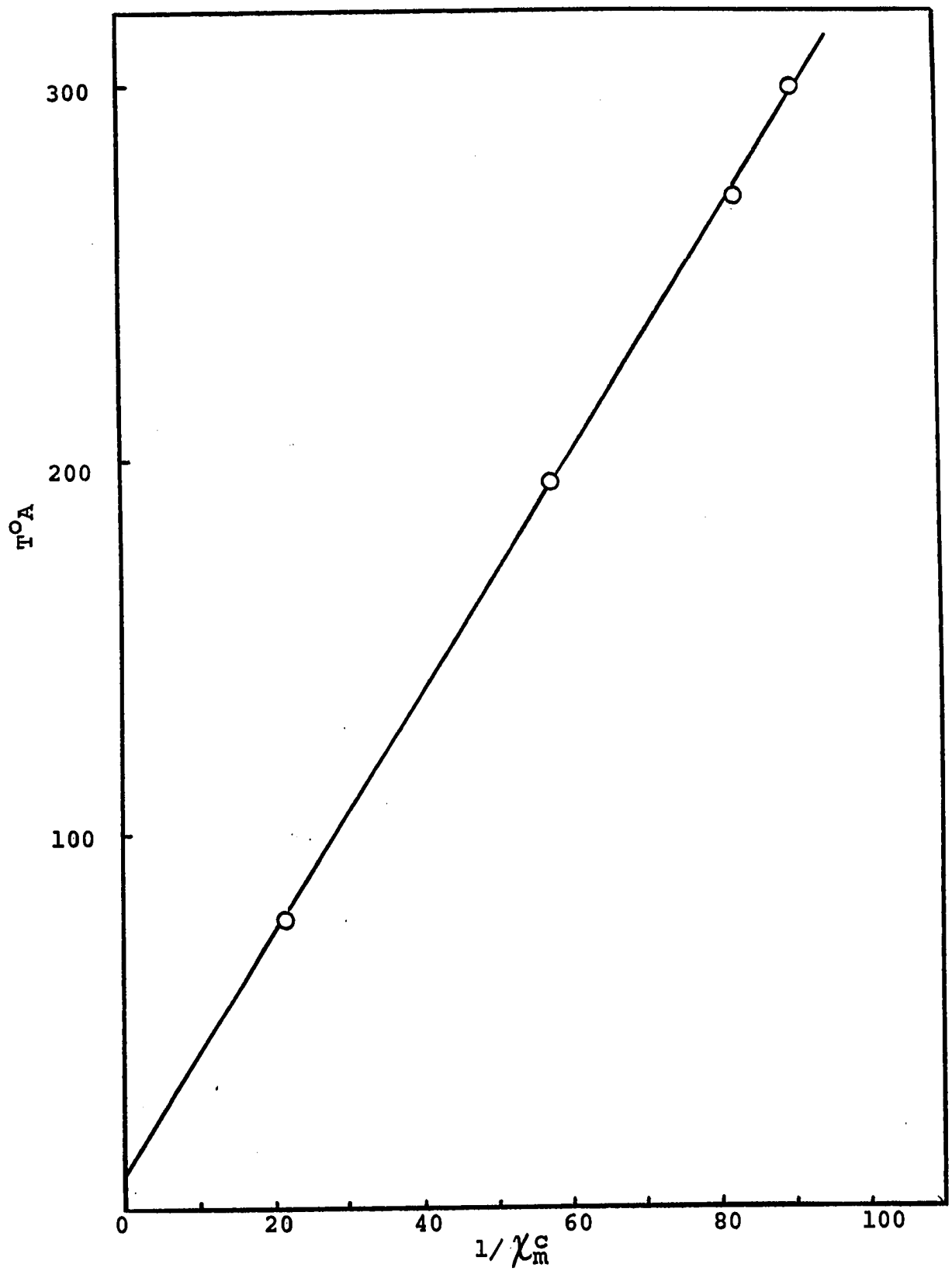

Fig. 26 -- $T^{o}A$ vs. $1/\chi_m^c$ for $Co(py)_4Cl_2$, $Co(py)_6Cl_2$

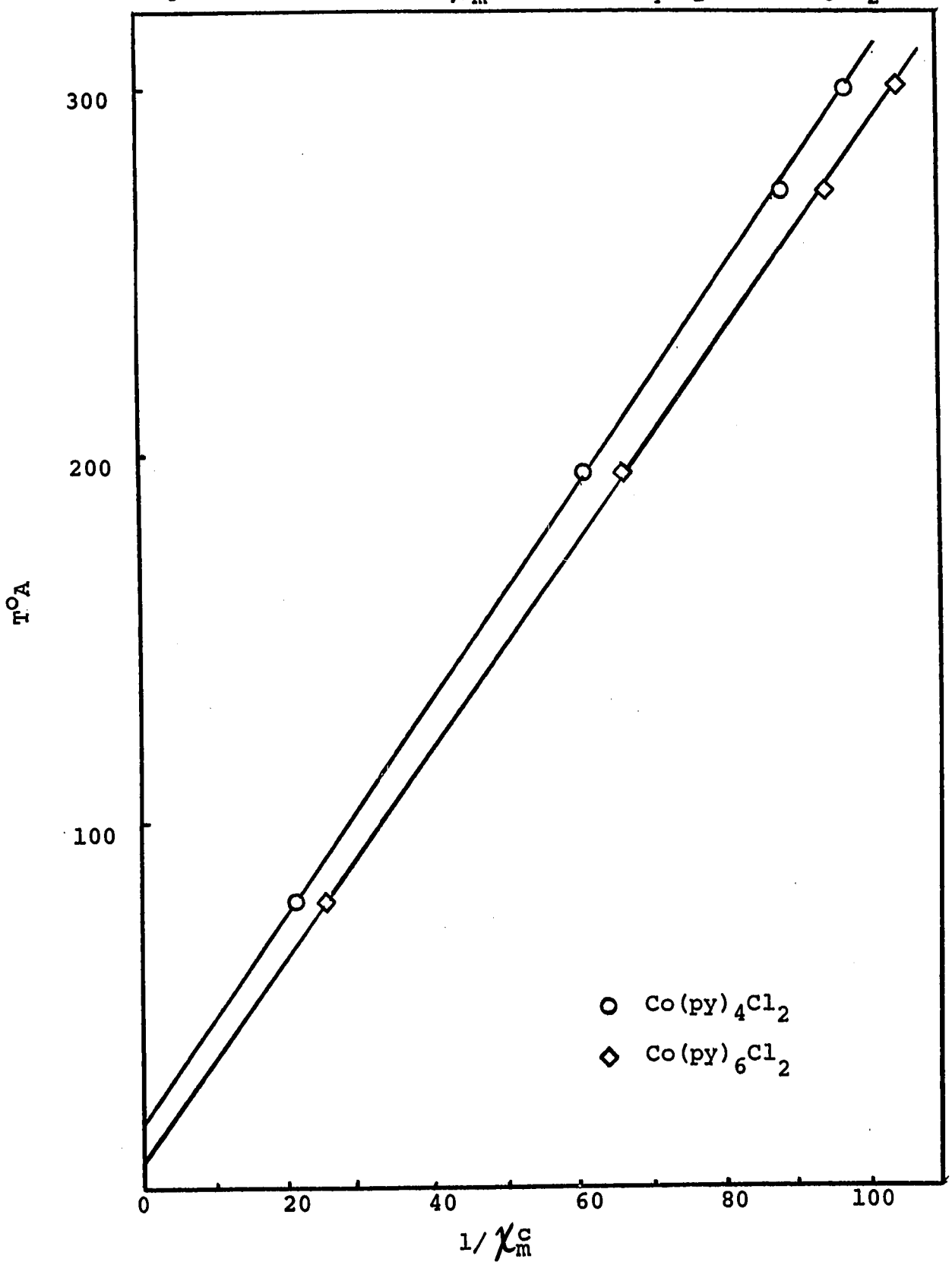

Fig. 27 -- χ_m vs. 1/T-Θ for $CoCl_2$

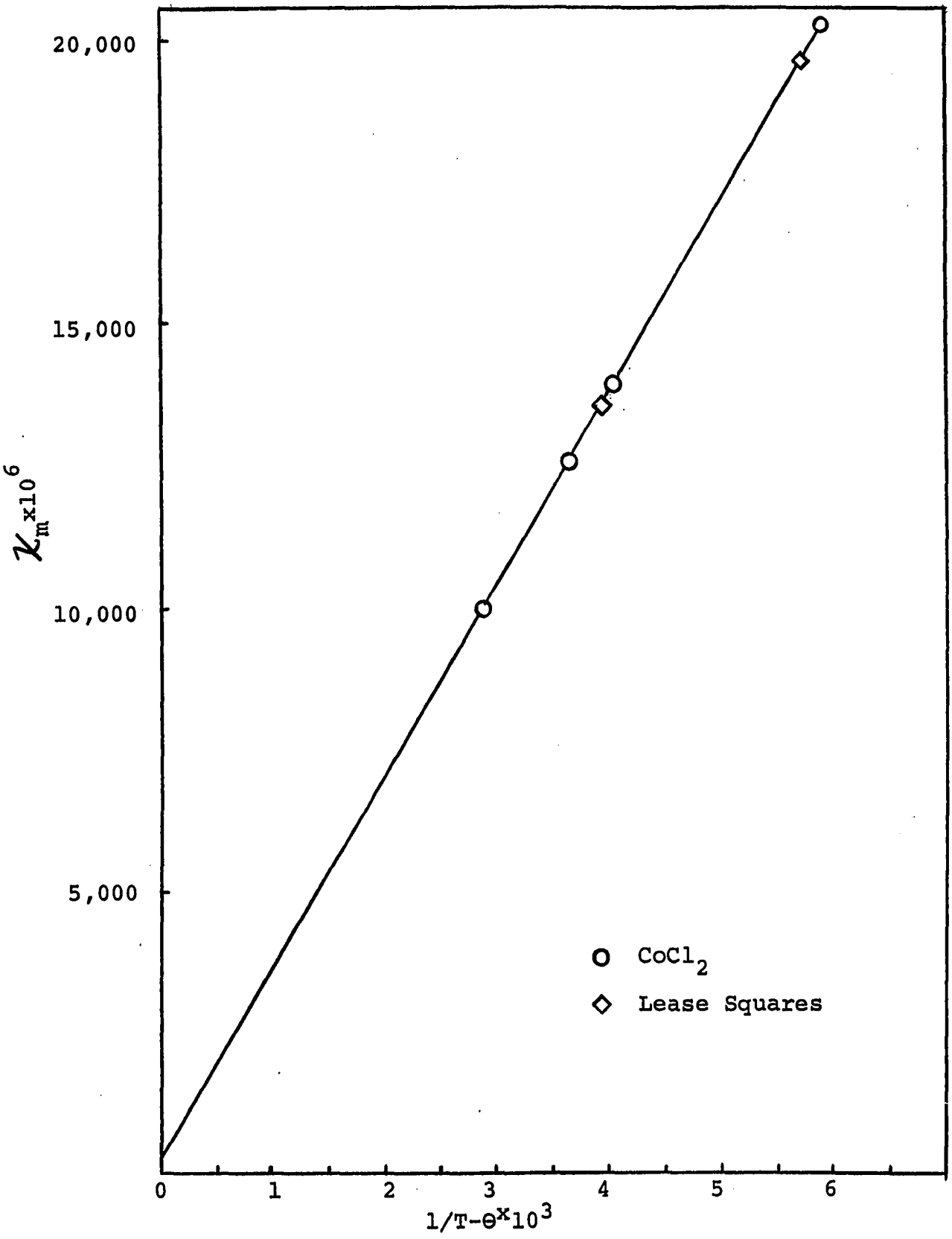

Fig. 28 -- χ_m vs. 1/T-θ for $\alpha Co(py)_2Cl_2$, $\beta Co(py)_2Cl_2$

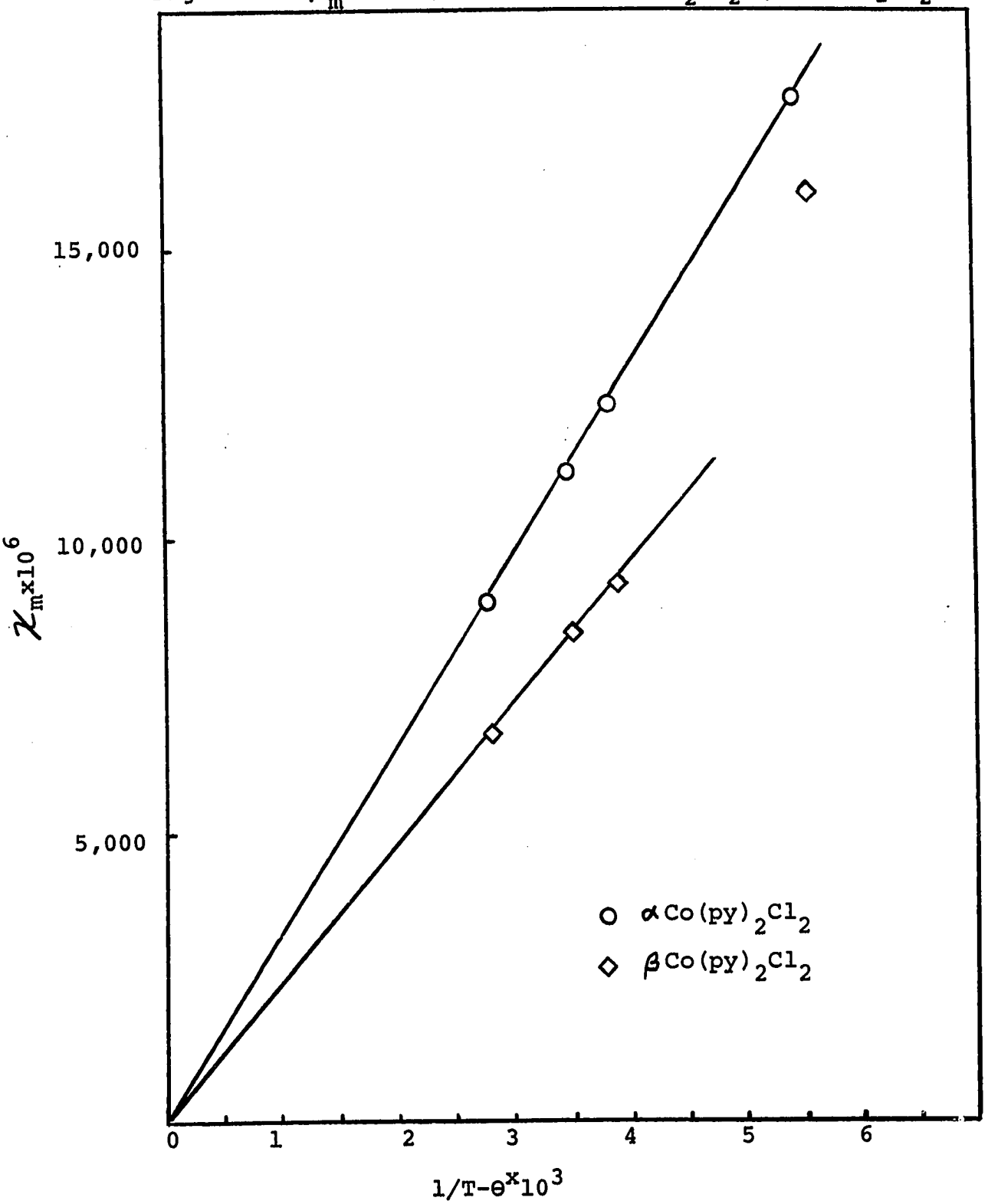

Fig. 29 -- χ_m vs. 1/T-θ for $Co(py)Cl_2$, $Co(py)_4Cl_2$

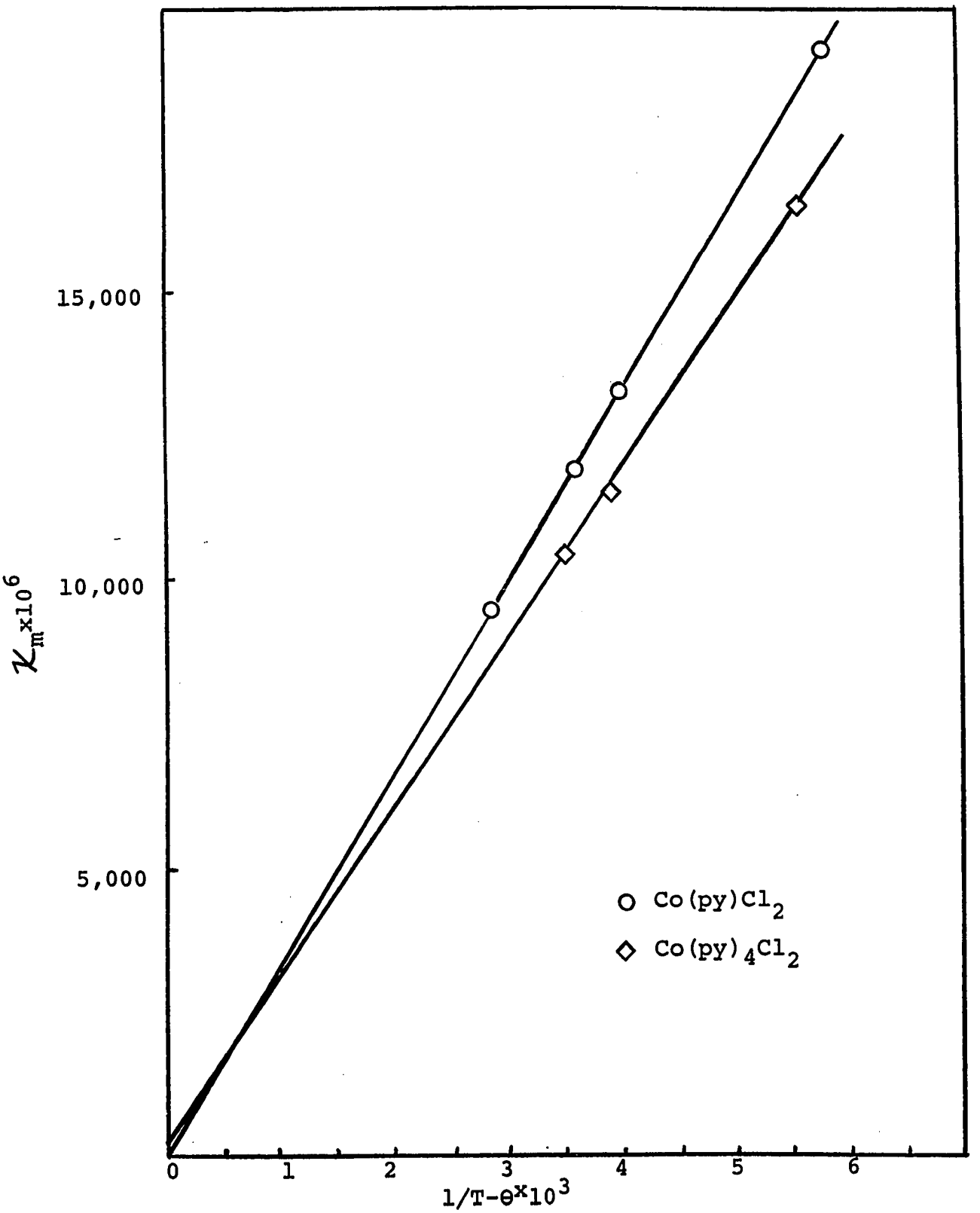

Fig. 30 -- χ_m vs. 1/T-θ for $Co(py)_6Cl_2$, $Co(py)_{2/3}Cl_2$

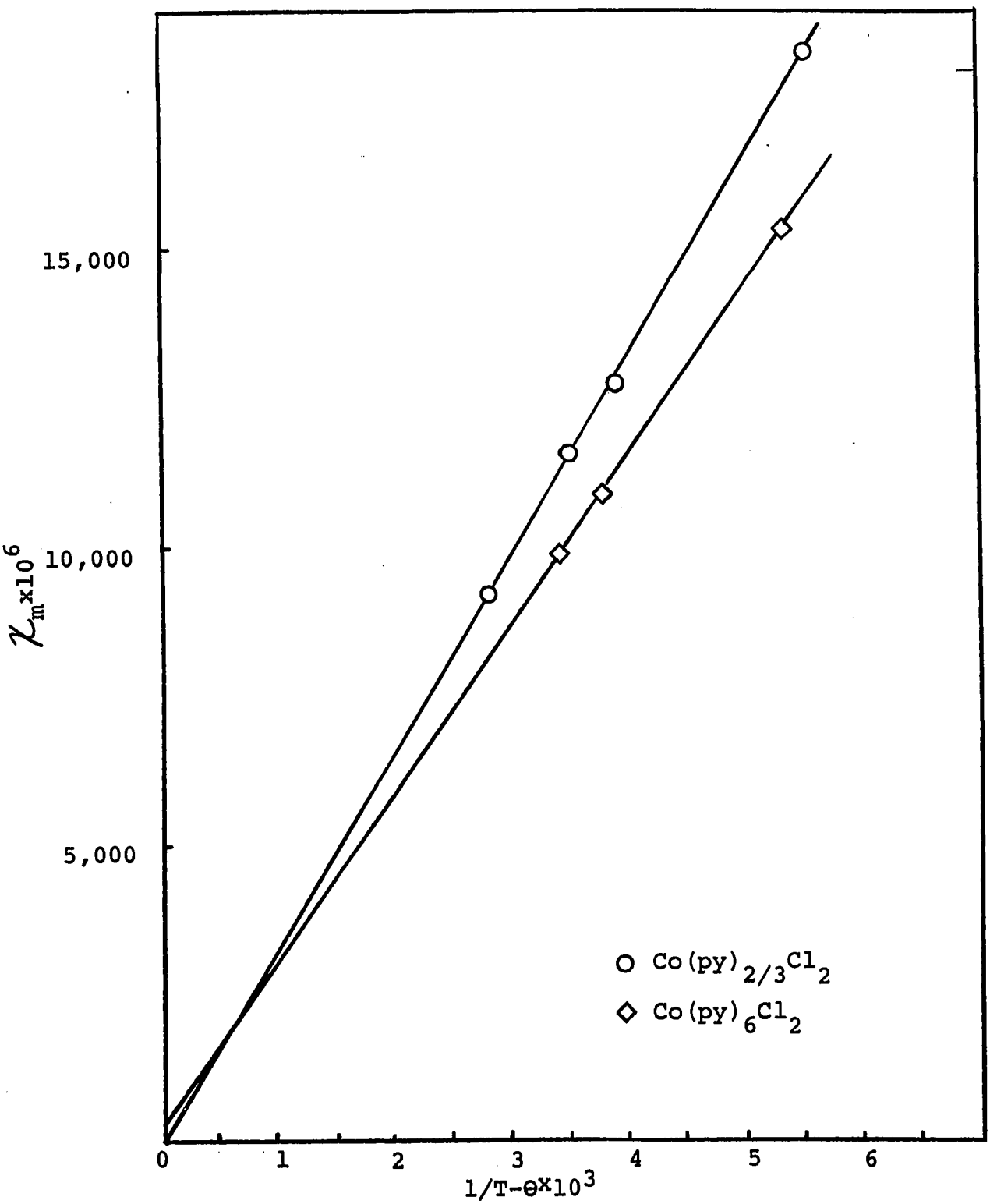

CHAPTER VI

GENERAL CONCLUSIONS AND DISCUSSION

Referring to Table 1, three of the pyridinate structures and $CoCl_2$ have been established by x-ray analysis and, as such, may be considered to be known exactly both in respect to site symmetry as well as crystal structure. From these known structures and the experimental evidence compiled, the unknown structures may be deduced (in so far as site symmetry and possible crystal symmetry) and a logical correlation obtained among the spectral, magnetic, and thermodynamic properties of the series.

Spectral evidence indicates that the species which has been referred to as $Co(py)_6Cl_2$ would better be shown as $\left[Co(py)_4Cl_2\right](py)_2$. That is, the inner coordination spheres of $Co(py)_6Cl_2$ and $Co(py)_4Cl_2$ are identical. The fact that the spectra are virtually identical and are fit satisfactorily under the tetragonal distortion scheme indicates that the ligand arrangement about the cobalt ion is the same. Since two additional molecules of pyridine must be fit into the crystal structure of $Co(py)_6Cl_2$, the nearest neighbor perturbation would be somewhat different in the two cases

and would account for minor differences in absorption peak shapes, intensities, and slight energy shifts.

It is not necessarily surprising to find that the inner coordination sphere of $Co(py)_6Cl_2$ contains four pyridines and two chlorides since the same general situation exists in the case of cobalt(II) chloride hexahydrate where it was shown (27) that the inner coordination sphere consisted of four water molecules and two chlorides. The other two waters form hydrogen bonding bridges between $Co(H_20)_4Cl_2$ octahedra. However, in the case of $Co(NH_3)_6Cl_2$ (and $Co(NH_3)_6Cl_3$) the inner coordination sphere consists of six ammonia molecules with the chlorides external to the $Co(NH_3)_6^{+2}$ octahedra. (As shown by the molecular distances: Co - N, 2.12 Å; Co - Cl, 4.37 Å (64)).

Further evidence for similar octahedral environments is provided by the similarity of the magnetic moments of $Co(py)_6Cl_2$ and $Co(py)_4Cl_2$, respectively 4.80 and 4.87 B. M. The moments are similar to other known "octahedral" environments under a tetragonal distortion potential. For example: $Co(H_20)_6Cl_2$, 4.98 B. M. and $Co(H_20)_4Cl_2$, 5.13 B.M.(32).

In general, a reduction is shown from the magnetic moment obtained in a more regular octahedral environment such as is seen in $CoCl_2$ (μ = 5.29 B.M.). This is attributed to the reduction of the orbital angular momentum contribution to the total moment due to the removal of

degeneracy within the t_{2g} octahedral level and hence the partial quenching of the orbital contribution with the loss of equivalency among the d_{xz}, d_{yz}, and d_{xy} orbitals. Referring to the $^4A_{2g}$ ground state configuration for z axis elongation given in Chapter IV, the e_g degenerate set (d_{xz} and d_{yz}) is completely filled and no orbital contribution is possible.

From the crystal structure data available for $Co(py)_4Cl_2$, especially the unit cell dimensions (a = b = 16 Å, c = 17 Å) and the bond lengths within the molecule, it may be shown that the major structural determining factor is simply close packing of the molecules (body centered tetragonal or ditetragonal bipyramidal, nine molecules) and the effect of intermolecular van der Waal's forces is secondary.

The molecules ($Co(py)_4Cl_2$) are situated in a manner such that the "correct" bonding portions of neighboring molecules are adjacent. That is, the two chlorides of the central $Co(py)_4Cl_2$ molecule (which is at the apex of the two pyramids) within the unit cell are immediately above and below four pyridine molecules which are bonded to molecules situated at the corners of the bases of the pyramids. Certainly electrons are donated from the pyridine molecule to the central cobalt ion (i.e. nitrogen electrons dislocated to some extent into the cobalt orbitals if a bond is to be formed). Thus the ring may be considered to be

electron deficient since the partial positive charge on the nitrogen would be delocalized onto the ring (reasonance stabilization).

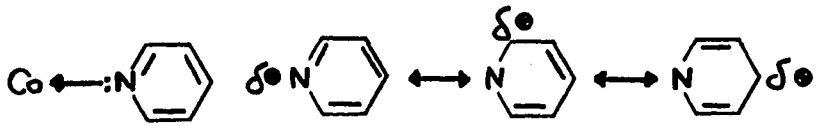

Therefore, the pyridine rings and the chlorides (which bear a partial negative charge) are correctly oriented for a possible interaction. However, the distance between the chlorides and the rings is rather large compared to what would be expected for a significant interaction.

Fig. 31 -- $Co(py)_4Cl_2$ Ditetragonal Bipyramidal Crystal Structure

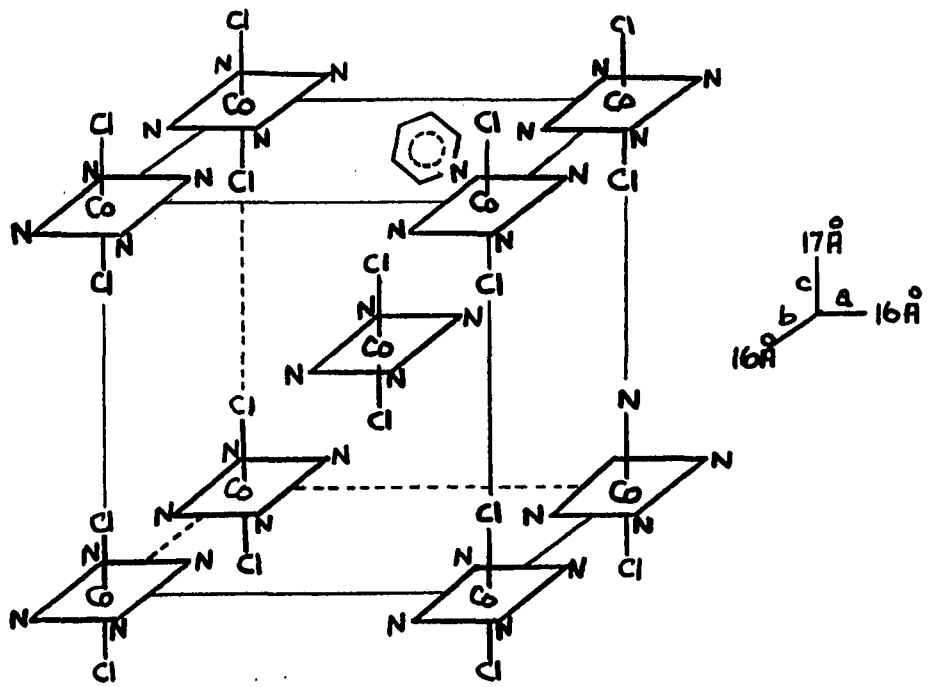

The distance between the chloride and the nearest hydrogen of a ring (i.e. the distance between the outer limits of the van der Waal's radii), even considering that the rings are rotated 45° with respect to the plane of the four nitrogens about the cobalt, is greater than one angstrom.

The incorporation of two additional pyridine molecules exterior to the inner coordination sphere would produce a considerable disordering within the close packed structure. Just how, exactly, the pyridine molecules are oriented with respect to the $Co(py)_4Cl_2$ molecules is unknown; however, the only possible bonding would be through a dipole-dipole interaction between pyridine (one contained within and the other exterior to the inner coordination sphere) or between the pyridine dipole and the chloride which carries a partial negative charge. Since only two additional pyridines are incorporated into the structure and there are, of course two chlorides per $Co(py)_4Cl_2$ molecule (whereas there are four pyridines), it would not be illogical to assume some interaction through the two chlorides. A structure which may be easily pictured would consist of a chain of $Co(py)_4Cl_2$ molecules oriented with respect to one another by a bridging pyridine molecule (with correct dipole orientation) between a chloride of one molecule and a pyridine ring of an adjacent molecule. Such chains would be crosslinked so that the net result is the association of one molecule of pyridine with each

chloride which fits the stoichiometry of the $Co(py)_6Cl_2$ complex.

Fig. 32 -- Postulated Structure $Co(py)_6Cl_2$

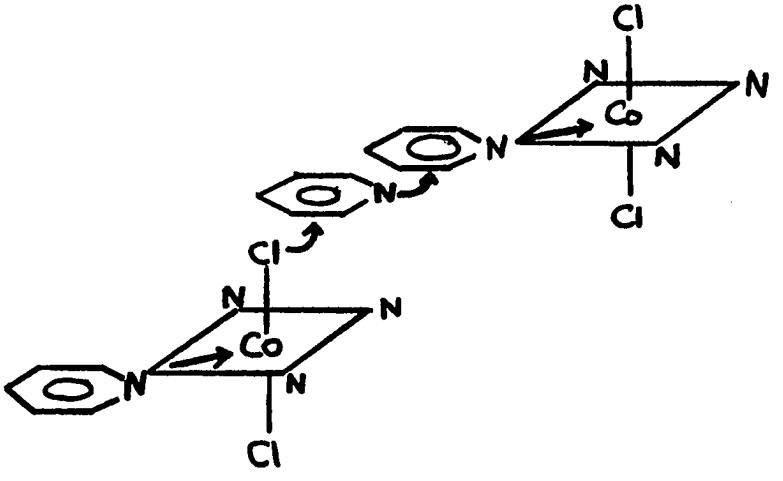

The fact that considerable structural ordering occurs with the removal of two moles of pyridine from $Co(py)_6Cl_2$ is evidenced by the fact that the difference in entropies of formation of $Co(py)_6Cl_2$ and $Co(py)_4Cl_2$ is 101 eu/mole.

This entropy difference may be better examined in the following manner. Taking the depyridination in general,

$$Co(py)_nCl_2(s) = Co(py)_{n-m}Cl_2(s) + mPy(v)$$

where $\Delta S = \sum [S_f(\text{products}) - S_f(\text{reactants})]$,

therefore, $\Delta S = [S_{f(n-m)} - S_{f(n)}] + mS_{fPy(v)}$.

Furthermore, the formation of the complex may be considered to take place in steps with the formation of the inner coordination sphere initially and then the union of these molecular units to form the crystal structure. This, of course, is an artificial concept. The actual formation

of the crystal may just as well occur by means of a concerted mechanism whereby the coordination sphere and the crystal structure are formed simultaneously. However, since entropy is a state function, the following is valid. Therefore, the entropy of formation of the whole crystal is the sum of the entropy of formation of the coordination sphere, $S_{f\ cs}$ and the entropy of formation of the crystal structure, $S_{f\ cryst}$,

$$S_{f(n-m)} = S_{\underset{Cryst}{f(n-m)}} + S_{f_{cs}(n-m)}$$

$$S_{f(n)} = S_{\underset{Cryst}{f(n)}} + S_{\underset{cs}{f(n)}}$$

and $$\Delta S = S_{\underset{Cryst}{f(n-m)}} + S_{\underset{cs}{f(n-m)}} - S_{\underset{Cryst}{f(n)}} - S_{\underset{cs}{f(n)}} + mS_{fPy(v)}$$

$$= \left[S_{f(n-m)} - S_{f(n)}\right]_{cryst} + \left[S_{f(n-m)} - S_{f(n)}\right]_{cs} + mS_{fPy(v)}$$

If the cobalt ion environment remains the same in $Co(py)_4Cl_2$ and $Co(py)_6Cl_2$ then the entropy contribution to the entropy of formation will be constant and the difference in entropies will cancel this contribution. That is, in terms of the above, $\left[S_{f(4)} - S_{f(6)}\right]_{cs} = 0$. Then from Table 13, $\left[S_{f(4)} - S_{f(6)}\right]_{cryst} = 101$ eu/mole.

The entropy of formation of $Co(py)_6Cl_2$ contains the entropy of formation of two moles of pyridine in the solid state. This is assuming that the entropy of formation of pyridine in the solid state would be approximately the same

in those instances where the pyridine molecules are oriented by dipolar interaction or by van der Waal's forces, in general within some solid matrix. This implies that the number of internal and external vibrational degrees of freedom of the pyridine molecule remains constant under such conditions. In this manner, the pyridine molecules within the crystal lattice of solid pyridine and those pyridine molecules external to the inner coordination sphere in $Co(py)_6Cl_2$ may be favorably compared.

The entropy of formation of solid pyridine may be estimated since the entropy of formation of liquid pyridine (42.8 eu/mole) and the heat of fusion (1.8 kcal/mole) of pyridine are known. Therefore the entropy of fusion is approximately 6 eu/mole and,

$$S_{fPy(s)} = S_{fPy(l)} - \Delta S_{fus.} \cong 36.8 \text{ eu/mole.}$$

The entropy of formation of two moles of solid pyridine is approximately 74 eu. This indicates that 101-74 or approximately 27 eu/mole is the entropy decrease due to a change in the crystal structure going from $Co(py)_6Cl_2$ to $Co(py)_4Cl_2$.

The removal of two moles of pyridine from $Co(py)_4Cl_2$ produces a known transition from the monomeric $Co(py)_4Cl_2$ to the polymeric octahedral $\alpha Co(py)_2Cl_2$ structure where two chlorides are shared between adjacent cobalts with the

pyridines situated above and below the cobalt. (This is directly analogous to the behavior of the corresponding hydrates.) The change to the polymeric system with the formation of actual "bonds" between molecular units is accompanied by a large decrease in the entropies of formation. (96.9 eu/mole entropy difference between $Co(py)_4Cl_2$ and $\alpha Co(py)_2Cl_2$). Of this entropy difference, approximately 23 eu/mole would constitute the sum of the change in inner coordination sphere and crystal structures. However in this case, the pyridine is removed from a fully bonded state and the comparison with the entropy of formation of solid pyridine would not necessarily be valid since bound pyridine would gain vibrational degrees of freedom.

The spectrum of $\alpha Co(py)_2Cl_2$ is similar in general form to that of $Co(py)_4Cl_2$ and $Co(py)_6Cl_2$, however it differs considerably in detail due to a change from z axis elongation to z axis compression and an accompanying slight rhombic distortion which removes the degeneracy of the ground state. This change in spectrum has been discussed previously in some detail.

The magnetic moment of $\alpha Co(py)_2Cl_2$ increases to a value of 5.05 B.M. This is explained in terms of the ground state d orbital occupancy in which the e_g level contains the unpaired electron. (Page 59, ground state configuration for axial compression) This means an orbital

angular momentum contribution is more likely, thus the increased magnetic moment.

The transition from violet, octahedral α $Co(py)_2Cl_2$ to deep blue, tetrahedral β $Co(py)_2Cl_2$ is accompanied by a definite increase in the disorder of the system due to a change from the polymeric octahedral to a monomeric tetrahedral system. The difference in entropies (11.4 eu/mole) is relatively small, however, since there is no release of pyridine into the vapor phase.

This general type of isomeric transition is known to occur in other cobalt-pyridine salts. For example, $Co(py)_2(SCN)_2$ and $Co(py)_2(OCN)_2$ both form polymeric octahedral and monomeric tetrahedral compounds; however, neither $Co(py)_2Br_2$ or $Co(py)_2I_2$ form the octahedral polymer(65).

The β $Co(py)_2Cl_2$ spectrum corresponds to the general tetrahedral form having the transition to the $T_{1g}(P)$ state at 600 mμ (similar to $CoCl_4^{=}$ and other such tetrahedral ions in solution as discussed previously) as compared to the system around 500 mμ for the $Co(py)_6Cl_2$, $Co(py)_4Cl_2$, and α $Co(py)_2Cl_2$ octahedral forms. The best experimental evidence for the tetrahedral configuration (other than direct x-ray determination) is the marked decrease in magnetic moment from 5.05 B.M. in α to 4.35 B.M. which is generally indicative of a tetrahedral environment in which there is no orbital angular momentum contribution.

A further analysis of the reactions involving $Co(py)_4Cl_2$, α $Co(py)_2Cl_2$ and β $Co(py)_2Cl_2$ is possible since the equilibrium

$$Co(py)_4Cl_2 = \beta Co(py)_2Cl_2 + 2py$$

has been studied in chloroform solution (4). The species present in a solution of either α or β $Co(py)_2Cl_2$ and pyridine in chloroform are octahedral $Co(py)_4Cl_2$ molecules, tetrahedral $Co(py)_2Cl_2$ molecules, and pyridine molecules. (This reaction has been mentioned previously in Chapter I.) From the temperature dependence of the equilibrium constant (determined spectrophotometrically), ΔS for this reaction was determined.

$$\Delta S = \left[(S_{f\beta} - S_{f(4)}) + 2S_{f(py)}\right]_{(CHCl_3)} = 46.8 \text{ eu/mole}$$

If the assumption can be made that the entropy of formation of pyridine in chloroform is similar to the entropy of formation of liquid pyridine then a further comparison can be made. The entropy of formation of pyridine in chloroform would contain the entropy of mixing which is, of course, an extensive property. Strictly for the purpose of a rough comparison, it may be argued that there is a similarity between the solution entropy of formation and the formation of the pure liquid. Certainly, the pyridine molecules will gain some translational and rotational freedom, but are still held within a liquid lattice with considerable dipole-dipole interaction. The magnitude of the

entropy increase would assuredly not be anything comparable to that attained in the transition from the liquid to the vapor state. If then the entropy of mixing is ignored and the $S_{f(py)(l)}$ is taken to be approximately 43 eu/mole,

$$(S_{f\beta} - S_{f(4)}) = -39 \text{ eu/mole.}$$

Since there is no lattice formation in solution (in the dilute solution, molecular interaction can be ignored and assuming solvent interaction will be generally the same for both molecules) then this difference may be taken as the approximate difference in coordination sphere entropies. That is,

$$(S_{f\beta} - S_{f(4)})_{cs} = -39 \text{ eu/mole}$$

Now from Table 13,

$$(S_{f\beta} - S_{f(4)}) = -85.5 \text{ eu/mole}$$

or $(S_{f\beta} - S_{f(4)})_{cryst} + (S_{f\beta} - S_{f(4)})_{c.s.} = -85.5$ eu/mole

then $(S_{f\beta} - S_{f(4)})_{cryst} = -85.5 + 39 = -47$ eu/mole.

This value is somewhat greater than the difference for $Co(py)_6Cl_2$ and $Co(py)_4Cl_2$ or $Co(py)_4Cl_2$ and $\alpha Co(py)_2Cl_2$ but this is not unreasonably large since the intermolecular forces between the tetrahedral monomers might well be rather weak.

The removal of one mole of pyridine from $\beta Co(py)_2Cl_2$ is accompnaied by a pronounced change in color (deep blue to a pale blue violet), in magnetic moment (4.35 to 5.14 B.M.) and in spectrum. The higher magnetic moment is indicative

of a change back to octahedral configuration and in particular a more symmetrical structure. The spectrum changes considerably; the large prominent peaks at 950 and 1250 mμ of the β $Co(py)_2Cl_2$ disappears and a new peak appears at 750 mμ in $Co(py)Cl_2$. Also as shown previously, the $Co(py)Cl_2$ spectrum is very close to $CoCl_2$, further indication of the resumption of octahedral coordination with a configuration close to that of $CoCl_2$.

The entropy of formation difference,

$$[S_{f(l)} - S_{f\beta}] = -45 \text{ eu/mole}$$

is indicative of ordering (or an increase in the number of degrees of freedom coincident with the establishment of higher symmetry) within the crystal structure or site symmetry. This is in agreement with a change from monomeric tetrahedral to a cobalt chloride like octahedral structure.

Thus the evidence (especially spectral and magnetic moment at this point) indicates that the cobalt environment in $Co(py)Cl_2$ is essentially the same as in cobalt chloride (i.e. the coordination sphere consists of six chlorides) with the pyridine nitrogen no longer bound directly to the cobalt.

There is apparently little further change in the inner coordination sphere as evidenced by the spectral and magnetic moment similarity (μ = 5.10 B.M. in $Co(py)_{2/3}Cl_2$) in either the removal of 1/3 mole pyridine per mole of $Co(py)Cl_2$ and the formation of $Co(py)_{2/3}Cl_2$ or the complete

depyridination with the removal of 2/3 mole pyridine per mole of $Co(py)_{2/3}Cl_2$. Further evidence of the structural similarity of $Co(py)Cl_2$, $Co(py)_{2/3}Cl_2$, and $CoCl_2$ is seen from the fact that the entropy difference between $Co(py)_{2/3}Cl_2$ and $CoCl_2$(23.9 eu/mole) is approximately twice that between $Co(py)Cl_2$ and $Co(py)_{2/3}Cl_2$ (12.2 eu/mole). The difference in pyridine content is, of course, in the same ratio.

Examining the entropies more closely,

$$[S_{f(2/3)} - S_{f(1)}] = [S_{f(2/3)} - S_{f(1)}]_{cryst} + [S_{f(2/3)} - S_{f(1)}]_{cs}$$
$$= -12.2 \text{ eu/mole.}$$

$$[S_{fCoCl_2} - S_{f(2/3)}] = [S_{fCoCl_2} - S_{f(2/3)}]_{cryst} + [S_{fCoCl_2} - S_{f(2/3)}]_{cs} = -23.9 \text{ eu/mole}$$

These are, however, the entropy differences per mole of complex. The differences in entropy per mole of pyridine removed are therefore given,

$Co(py)Cl_2 \longrightarrow Co(py)_{2/3}Cl_2$: $3(-12.2) = -36.6$ eu/molePy

$Co(py)_{2/3}Cl_2 \longrightarrow CoCl_2$: $3/2(-23.9) = -35.8$ eu/molePy

Assuming that $CoCl_2$, $Co(py)_{2/3}Cl_2$, and $Co(py)Cl_2$ have the same coordination sphere, these contributions will cancel. Therefore,

$$[S_{f(2/3)} - S_{f(1)}]_{cs} = 0$$
$$[S_{fCoCl_2} - S_{f(2/3)}]_{cs} = 0.$$

Furthermore since the pyridine is evidently exterior to the inner coordination sphere, the entropy of formation of pyridine in these complexes would be approximated by $S_{fPy(s)}$ (36.8 eu/mole) as discussed previously. It can be seen that both entropy differences above correspond very closely to this value. This indicates that the total difference in entropy in both cases is due to the formation of pyridine in the solid state. That is,

$$\left[S_{f(2/3)} - S_{f(1)}\right]_{cryst} = 0$$

$$\left[S_{fCoCl_2} - S_{f(2/3)}\right]_{cryst} = 0.$$

This does not prove that the crystal structures are the same in these compounds but rather indicates that the entropies of formation are similar.

If the above assumptions are correct, then the entropy of reaction per mole of pyridine removed for $Co(py)Cl_2$ going to $Co(py)_{2/3}Cl_2$, and $Co(py)_{2/3}Cl_2$ going to $CoCl_2$, should each be equal to the entropy of formation of pyridine vapor from pyridine solid (i.e. the entropy of sublimation). From Table 12 the reaction entropies are seen to be in order 12.9 eu/mole and 26.2 eu/mole. Therefore per mole of pyridine,

$$\Delta S_{1 \rightarrow 2/3} = (3)(12.9) = 38.7 \text{ eu/mole Py}$$

$$\Delta S_{2/3 \rightarrow CoCl_2} = (3/2)(26.2) = 39.3 \text{ eu/mole Py}$$

The entropy of sublimation may be estimated as the sum

of the entropy of vaporization and the entropy of fusion,

$\Delta S_{sub.} = 32.6 + 6 = 38.6$ eu/mole Py.

This value compares favorably with the reaction entropies.

The apparent fact that the pyridine is external to the coordination sphere of the cobalt in $Co(py)Cl_2$ (and $Co(py)_{2/3}Cl_2$) is in opposition to the behavior of cobalt(II) chloride monohydrate where the site symmetry remains octahedral and the water remains within the coordination sphere. The reflectance spectrum of the monohydrate is, therefore, generally the same as that of the previous octahedral compounds in the series. The structure of the monohydrate (66) is similar to the dihydrate in that long polymer chains are formed by the sharing of chlorides between adjacent cobalts, but in the monohydrate, the water molecules above and below the chloride plane are also shared between cobalts of adjacent chains. The sharing of a water molecule is facilitated by the fact that the oxygen has two lone pairs of electrons. A similar structure for the pyridine molecule would be, therefore, less likely and, apparently, the more stable structure is a rearrangement such that a site symmetry similar to that of cobalt(II) chloride is attained. The exact crystal structure of $Co(py)Cl_2$ cannot be determined with the information available.

The $Co(py)_{2/3}Cl_2$ type compound apparently does not occur with other ligands (i.e. they are not reported) and its crystal structure remains undetermined.

REFERENCES

(1) N. S. Gill and E. Nyholm, Jour. Inorg. Nucl. Chem., 18 (1961), 88.

(2) L. Katzin El Al., Journal of the American Chemical Society, 72 (1950), 5471.

(3) L. Katzin Et Al, Jour. Amer. Chem. Soc., 75 (1953), 2830.

(4) H. A. King Et Al, Jour. Chem. Soc., 166 (1963), 5449.

(5) A. V. Ablov, Et Al, Zhur. Neorg. Khim., 4 (1959), 2480.

(6) J. A. Friend, D. P. Mellor, Journal of the Proceedings of the Royal Society of New South Wales, 81, (1947), 154.

(7) M. A. Porai-Koshits, Akad. Nauk. SSSR, No. 29, (A55), 19.

(8) F. A. Cotton, R. Holm, Journ. Amer. Chem. Soc., 82 (1960), 2983.

(9) Gmelin's Handbuch der Anorganishe Chemie, vol. 58 (1963), Verlag Chemie.

(10) F. Reitenstein, Annalen, 282 (1894), 267.

(11) T. Hantzsh and L. Schlegel, Zeit. Fur Anorg. Chemie, (1927), 273.

(12) Gox Et Al., Jour. Chem. Soc., (1937), 1556.

(13) C. Furia, M. Geroni, Ricerva Sci., 30 (1960), 1016.

(14) T. I. Malinovskii, Soviet Physical Crystallography, 2 (1957), 732.

(15) J. D. Dunitz, Acta Crystalographia, 10 (1957), 307.

(16) D. Melior and C. D. Coryell, Jour. Amer. Chem. Soc., 60, (1938), 1786.

(17) W. Brode, Jour. Amer. Chem. Soc., 53 (1931), 2457.

(18) C. J. H. Schutte, Zeit. Naturforshung, 18u (1963), 525.

(19) N. S. Gill Et Al., Jour. Inorg. Nucl. Chem., 18 (1961), 79.

(20) R. P. Bauman, Absorption Spectroscopy, John Wiley, New York, 1962.

(21) R. J. H. Clark Et Al., Inorg. Chem., 4 (1963), 350.

(22) W. Heiber, Zeit. Anorg. Chem., 186 (1930), 104.

(23) L. R. Ocone Et Al., Jour. Inorg. Nucl. Chem., 15 (1960), 70.

(24) O. Stellung, Zeit. Fur Phys. Chem., 16 (1932), 317.

(25) L. R. Ocone Et Al., Jour. Inorg. Nucl. Chem., 15 (1960), 1412.

(26) S. Sugden, Jour. Chem. Soc., (1943), 328.

(27) J. Mizuno, Jour. Phys. Soc. Japan, 15 (1960), 1412.

(28) N. Elliot, Jour. Chem. Phys., 21 (1953), 890.

(29) J. Sacconi, Et Al., Jour. Chem. Soc.,(1958), 848.

(30) J. Zachoual, Et Al., Collection Czech. Chem. Comm., 28 (12), (1963), 3450.

(31) H. M. Powell and A. F. Wells, Jour. Chem. Soc.,(1935), 359.

(32) W. K. Grindstaff, Ph.D. Dissertation, Univ. of Okla., 1966.

(33) C. H. Sorum, Semimicro Qualitative Analysis, Prentice Hall, Inc., New York, 1960.

(34) "Montecatini" Societa Generale per l'Industria Mineriae Chimica, British Patent 924,244, April 24, 1963.

(35) W. W. Wendlandt, T. D. George, Chem. Analysis, 53, 100.

(36) G. H. Ayres, Quantitative Chemical Analysis, Harper, 1958, 609.

(37) N. H. Furman, Ed., Scotts Standard Methods of Chemical Analysis, 5th Edit., Vol. 2, 315.

(38) I. Koltoff, M. Bruckenstein, Jour. Amer. Chem. Soc., 78, (1956), 1.

(39) C. N. Reilly, D. T. Sawyer, Experiments for Instrumental Methods, McGraw-Hill, 1955.

(40) C. D. Hodgeman, Ed., Handbook of Chemistry and Physics, 43rd, Chem. Rubber Pub. Co., 1961.

(41) S. D. Christian, Jour. Chem. Ed., 43, (1966), 432.

(42) NBS, C500, Selected Values of Chemical Thermodynamics Constants, 253.

(43) W. N. Hubbard, Jour. Phys. Chem., 65 (1961), 1326.

(44) J. Timmermans, Physio-Chemical Constants of Organic Compounds, Vol. 2, Elsevier Pub. Co., 1965, 358.

(45) G. S. Parks Et Al., Jour. Amer. Chem. Soc., 58 (1936), 400.

(46) W. Hieber, A. Woerner, Zeit. Electrochemie, 40 (1934), 256.

(47) J. Ferguson Et Al., Jour. of Chem. Phys., 39 (1963), 881.

(48) J. C. Slater, Quantum Theory of Atomic Structure, Vol. I, McGraw-Hill, 1960, 215.

(49) C. J. Ballhausen, Introduction to Ligand Field Theory, McGraw-Hill, 1962.
(a) p. 61 (b) p. 100 (c) p. 111 (d) p. 14

(50) H. Eyring, J. Walter, G. E. Kimball, Quantum Chemistry, John Wiley, 1944, p. 369, p. 98.

(51) K. W. H. Stevens, Proceeding of the Royal Physics Soc., A65 (1952), 209.

(52) F. A. Cotton, Chemical Applications of Group Theory, Interscience, 1963.

(53) C. J. Ballhansen, W. Moffitt, Jour. of Inorg. and Nucl. Chem., 3 (1956), 178.

(54) J. Ferguson, J. Chem. Phys., 32 (1960), 533.

(55) E. B. Wilson, J. C. Declus, P. C. Cross, Molecular Vibrations, McGraw-Hill, 1955.

(56) K. Nakamoto, IR Spectra of Inorganic and Coordination Compounds, John Wiley, 1963.

(57) NBS, C467, Atomic Energy Levels, Vol. II.

(58) P. W. Selwood, Magneto Chemistry, Interscience, 1943, p. 10.

(59) D. M. Adams, J. B. Raynor, Advanced Practical Inorganic Chemistry, John Wiley, 1965, p. 150.

(60) J. Lewis, R. G. Wilkens, Modern Coordination Chemistry, Interscience, 1960, p. 403.

(61) T. M. Dunn, D. S. McClure, R. G. Pearson, Aspects of Crystal Field Theory, Harper and Row, 1965.

(62) C. C. Lin Et Al., Jour. of Chemical Physics, 42 (1963), 3326.

(63) E. Hejmo, M. Ogorzalek, Roczniki Chem., 34 (1960), 1135.

(64) G. Bodtker-Naess, O. Hassell, Z. Anorg. Chem., 211 (1933), 21.

(65) S. M. Nelson, Proc. Chem. Soc., (London), (1961), 372.

(66) Z. G. Pinsker, Izvest. Akad. Nauk. SSSR, 13 (1949), 473.